COMMISSION ON COLLEGE PHYSICS

Cosmic Rays

MARTIN A. POMERANTZ

POMERANTZ Cosmic Rays

VAN NOSTRAND REINHOLD MOMENTUM BOOKS

PUBLISHED FOR THE COMMISSION ON COLLEGE PHYSICS

No. 1. **ELEMENTARY PARTICLES**—*David H. Frisch and Alan M. Thorndike*

No. 2. **RADIO EXPLORATION OF THE PLANETARY SYSTEM**
—*Alex G. Smith and Thomas D. Carr*

No. 3. **THE DISCOVERY OF THE ELECTRON:** The Development of the Atomic Concept of Electricity—*David L. Anderson*

No. 4. **WAVES AND OSCILLATIONS**—*R. A. Waldron*

No. 5. **CRYSTALS AND LIGHT:** An Introduction to Optical Crystallography
—*Elizabeth A. Wood*

No. 6. **TEMPERATURES VERY LOW AND VERY HIGH**—*Mark W. Zemansky*

No. 7. **POLARIZED LIGHT**—*William A. Shurcliff and Stanley S. Ballard*

No. 8. **STRUCTURE OF ATOMIC NUCLEI**—*C. Sharp Cook*

No. 9. **AN INTRODUCTION TO THE SPECIAL THEORY OF RELATIVITY**
—*Robert Katz*

No. 10. **RADIOACTIVITY AND ITS MEASUREMENT**
—*Wilfrid B. Mann and S. B. Garfinkel*

No. 11. **PLASMAS—LABORATORY AND COSMIC**—*Forrest I. Boley*

No. 12. **INFRARED RADIATION**—*Ivan Simon*

No. 13. **THE PHYSICS OF MUSICAL SOUND**—*Jess J. Josephs*

No. 14. **THE FREEZING OF SUPERCOOLED LIQUIDS**—*Charles A. Knight*

No. 15. **RADIO EXPLORATION OF THE SUN**—*Alex G. Smith*

No. 16. **MAGNETS**—*L. W. McKeehan*

No. 17. **THE WORLD OF HIGH PRESSURE**—*John W. Stewart*

No. 18. **MAGNETOHYDRODYNAMICS**—*Noel C. Little*

No. 19. **THE WINDS:** The Origins and Behavior of Atmospheric Motion
—*George M. Hidy*

No. 20. **THE DISCOVERY OF NUCLEAR FISSION**
—*Hans Graetzer and David L. Anderson*

No. 21. **THE WAVES:** The Nature of Sea Motion—*George M. Hidy*

No. 22. **COSMIC RAYS**—*Martin A. Pomerantz*

No. 23. **CRUCIAL EXPERIMENTS IN MODERN PHYSICS**—*George L. Trigg*

MARTIN A. POMERANTZ

VAN NOSTRAND REINHOLD COMPANY REGIONAL OFFICES:
New York, Cincinnati, Chicago, Millbrae, Dallas

VAN NOSTRAND REINHOLD COMPANY INTERNATIONAL OFFICES:
London, Toronto, Melbourne

Library of Congress Catalog Card No. 71–94017

Published by Van Nostrand Reinhold Company
450 West 33rd Street, New York, N.Y. 10001

Published simultaneously in Canada by
Van Nostrand Reinhold Ltd.

10 9 8 7 6 5 4 3 2 1

0442087217 ✓

Preface

The primary aim of this book is to convey to readers with a wide diversity of interests and backgrounds a sense of the excitement that pervades cosmic-ray research, as well as some feeling for the broad range of fundamental physics that falls within its purview. In addition to the intrinsic intellectual appeal of the ubiquitous stuff of which the whole universe is made, cosmic rays have implications in many disciplines, some far beyond the confines of physical science.

I have tried to achieve a level that is suitable for, but not limited to, an undergraduate whose only prior contact with physics was the beginning course. Thus, on the one hand, although this volume is not intended as a text for a graduate course, it might well serve as its syllabus. On the other hand, although some aptitude in physics (in addition to considerable patience) is required for thoroughly digesting the contents, I have tried to organize the material in such a manner that, hopefully, some appreciation of aesthetic values may be gleamed in this seemingly esoteric pursuit.

The emphasis is on ideas rather than experimental and theoretical details. In the interest of producing a nonencyclopedic narrative, individuals are named only in the process of setting the stage by sketching some of the pioneering steps that ushered in new ways of looking at things. I beg my colleagues' understanding and forgiveness for several sins of commission and omission. First, it was necessary to exercise some poetic licence in communicating concepts. Furthermore, I have perforce been somewhat cavalier in presenting results without due acknowledgment. Finally, large areas of research, in which exceedingly elegant work is being carried out, have barely been mentioned. I apolo-

gize for the somewhat egocentric approach, but it seems to be inevitable for a book on cosmic rays to be like the Bostonian's map of the United States.

I have enjoyed the good fortune of being associated with two generations of cosmic ray physicists. Together with just a few others who are still active workers in the field, I experienced the rare privilege of knowing personally practically all of the pioneers in cosmic rays, including their discoverer. And, thanks to the welcome movement toward international cooperation, and the shrinking size of the world, it is now possible to count among one's friends a very large number of scientists in many lands who are drawn together by the variegated facets of this fascinating subject.

To many individuals and institutions much too numerous to list, I express my deep gratitude for their help.

MARTIN A. POMERANTZ

Table of Contents

To Molly

1 *The Heroic Age of Cosmic Ray Exploration*

The beginning is the most important part of the work.
PLATO

Cosmic rays have been pelting the earth incessantly for countless eons. Every second, some ten or twenty of the progeny of these subatomic visitors from afar strike the body of each of us. But man first became aware of their presence only at the beginning of this century. Then, as has happened so frequently in the history of science, it was noted that certain experimental apparatus behaved in an unexpected manner.

Inquisitive minds, not content with the "obvious" explanation of this disturbing effect which interfered with the measurements that were then being carried out in a number of laboratories, ultimately established the existence of a new fundamental phenomenon. But even then, many decades were to pass before the broad implications of this discovery became comprehensible.

A considerable body of knowledge about the once mysterious cosmic radiation has now been amassed, and this esoteric and still romantic subject has attained prominence even among the general public. This is attributable to several factors, not the least of which is the preeminent role played by cosmic ray physicists in the space age. By virtue of their philosophical and experimental heritage, they have been in the vanguard, making sometimes spectacular and usually exciting discoveries with equipment carried by spacecraft to the farthest reaches of the earth's atmosphere and far beyond. To provide a frame of reference in which one can better appreciate the degree of sophisti-

cation of present day cosmic ray research, let us trace its early history from its very humble beginnings.

THE DAWN OF COSMIC RAY RESEARCH

At the turn of the century, studies on x rays, discovered in 1895 by Wilhelm Conrad Röntgen, and radioactivity, first observed by Henri Becquerel the following year, were in vogue. These experiments generally involved use of the ionization chamber, a vessel containing gas which becomes conducting when exposed to radiations endowed with sufficient energy to detach some of the atomic electrons. The resulting current, arising from the motion of the free positive and negative charges, or *ion pairs*, was measured with an electrometer.

The most primitive electrical instrument that can be used as a radiation sensor is the familiar gold-leaf electroscope. This simple device indicates, by its rate of discharge, the extent to which the conductivity of the surrounding air is modified by the presence of ionizing radiation. Long before radioactivity was recognized, electroscopes had revealed that the atmosphere is not a perfect insulator. Indeed, free air always seemed to contain something like 500 to 1000 ions per cubic centimeter, corresponding to a rate of formation of roughly 10 ion pairs per cubic centimeter per second. After Becquerel's discovery it was quite natural to attribute the residual leakage of electroscopes to the presence of radioactive material in the air and in the soil.

This explanation seemed to be confirmed in 1901 by the experiments of C. T. R. Wilson, in England, and J. Elster and H. Geitel, in Germany. They measured the conductivity of stagnant air in a dust-free, sealed vessel enclosing an electroscope, and found that some residual ionization still persisted. But, eventually, a nagging question arose. Could internal radioactive impurities account *entirely* for the current that always remained despite all efforts to eliminate contaminations?

Perhaps radium emanation and its disintegration products produced some type of radiation that was capable of penetrating even the walls of an ionization chamber. Testing this hypothesis, E. Rutherford and H. L. Cooke, in England, and J. C. Mc-

Clennan and E. F. Burton, in Montreal, found in 1903 that very thick shielding by water or other inactive materials reduced the ionization of air in a closed vessel by about 30%. However, there was no appreciable further change when the thickness of the lead shield exceeded about 2 inches.

Measurements were then made by McClennan on land and aboard a ship at sea, in what appears to have been the first cosmic ray expedition. Later, he even took his apparatus out on the ice of Lake Ontario. These observations suggested that the ionization was greater over land, and could be ascribed to penetrating gamma radiation from the soil, which always contains traces of radioactive impurities (uranium, thorium, radium, and their decay products). The residual ionization over water was attributed to minute radioactive impurities in the walls and gas filling of the ionization chambers, and to γ rays from the surrounding air. However, A. S. Eve, in Montreal, was skeptical. In the first quantitative analysis of this problem, he showed, in 1905, that the radium and thorium emanations in the air were not sufficiently abundant to produce more than one-tenth of the effect that was observed over water. Subsequently, other attempts were made to account quantitatively for the observed 10 to 20 ion pairs/cm^3/sec, culminating in the conclusion by an Italian physicist, D. Pacini, in 1910, that the observed excess ionization might be produced by sources other than the known radioactive substances.

Early experiments designed to assess the contribution from the ground by taking ionization chambers up into towers were inconclusive because of the excessive background of radioactive substances in the stone structures that were selected for this purpose. Ironically, however, the first definitive experiment aimed at determining the altitude variation seemed to indicate that the ionization *decreased* with altitude! In 1910, Father Th. Wulf determined that the residual ionization on the ground in Paris was 6 ion pairs/cm^3/sec (after subtracting the chamber background) while at the top of the Eiffel Tower, 300 meters above the ground, the strength was reduced to 64% of that value. However, he had anticipated that the intervening layer of air would cause a much greater decrease, to about 10% of the ground value.

Wulf concluded that either another source of γ rays existed in the upper layers of the atmosphere, or the absorption of γ rays in air was apparently smaller than had been assumed hitherto.

Meanwhile, K. Bergwitz had, in 1909, already made balloon ascents that showed a more marked decrease of the total ionization, which at 1300 meters was down to about 25% of the value on the ground. This was interpreted as being in better accord with expectation if the ground were the source of gamma radiation that was responsible for the residual ionization. However, there was some question about the validity of Bergwitz' measurements, since his electrometer was damaged during the flight by deformation of his pressure vessel. This prompted A. Gockel to make three balloon ascents over Switzerland in 1910 and 1911. From his measurements of the ionization up to 4500 meters, Gockel concluded that the "decrease of the radiation with height . . . was still less than was found earlier." The source of the ionization at high altitudes, according to Gockel, was disintegration products of the known radioactive substances.

In order to avoid the pitfalls encountered by Bergwitz, Gockel had connected his ionization chamber to a rubber balloon that expanded as the external pressure decreased, thereby avoiding a pressure differential between the gas filling and the outside air. Consequently, the pressure of the gas in the vessel varied with altitude. Under the prevailing conditions, the measured ionization was proportional to the gas pressure. If Gockel had only corrected his measurements for this variation of instrumental sensitivity with pressure, he would have concluded that there was a significant *increase* in ionization as the balloon ascended!

It was a happy circumstance that Victor Hess, an Austrian physicist, was an ardent amateur balloonist. After reading about Wulf's Eiffel Tower experiment, he decided that the accumulated evidence pointed to the presence of a previously unknown source of ionization. He initiated a program to check this possibility experimentally by measuring directly the absorption in air of γ rays from an intense radium source (1500 milligrams). His measurements, made outdoors by varying the distance between a closed ionization chamber and the source up to 90 meters, firmly established that γ rays from the ground are almost completely

absorbed at a height of 500 meters. Then, he designed an instrument that could survive the rigors of an open balloon gondola—an airtight ionization chamber with walls sufficiently thick to withstand a pressure differential of one atmosphere, and containing a temperature-compensated Wulf fiber electrometer.

In 1911, the first of a series of ten balloon flights (each carrying two or three instruments operating simultaneously) reached 1070 meters. Hess concluded that the radiation at that height was not appreciably different from that at sea level. But, in the following year, he attained an altitude of 5350 meters (Plate I). After an initial decrease, the ionization current above 800 meters seemed to increase. Between 1400 and 2500 meters the sea level value was clearly exceeded and at 5000 meters the reading was several times as great as on the ground. Hess saw no possibility of accounting for his results in terms of radioactive substances in the air but was forced "to have recourse to a new hypothesis; either invoking the assumption of the presence at great altitudes of previously unknown matter, or the assumption of an extra-terrestrial source of penetrating radiation." Twenty-five years later, Hess received a Nobel Prize for his discovery.

Further flights by W. Kolhörster, a German physicist, who reached a height of 9300 meters in 1914, provided clear confirmation that should have made Hess's conclusion incontrovertible. The ionization continued to increase until it attained a value about fifty times that at sea level. Assuming that, as in the case of x and γ rays the intensity drops off exponentially with distance x according to the law

$$I_x = I_0 \exp(-\beta_i x) \tag{1-1}$$

Kolhörster determined from his data the absorption coefficient $\beta_i \simeq 1 \times 10^{-5}$ per cm of air, representing almost ten times the penetrating power of the most penetrating γ rays then known.

THE RADIATION ERA

In retrospect, it is not surprising that the earlier workers were inclined to question whether the residual ionization in a supposedly "clean" vessel was representative of anything other than

some stubborn contamination that defied all efforts to remove it. Indeed, most of it *was* attributable to such causes. For, in fact, the ionization produced by cosmic rays in air at sea level is only about 20 percent of that arising from natural radioactivity!

By the same token, it is readily understandable that this new phenomenon should be identified as electromagnetic radiation, similar to the known γ rays, although much less easily absorbed in passing through matter. The only other available candidate, the electron, appeared not to be naturally adapted to yielding the exponential type of absorption law that seemed to be followed by the penetrating radiation. Furthermore, β rays from radioactive substances, the most penetrating charged particles then known, were absorbed in less than 1 millimeter of lead.

The extension of the measurements to high altitudes provided the crucial evidence that should have removed all doubt concerning the existence of an unknown radiation with a penetrating power exceeding by many times that of γ rays from natural radioactive substances. But a stubborn skepticism in some circles concerning the reality of the new penetrating radiation from above (*Ultrastrahlung* or *Höhenstrahlung*) combined with a World War to result in a hiatus in the experimental investigations. High altitude experiments were not resumed until 1922, when R. A. Millikan and I. S. Bowen started sending up balloons carrying small self-registering electroscopes.

Once again, the waters were to be muddied by a chance circumstance—the choice of launching sites—that led to a discrepancy between the American and European results. The ionization at very high altitude over San Antonio, Texas, was only 25 percent of that over Central Europe! This consequence of the then unknown *latitude effect* triggered off a renewed attack, exemplified by Millikan's subsequent conclusion in 1924, based upon ionization measurements atop Pike's Peak, that ". . . there exists no such penetrating radiation (of cosmic origin). The whole of the penetrating radiation is of local origin. How such quantities of radioactive material get into the upper air is as yet unknown."

This proved to be but one of a great many erroneous conclusions about cosmic rays. The state of flux of ideas about cosmic rays in the early days is admirably portrayed in one of the in-

numerable anecdotes about Millikan. Appearing as an expert witness in the trial of a man who was being prosecuted for selling bottles of water with a label claiming that the liquid had curative effects because it had been irradiated by cosmic rays, Millikan is supposed to have pointed out that, indeed, the contents of the bottles *had* been irradiated by cosmic rays. And, as for the claimed medicinal properties, who *hadn't* made incorrect statements about cosmic rays?

Measurements of the change in ionization with depth in snow-fed lakes (to minimize background radioactivity) at different altitudes (Muir Lake at 3590 meters, Arrowhead Lake at 2060 meters) finally convinced Millikan in 1926 that "very hard etherial rays of cosmic origin were entering the earth uniformly from all directions." He christened them "cosmic rays." But all was not yet serene. One of the stormiest marathon debates between two giants in the history of science, Millikan and Compton, was still to ensue.

The consequences of the generally accepted assumption that cosmic rays were γ rays endowed with tremendous energies were pursued assiduously during the years that followed this much belated universal agreement as to their existence. The ultimate goal was to determine the energy spectrum of these incoming high frequency photons that quantum theory had already associated with high energy. This was accomplished by assigning an initial arbitrary photon frequency distribution, and then tracing its consequences with respect to the variation of the ionization as a function of depth in the atmosphere, or in lakes, or under other absorbing media. By trial and error, the spectrum providing the best fit to the observations was found. Although the difficulties of envisaging cosmic rays as energetic electrically charged particles seemed insuperable, the required extrapolation of the then known laws of γ-ray absorption was still fantastic. In some cases, the procedure was equivalent to extrapolating for several hundred miles a curve drawn on an ordinary piece of graph paper covering the range over which the law that it represented had been experimentally verified.

The game consisted of dividing the incoming beam into several distinct bands of photons with characteristic absorption co-

efficients β_i, such that the combination would yield the observed ionization *vs* depth curve. Each β_i was associated with the corresponding photon frequency ν_i. The energies $W_i = h\nu_i$ were then related to the energies of certain atom-building processes, as suggested by the mass defects of atoms revealed by F. W. Aston's measurements of isotopic masses in 1927.

Just as the atomic spectrum had led to a thorough understanding of atomic structure, it was speculated that the cosmic ray spectrum could reveal how more complex forms of matter are formed from hydrogen. As is shown in Fig. 1-1, Millikan and

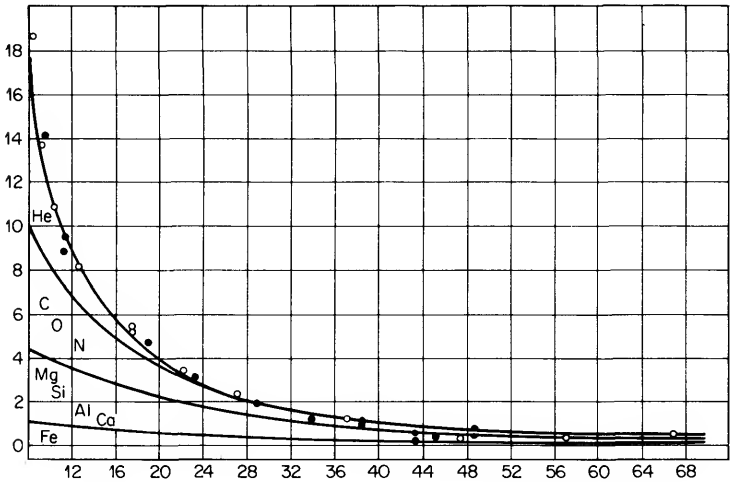

FIG. 1-1 Millikan and Cameron's comparison of experimental data (dots and circles) with a built-up curve compounded from four absorption coefficients. Abscissas: depth in equivalent meters of water beneath surface of atmosphere. Ordinates: ionization in ions per cubic centimeter per second.

G. H. Cameron interpreted their observations as providing evidence for the existence of four energy bands associated with atom-building "in the depths of space." The four bands were identified with "acts of formation of hydrogen into the celestially common elements helium, oxygen (C, N, O), and silicon (Na, Mg, Al, Si and S)." It is easy to appreciate the reluctance of its originator to relinquish this most alluring hypothesis envisioning cosmic rays as the birth-cries of the elements.

THE CORPUSCULAR ERA

Meanwhile, certain experimental developments seemed to point to the possibility that the observed ionization produced by cosmic rays might be attributable to electrically charged particles. In 1927, a Russian physicist, D. Skobelzyn, observed tracks arising from the passage through his Wilson cloud chamber of β rays having energies at least an order of magnitude greater than those emitted by the known radioactive substances. Furthermore, these occurred at a sufficient rate to account for the whole of the cosmic ray ionization.

At the same time, a Dutch physicist, J. Clay, was conducting the decisive experiment that, following the familiar pattern in the history of cosmic rays, *should* have ended the controversy—but didn't.

J. J. Thomson had shown in 1897 that moving electrically charged particles are deflected by magnetic fields. As early as 1904, C. Störmer, a Norwegian who used to remarkable advantage his ideal location in the zone of maximum auroral occurrence, had started his brilliant analysis of the effects of the geomagnetic field upon the motion of incoming charged particles (presumably the cause of the magnificent auroral displays that he was studying). Störmer's results revealed that, for electrons of a certain energy, which could reach the earth at high latitudes, there was an inaccessible equatorial zone. Thus, if cosmic rays were electrically charged corpuscles with the appropriate energies, fewer should arrive at the equator than at higher latitudes. On the other hand, if the incoming cosmic rays were electromagnetic, they would not be affected by the earth's magnetic field.

So Clay mounted his apparatus aboard a ship traveling between Holland and Java. In three different voyages, the intensity was consistently lower (by about 11 percent) near the equator.

But a number of other investigators failed to confirm the crucial findings first published by Clay in 1927. The reasons for these apparent discrepancies are now obvious. The most flagrant blunder committed by some of those who disagreed with Clay's

conclusion that the ionization changed with latitude in going toward the equator was that they generalized from observations made north of the so-called *knee* of the latitude effect (cf. Chapter 4). At high latitudes, the ionization near sea level reaches a constant plateau value determined not by the earth's magnetic field, but rather by absorption in the atmosphere.

In 1929, W. Bothe and W. Kolhörster demonstrated by experiments with Geiger-Mueller counters in coincidence (cf. Chapter 3) that the penetrating power of the ionizing particles was comparable with that deduced from the variation with depth of the total cosmic radiation. They also pointed out that the lower energy particles among those they observed would be excluded from the equatorial zone, as indicated by the experiments of Clay. Perhaps, they speculated, these ionizing corpuscles might be the primaries themselves!

And now, the climax neared as A. H. Compton mounted a program of heroic proportions. Beginning in 1930, exceedingly careful measurements with the "improved cosmic ray meter" shown in Fig. 1-2 were made in a world-wide survey by twelve expeditions involving eighty cooperating physicists at a hundred stations. The results dispelled all the doubts, including those that had even started to plague Clay himself. As Compton put it so succinctly, "Isocosms* are not to be argued with."

THE MODERN ERA

When the corpuscular nature of the primaries became textbook gospel, cosmic ray research really came of age. Then, interest in this challenging and rewarding field burgeoned. Whereas the annual output of published papers, both theoretical and experimental, had been less than 10 between 1912 and 1920, the number rose to more than 200 per year between 1933 and 1936, and more rapidly thereafter.

It was inevitable that cosmic ray research should develop along two main lines. One, the subject of this book, is concerned with

* Lines of equal cosmic ray intensity plotted on a world map. These appeared to follow the contours of constant values of the horizontal component of the earth's magnetic field (isomagnetic lines).

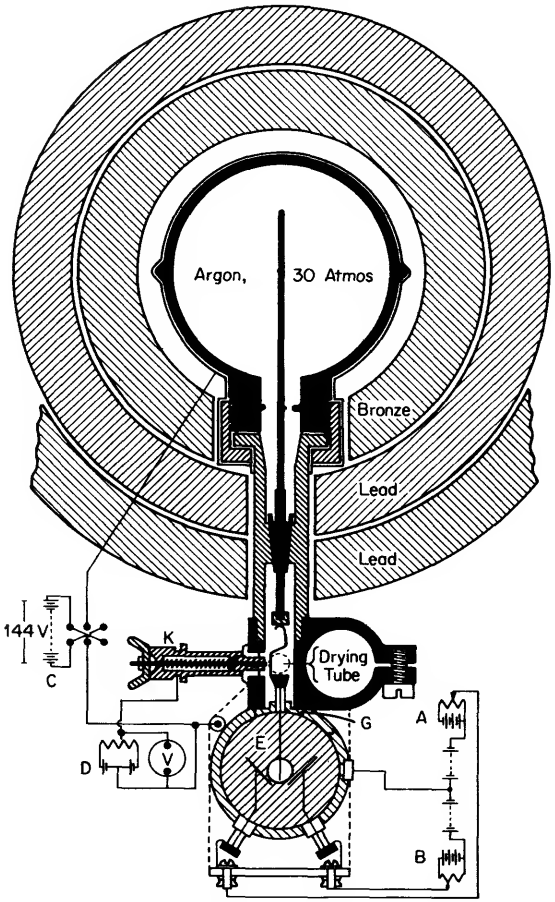

FIG. 1-2 Portable cosmic ray meter designed for the world-wide survey organized by Compton in 1930. After more than three decades a larger version, the Model C ionization chamber, is still continuously recording the cosmic-ray intensity at several widely separated stations.

the cosmic rays themselves—what are they, where do they come from, how do they get here, and so on. The other involves the utilization of this windfall of high-energy subatomic particles for studying their interactions with matter.

The latter category at first was of far-reaching interest as a

proving ground for testing the validity of the laws of quantum electrodynamics in extreme energy regions where breakdowns were theoretically predicted. Then, the cosmic rays served as a medium for discovering and investigating the properties of new "elementary" particles. Finally, they provided the means for studying high energy nuclear interactions, with the aim of shedding light on processes which are germane to the basic understanding of nuclear forces. As man-made machines capable of accelerating particles up to cosmic ray energies became available, a sort of bifurcation occurred, and high-energy nuclear physics, or particle physics, was recognized as an established field in its own right.*

Nevertheless, strong bonds of mutual interest have persisted, and the two breeds have retained a common meeting ground. This is because, on the one hand, particles endowed with vastly higher energies than man will be able to produce in the laboratory will always be present among the cosmic rays; whereas, on the other hand, in order to interpret observations with cosmic ray instruments in the lower atmosphere, it is necessary to understand in detail the complicated processes involved in the transfer of energy from the *primary* cosmic rays (which are initially incident upon the outer limits of the earth's atmosphere, but which do not penetrate very deeply because of their propensity for interacting with the atmospheric constituents) to their progeny, *secondary* cosmic rays (which are ultimately detected at ground level).

How did our knowledge about cosmic rays develop after their identity as electrically charged particles was established? The story will unfold in subsequent chapters, but, as a prelude, let us summarize in capsule form what has been learned thus far.

Primary cosmic rays are the atomic nuclei of elements with which we are familiar on earth. Hydrogen nuclei—protons—are the most abundant, followed by the second element on the periodic table, the nuclei of helium atoms—alpha particles. Roughly speaking, these are present in about the same proportion as the relative abundances of these elements throughout the

* See MOMENTUM Book No. 1, *Elementary Particles*, by D. H. Frisch and A. M. Thorndike, Van Nostrand, Princeton (1964).

universe—about 10 hydrogen to 1 helium. On the other hand, heavier nuclei, although relatively scarce (about 1 percent), are overabundant in the cosmic-ray beam. Nuclei considerably heavier than iron are found to be exceedingly rare members of the cosmic-ray family. There are also some electrons, to the extent of a few percent.

The energies of primary cosmic rays range from a lower limit under 10^6 eV to an upper limit of at least 10^{20} eV. Whereas roughly one particle having an energy near 10^9 eV passes through one square centimeter at the top of the atmosphere each second, only a single 10^{20} eV particle impinges on an area of a hundred square kilometers in a year. The number of cosmic rays above a given energy E falls off approximately as $E^{-1.5}$.

In interplanetary space, a total of about four cosmic-ray particles passes through each square centimeter every second. The corresponding energy density amounts to approximately 10^{-12} ergs per cubic centimeter, about equivalent to the energy that reaches us in the form of starlight, or to the energy that is associated with magnetic fields in space.

The cosmic rays arrive essentially isotropically except for some local effects of solar origin. Most, but probably not all, of the cosmic rays originate in our galaxy, and hence are called *galactic cosmic rays* to distinguish them from energetic particles emanating from the sun. Various acceleration mechanisms may be responsible for imparting to them their high energies, and they may wander through the galaxy for very long periods before reaching the solar system. They alone are the only bits of matter that reach us from outside the solar system.

This recital of their nature and properties suggests that cosmic rays play the role of a virtuoso in the broad concert of science. For, indeed, interest in these gadabouts of the universe far transcends the realm of physics, and considerable impetus for studying them stems from their broad interdisciplinary ramifications. Cosmic rays serve as a unique tool for investigating a variety of problems, not only in the physical sciences, but in such seemingly remote fields as archeology and geology; their study is of fundamental interest to astronomy, astrophysics, solar physics, cosmology, geophysics, and high-energy nuclear physics. The scale

of distances over which they function as effective probes ranges from the interior of atoms to the environs of our planet on out to the most distant reaches of the galaxy in which our solar system is located (the Milky Way) and even beyond. It will become increasingly evident in the sequel that the heroic age of cosmic-ray exploration is not likely to come to an end in the foreseeable future!

2 *Collisions of Cosmic Rays with Matter*

By their fruits, ye shall know them.
MATTHEW VII, 20

The label "cosmic radiation" has generally been attached to the totality of all the different *primaries* impinging on the top of the atmosphere, together with the *secondaries* comprising all succeeding generations of their multifarious progeny. The vital statistics of the particles that play significant roles in the phenomenology of cosmic rays are summarized in Table A-1 (Appendix). Various other evanescent members of the rapidly growing family of "elementary" particles that rarely appear among the cosmic rays are best ignored for our purposes, since interest in them properly falls within the domain of high-energy physics.

A variety of atomic and nuclear processes come into play as cosmic rays plow through matter, "frittering away their energy" to borrow a phrase from picturesque Millikanese. The prerequisite of all methods for studying cosmic rays is a thorough understanding of their interactions, for it is only the consequences of their collisions that render them "directly" observable rather than theoretically assumed. Knowledge about their interactions is essential both for designing detectors and for interpreting observations in the light of instrumental responses. Thus, appropriate sensors can be developed not only for detecting particles, but for determining their relevant characteristics.

Furthermore, we must be able to trace backward from observations within the atmosphere to the incident primaries which they represent. Finally, even interstellar space is not devoid of

matter, hence the primaries themselves have suffered collisions on their long and tortuous journey toward the solar system. Clearly, these need to be taken into account in studies on the origin of cosmic rays.

Particle interactions generally fall into one of two categories, depending upon whether the nature of the force is *electromagnetic* or *nuclear*. Electromagnetic forces may cause the transfer of energy by excitation, ionization, radiation, photoelectric emission, Compton scattering, pair production, and particle annihilation. Nuclear forces come into play when nucleons interact to produce mesons, or to induce nuclear disruptions. In some cases, such as photodisintegration of nuclei and photoproduction of mesons, both types of force may be involved.

Let us now consider how the various components of the cosmic radiation behave when they encounter matter. But before discussing the different types of interaction in which energy is transferred, it is helpful to become acquainted first with a few concepts that are useful in describing absorption processes.

Relativistic Energy. When the speed v of a particle of mass M_0 approaches the speed of light c, its energy can no longer be represented by $\frac{1}{2} M_0 v^2$ as in ordinary Newtonian mechanics. Otherwise, the limiting energy that could be attained by any particle would be $\frac{1}{2} M_0 c^2$! Relativity theory, which prescribes the limiting velocity c in the first place, tells us how to handle this situation. We must forego the fun of deriving the relativistic transformations here,* and will note only the results that are essential for understanding the behavior of cosmic rays. The significant parameter is the ratio of particle velocity to the speed of light, $\beta = v/c$. We start with a few assertions.

The mass M_β of a particle moving with speed $v = \beta c$ is

$$M_\beta = \frac{M_0}{(1 - \beta^2)^{\frac{1}{2}}} \tag{2-1}$$

where M_0 is the *rest mass* of the particle. The *momentum* p and *total energy* U of this particle are given by:

* See MOMENTUM Book No. 9, *An Introduction to the Special Theory of Relativity*, by R. Katz, Van Nostrand, Princeton (1964).

$$p = M_\beta v = \frac{M_0 \beta c}{(1 - \beta^2)^{\frac{1}{2}}} \tag{2-2}$$

$$U = M_\beta c^2 = \frac{M_0 c^2}{(1 - \beta^2)^{\frac{1}{2}}}. \tag{2-3}$$

Equation (2-3) says that the total energy U_0 of a stationary particle ($\beta = 0$) is equal to $M_0 c^2$, in accordance with the well-known Einstein mass-energy equivalence principle.

The *kinetic energy* E is obviously smaller than the total energy U by the amount of energy associated with the rest mass:

$$E = U - M_0 c^2. \tag{2-4}$$

Hence

$$E = M_0 c^2 \left[\frac{1}{(1 - \beta^2)^{\frac{1}{2}}} - 1 \right]. \tag{2-5}$$

It is advantageous to express particle energies in units of the rest energy of the particle. At very high energies, $E \gg M_0 c^2$, the total energy and kinetic energy are roughly equal, and

$$E/M_0 c^2 \simeq U/M_0 c^2 \simeq 1/(1 - \beta^2)^{\frac{1}{2}}. \tag{2-6}$$

Thus, two very energetic particles ($E \simeq U$) with different rest masses but the same energy in units of $M_0 c^2$ move with the same speed. For example, referring to Table A-1, we see that the value of β for a 10,000 MeV muon ($E/M_0 c^2 = 10^4/10^2 = 100$) is the same as for a 50 MeV electron ($E/m_0 c^2 = 50/0.5 = 100$). The same advantage is gained by expressing momentum in units of $M_0 c$. Comparing Eq. (2-2) and (2-3), we see that at very high velocities ($\beta \simeq 1$)

$$p/M_0 c \simeq U/M_0 c^2 \tag{2-7}$$

or

$$pc \simeq E. \tag{2-8}$$

The relationships among p, U, E, and β are shown in Fig. 2-1. Its usefulness stems from Eqs. (2-2) and (2-3), which say that $p/M_0 c = \beta/(1 - \beta^2)^{\frac{1}{2}}$ and $U/M_0 c^2 = 1/(1 - \beta^2)^{\frac{1}{2}}$.

While we are talking about relativity effects, we should point out that τ, the lifetime before decay of a moving unstable particle, is given by a relationship exactly like Eq. (2-1):

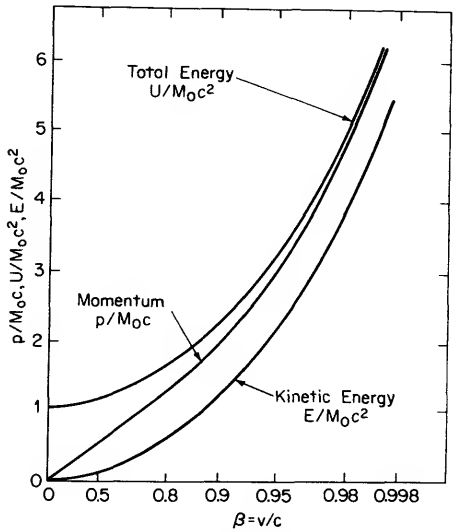

FIG. 2-1 Total and kinetic energy in units of M_0c^2, and momentum in units of M_0c, as a function of β.

$$\tau = \frac{\tau_0}{(1 - \beta^2)^{\frac{1}{2}}} \tag{2-9}$$

where τ_0 is the *proper lifetime* measured in the coordinate system in which the particle is at rest. Consequently, making use of the fact that $1/(1 - \beta^2)^{\frac{1}{2}} = U/M_0c^2$, we find that

$$\tau = (U/M_0c^2)\tau_0. \tag{2-10}$$

Thus, to a stationary observer, the lifetime of a relativistic particle ($\beta \simeq 1$) appears to be proportional to its energy! For example, the *mean lifetime* of a 10^{14} eV muon is approximately $(10^{14}/10^8)\tau_0 = (10^6)\ (2 \times 10^{-6})$ sec $= 2$ sec.

Absorber Thickness. It is obvious that a particle passing through 1 cm of water sees more entities with which it can interact than it would if the water were replaced by 1 cm of air at STP. To be sure, the ratio of densities, $\rho_{H_2O}/\rho_{air} \simeq 800$, is the same as the ratio of the amounts of the two substances encountered by the particle in this example. On the other hand, if the air path length is increased, say to 8 m, then the total quantity of absorber is 800 times the original amount. We must therefore specify both

the *density* ρ and the *path length* x. Merely by multiplying these quantities, we obtain a valid measure of the total *mass* of absorber traversed. Thus, in the above example, the mass of 8 meters of air is equal to the mass of 1 centimeter of water. The quantity ρx is a sort of *surface density,* measured in grams per square centimeter.

At sea level, the superposed atmospheric mass is $\rho_{Hg} h_{Hg} =$ (13.6 gm/cm^3) (76 cm) $\simeq$ 1000 gm/cm^2. Conveniently, the atmospheric depth in gm/cm^2 is almost exactly equal to the pressure in millibars. In the vernacular, we sometimes say "grams" in referring to absorber thickness, or atmospheric depth, when we really mean "grams per square centimeter."

Cross Section. Let us imagine that a beam of particles passes through a target, as illustrated in Fig. 2-2, uniformly irradiating the area A_s.

The particle *flux* ϕ is defined as the number of particles n passing through unit area in unit time, e.g. n/cm^2/sec. In a unit vol-

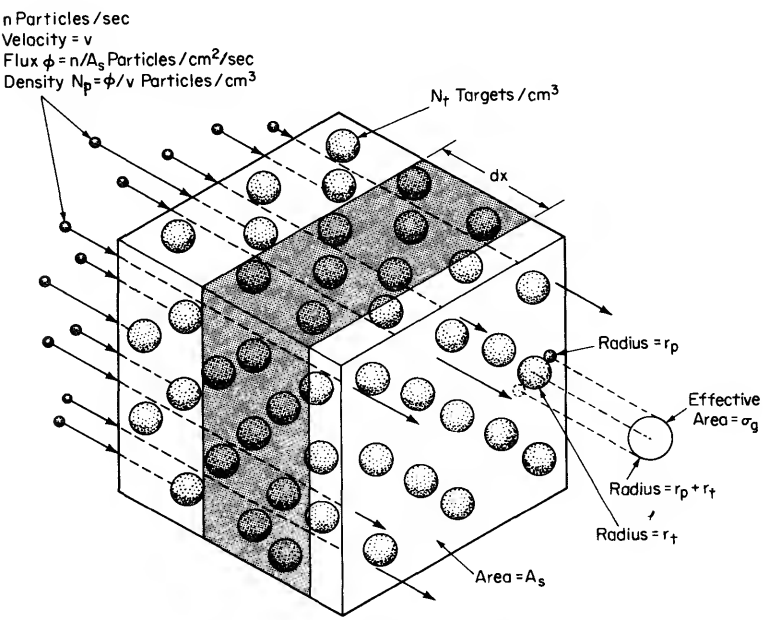

FIG. 2-2 Schematic representation of the meaning of cross section.

ume, the target contains N_t uniformly distributed identical bodies. Suppose both the projectiles and the entities comprising the target are hard spheres, with radii r_p and r_t respectively. The bombarding particle collides with one of the objects in the target if it comes within the effective area $\sigma_g = \pi(r_p + r_t)^2$ The chance of a collision as the incident particle attempts to pass through the thin lamina dx is simply the ratio: (total projected effective area of all the centers in A_s)/(total area A_s).

Referring to the figure, this ratio is

$$\frac{\sigma_g(N_t A_s dx)}{A_s} = N_t \sigma_g dx, \tag{2-11}$$

where σ_g is the *geometric cross section*. The unit of cross section is the *barn* (10^{-24} cm^2) or the *millibarn* (10^{-27} cm^2). The radius of a nucleus is approximately $1.2A^{1/3} \times 10^{-13}$ cm, where A is the mass of the nucleus in atomic mass units; hence the nuclear geometric cross section is about $0.05A^{1/3}$ barns. Most interactions do not correspond to billiard-ball collisions. The cross section σ_i is the effective area for a given type of interaction i presented by one target particle per unit area perpendicular to the direction of the beam.

Mean Free Path. In Eq. (2-11), note that $N_t\sigma_g$, the product of the number of absorbing centers per unit volume and the effective area of each center, is the number of centers encountered by a single particle in traversing unit distance through the target. Its reciprocal is the distance, on the average, between the centers along its route, the *mean free path* λ_g. Thus, in general,

$$1/N_t\sigma_i = \lambda_i. \tag{2-12}$$

In the above discussion, the mean free path represented the *interaction length* λ_i. If the initial collision is not catastrophic, but merely maims the bombarding particle, the absorption mean free path, or *absorption length* λ_a can exceed the interaction length.

Attenuation. When there are many particles in a beam, we can measure the *attenuation,* or fractional reduction of the flux suffered from interactions. The number of casualties depends upon how many mean free paths have been traversed. Thus,

$$-d\phi/\phi = (dx/\lambda). \tag{2-13}$$

Integration gives

$$\phi_x = \phi_0 \exp(-x/\lambda). \tag{2-14}$$

Absorption Coefficient. The absorption coefficient is equal to $1/\lambda$. If λ and x are expressed in cm, β_l is the *linear absorption coefficient* (cm^{-1}). If λ and x are expressed in gm/cm^2, β_m is the *mass absorption coefficient* (cm^2/gm).

ELECTROMAGNETIC INTERACTIONS

The theoretical analysis of electromagnetic interactions employs quantum electrodynamics. The formulas thus derived have been checked by a variety of experimental techniques. The energy-transfer processes, governed by conservation laws, stem from the interrelationships between particles and fields. The particles are both the sources of the fields (or the fields themselves), and the recipients of their effects.

Electromagnetic fields in the macroscopic world are completely described by classical Maxwell theory. However, when we are dealing with microscopic systems, quantum laws hold sway, and a field becomes a flux of photons. Particles now play a dual role: (1) as radiation quanta, their electromagnetic properties reside in their *charge* and *magnetic moment;* (2) as constituents of matter, their mechanical properties are inherent in their *mass* and *spin.*

All interactions are treated in terms of a field of force. In the case of ionization, for example, this is the familiar force between electrical charges that is described by Coulomb's law:

$$\mathbf{F} = \frac{1}{4\pi\epsilon_0}\frac{q_1 q_2}{r^2}\mathbf{r}_1 \tag{2-15}$$

where $\mathbf{F}$ is the force, *in vacuo,* between two charges q_1 and q_2 of bodies that are very small compared with the distance r between them, $\mathbf{r}_1$ is a unit vector along the line joining q_1 and q_2 indicating the direction of that line, and ϵ_0, the permittivity of free space, is a constant [$= 1/(36\pi \times 10^9)$farad/m in MKS units].

The consequences of a collision depend upon the distance of

closest approach of the interacting entities—the *impact parameter* d in Fig. 2-3. This quantity figures prominently in the theoretical analyses leading to the results that we shall now examine.

Charged Particles. When the impact parameter greatly exceeds the atomic radius ($d \gg r_{\text{atom}}$), the entire atom reacts as a whole to the passing charge. As a result, the charged particle loses energy gradually by exciting atoms along its route (*excitation*) and freeing those electrons to which it imparts amounts of energy greater than their binding energies (*ionization*). Figure 2-3 shows sche-

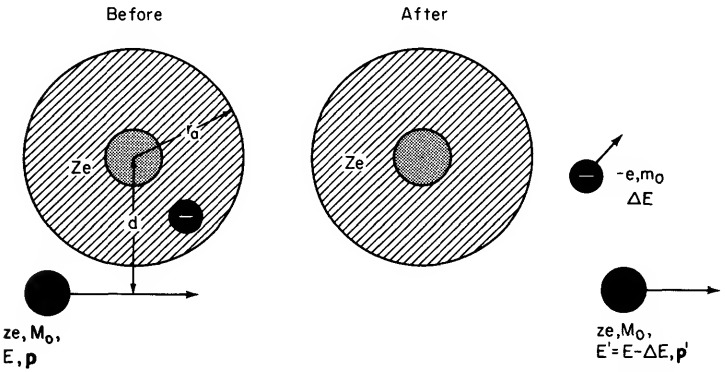

FIG. 2-3 Schematic representation of an ionizing interaction. The collision changes the originally neutral atom into a positive ion.

matically an ionizing event produced by a particle with z units of the electronic charge e when it interacts with an atom with atomic number Z. The magnetic moment does not play an important role in this case, since the magnetic force varies as $1/r^3$, whereas the electrostatic force falls off more slowly, as $1/r^2$.

In an ionized gas, the emitted electrons constitute free negative charges and the originally neutral atoms positive charges (*ion pairs*), until they recombine. In the case of a solid, the subsequent history of the liberated charge carriers depends upon whether it is a metal or an insulator. Free electrons in the conduction band of a metal, as well as bound electrons, may extract energy from a passing charged particle. We have found in our laboratory that a thin insulating crystal, such as MgO, becomes a conductor

temporarily when high energy electrons are shot through it, boosting bound electrons over the band gap into the normally unoccupied conduction band. (Even the most ardent cosmic ray aficionados sometimes like to try experiments that *they* have concocted, as a change from having to wait for nature to perform them!)

High energy secondary electrons, originally referred to as *knock-on electrons* but now generally called *delta rays* because of the characteristic appearance of their tracks in a Wilson cloud chamber or a photographic emulsion, can be ejected when the impact parameter is comparable with the atomic radius ($d \simeq r_{\text{atom}}$). In this case, the moving particle collides with a single electron which responds as though it is essentially free.

When the incident particle penetrates deeply into the atom ($d < r_{\text{atom}}$), its trajectory can be deflected by the electric field of the nucleus. In this case, the Coulomb field of the point charge $+Ze$ centered at the nucleus acts upon a particle that passes at a distance large compared with the nuclear radius ($\sim 10^{-13}$ cm) but small compared with the atomic radius ($\sim 10^{-8}$ cm). Because of the deceleration $d\mathbf{p}/dt$ associated with the change of direction of motion of the charged particle, electromagnetic radiation is generated. Classical electrodynamics predicts that the intensity is proportional to the square of the acceleration. If only soft quanta are emitted, the incident particle merely undergoes *inelastic scattering*.

But, according to quantum electrodynamics, a single γ ray with up to the entire particle energy can emerge from a *radiative collision*. Figure 2-4 depicts such an event in which *bremsstrahlung* (German: braking radiation) is produced. Furthermore, although it is not possible according to classical theory for a charged particle, such as an electron, to be deflected by a nucleus *without* emission of radiation, in quantum theory there is a finite probability for the particle to be deviated without emission of a photon, and hence to undergo *elastic scattering* through *nonradiative collisions* (Fig. 2-5).

In the formalistic language of quantum electrodynamics, we may regard the emission of bremsstrahlung as the transition from an initial state in which the electron has a certain positive kinetic

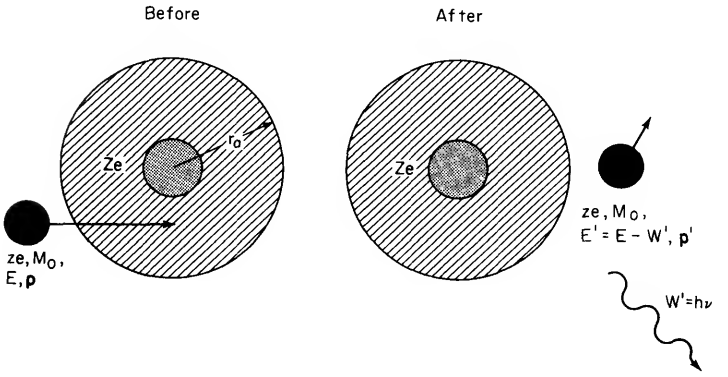

FIG. 2-4 Schematic representation of a radiative collision, resulting in the emission of bremsstrahlung.

energy E and momentum p in the radiation field containing zero photons, to a final state in which the electron energy is lower ($E' < E$) but still positive in a field containing one photon of energy $W' = h\nu$.

In elastic scattering, the energy of the electron remains unchanged ($E' = E$) in a field containing zero photons both before and after the interaction, but the direction of the electron's momentum vector is changed, although its magnitude remains the same.

Needless to say, we have idealized the situation somewhat by

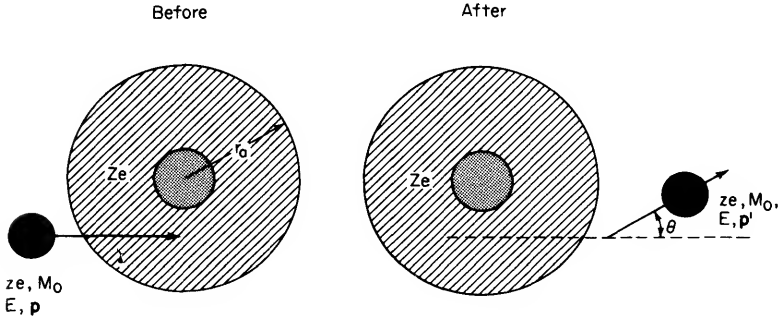

FIG. 2-5 Schematic representation of a nonradiative collision, resulting in elastic scattering.

associating each process with a different range of the *impact parameter/atomic radius* ratio. Thus, for example, bremsstrahlung may occur when the distance of important interaction is comparable with or even larger than the radius of the atom. The effects of *screening* of the nuclear charge by the outer electrons must then be taken into account in the theoretical calculations. Similarly, very close approaches to the nucleus invalidate the approximation that the nucleus is a point source of the field. Actually, very close impacts do not contribute significantly to the energy loss by bremsstrahlung.

Photons. We have delineated three modes of electromagnetic interaction of charged particles, related to the ratio of the distance of approach to the radius of the atom: (1) with the atom as a whole (excitation, ionization); (2) with a single essentially free electron (δ-ray emission); and (3) with the nucleus (bremsstrahlung). Similarly, there are three processes whereby photons interact through their electromagnetic fields, depending upon how their wavelengths compare with the dimensions of atoms and of electrons: (1) the photoelectric effect; (2) Compton scattering; and (3) pair production.

At low energies, corresponding to long wavelengths (remember that $W = h\nu = hc/\lambda$) the *photoelectric effect* predominates. As is seen in Fig. 2-6, this process is analogous to ionization in that the energy is transferred to the atom as a whole, except that the *entire* photon energy is imparted to a single electron. Since

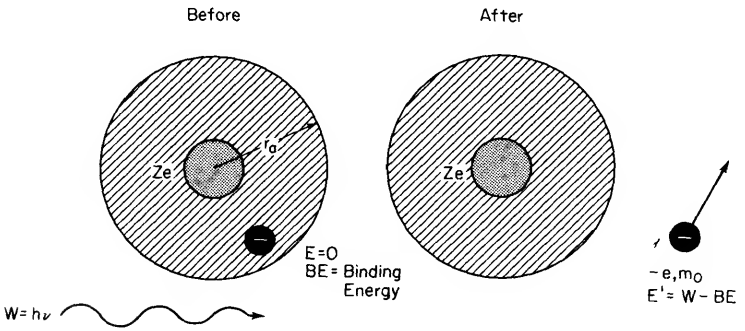

FIG. 2-6 Schematic representation of photoelectric emission.

this is a catastrophic collision, it turns out that the absorption law is of the exponential form, $I_x = I_0 \exp(-\beta_i x)$, first encountered as Eq. (1-1). This points up a fundamental difference between the behavior of particles which lose their entire energy in single acts and those that dissipate their energy gradually. In the latter case, the energy of the particle at any point determines, at least approximately, how far it will subsequently travel in a given absorber.

The electron may be freed from the atom if it receives an amount of energy exceeding its binding energy (ionization), or it may be excited into a bound state of higher energy (excitation) if the photon energy is less than the binding energy. Of course, in the latter case, the atomic quantum rules must be obeyed, which means that the photon energy must be exactly equal to the energy difference between the initial and final bound states.

As the photon energy is increased, the *Compton effect,* which has no classical counterpart, sets in. Here, as is shown in Fig. 2-7, a photon transfers some energy and momentum to an electron that initially is essentially free and at rest.

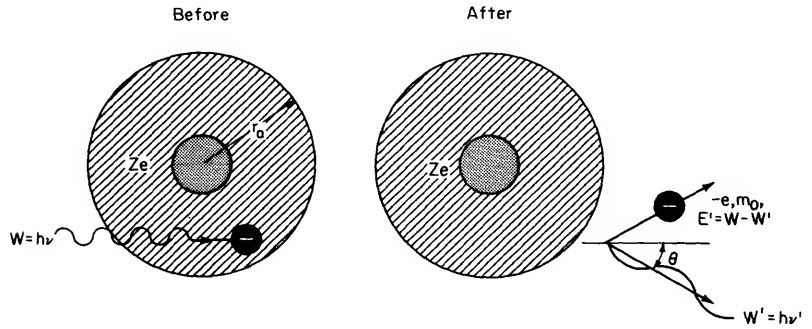

FIG. 2-7 Schematic representation of Compton scattering.

Again speaking formalistically, the Compton effect can be considered to be a transition from an initial state in which there is an electron with zero energy ($E = 0$) in a radiation field containing one photon of energy $W = h\nu$ to a final state in which the electron energy is E' and the radiative field contains one photon of energy $W' = h\nu' = W - E'$.

At still higher energies, when the γ-ray energy exceeds twice the electron rest energy ($2m_0c^2 = 1.02$ MeV), *pair production,* the conversion of a γ ray into a positive and negative electron, can occur. The energetics of this interaction are indicated in Fig. 2-8. Note that the nuclear recoil is required for momentum conservation!

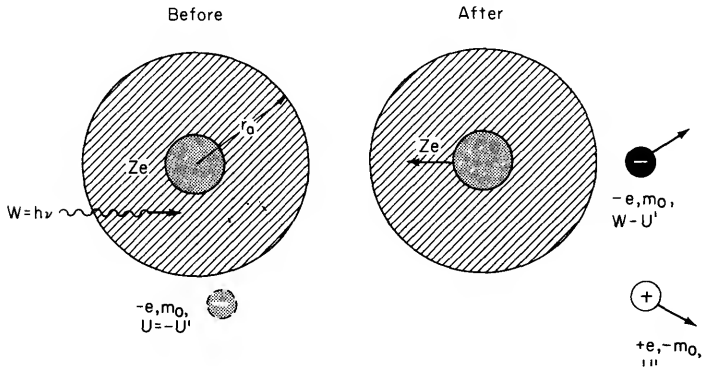

FIG. 2-8 Schematic representation of pair production.

This remarkable process in which matter materializes from electromagnetic radiation is a sort of photoelectric effect in the context of the Dirac theory, which envisages an "infinite sea" of electrons in negative energy states. One of these electrons, with total energy $-U_-$, is initially in the radiation field of the photon with energy $W = h\nu$. The final state after the interaction, as depicted in Fig. 2-9, finds this ejected electron in the normal world, with positive energy, $+ U_-$. But, in addition, the hole left in the continuum of negative energy states now acquires positive energy U_+ and a positive charge $-(-e) = +e$. This constitutes a positron with total energy $U_+ = W - U_-$, and kinetic energy $E_+ = W - (2m_0c^2 + E_-)$.

The inverse process may also occur, and its consequences can be envisioned by reversing the direction in Fig. 2-9. The electron makes a transition to the vacant negative energy state that corresponds to the positron, hence both particles disappear. Conservation of momentum requires that if a free electron and a

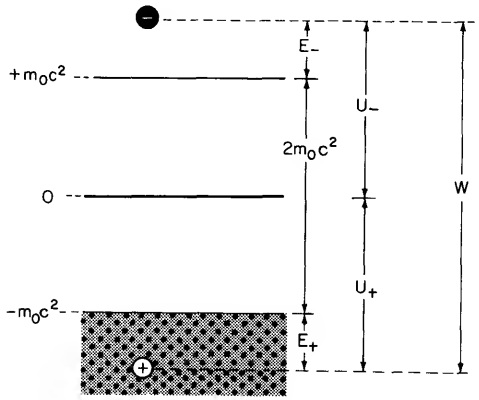

FIG. 2-9 Energy-level diagram illustrating the energetics of the pair-production process.

positron, both at rest, combine, two oppositely directed quanta, the *annihilation radiation,* each with energy corresponding to the electron rest energy ($m_0c^2 = 0.511$ MeV) must appear. If a nucleus participates, single quantum annihilation can occur.

Again, as in the discussion of charged particle interactions, we have simplified the picture by not mentioning such effects as the interaction of outgoing atomic electrons with the nuclear Coulomb field, the role played by electrons in different shells, and relativity considerations.

CHARGED PARTICLE ENERGY LOSSES

A great deal might be said about the development of our understanding of all of these processes, starting in 1904 with Bragg's experiments on the specific ionization of alpha particles, followed by the evolution of empirical absorption laws, the work of Rutherford on alpha-particle scattering, and the theoretical treatment of collision laws by J. J. Thomson and by N. Bohr. After deriving the classical relationships, we might then consider in detail the quantum mechanical treatment, pioneered by H. A. Bethe, H. J. Bhabha, F. Bloch, A. G. Carlson, A. H. Compton, W. Heitler, H. J. Massey, C. Møller, N. Mott, J. R. Oppenheimer, R. Serber, to cite a few who provided the structure upon which our

understanding of collision phenomena is based. But, for practical reasons, we must circumvent this formidable undertaking here. Fortunately, if we are willing, for the sake of expediency, to accept some formulas and graphs on faith, we can scrutinize them to extract their rich and comprehensible content.

Ionization and Excitation. The rate at which a particle loses energy by excitation and ionization, expressed in units of electron volts per gram per square centimeter, is

$$-(dE/dx)_{\text{ion}} = \frac{2}{\beta^2}\left[(N_A/A)(Z)(\pi r_0^2)\right] z^2 m_0c^2 \left[\ln \frac{(2m_0c^2\beta^2)^2}{\bar{I}^2(1-\beta^2)} - 2\beta^2\right], \tag{2-16}$$

where E = energy in electron volts,
x = thickness of absorber in gm/cm^2,
$\beta = v/c$; v = particle speed, c = speed of light,
N_A = Avogadro's number = 6.02×10^{-23} atoms per gram atom,
z = charge on incident particle in units of electronic charge,
m_0c^2 = electron rest energy = 0.511 MeV,
r_0 = classical electron radius = $e^2/m_0c^2 = 2.8 \times 10^{-13}$ cm, and,
$\bar{I}$ = mean ionization potential of the atoms of the absorber $\simeq 13.5Z$ (= 13.5 eV for Hydrogen).

The term $[(N_A/A)(Z)(\pi r_0^2)]$ is actually the area covered by electrons in 1 gm/cm^2 of the absorber. Note that the rate of loss of energy is independent of the mass of the incident particle, but depends on the *square* of its charge. Thus, the *specific energy loss* of an α particle is four times that of a proton traveling with the same velocity. When $v \ll c$, $(dE/dx)_{\text{ion}}$ varies inversely as v^2, because of the way the probability that a given interaction will occur depends upon the length of time that the interacting entities are sufficiently close for something to happen. The logarithmic term takes care of the Lorentz contraction as v approaches c.

The entire energy dependence of $(dE/dx)_{\text{ion}}$ appears in β, and the absolute value of the rate of energy loss depends only upon the atomic constants of the absorber, and the charge and velocity of the particle. Consequently, except for certain frills which

need not concern us here, the universal curve shown in Fig. 2-10 describes the energy loss by ionization and excitation for any type of singly-charged particle.

The $1/v^2$ dependence in the nonrelativistic region and the slow increase above the minimum are evident. The lowest point on the curve occurs at $\beta = 0.95$. This corresponds to a total energy U equal to three times the rest energy, or a kinetic energy $E = 2\ M_0c^2$. Particles having values of β near or above this value are *relativistic,* or *minimum ionizing.* Typical minimum values of $(dE/dx)_{\text{ion}}$ are 1.1 MeV/gm/cm² for lead and 1.8 MeV/

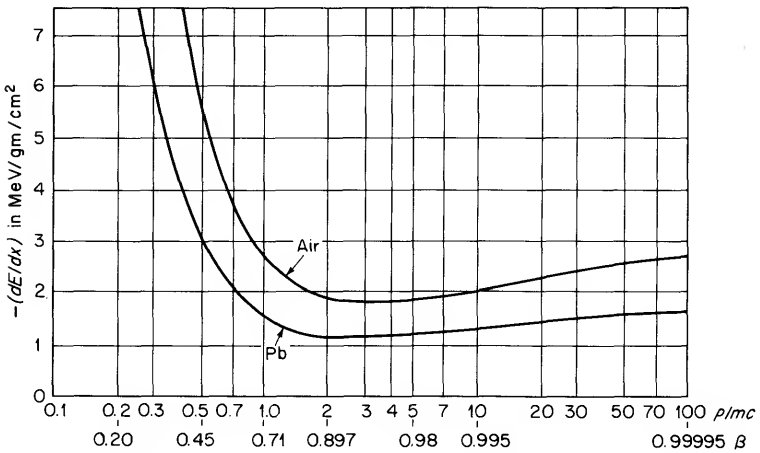

FIG. 2-10 Energy loss by ionization and atomic excitation as a function of velocity. The ordinates refer to singly charged particles. For multiply charged nuclei, the indicated values would be multiplied by Z^2.

gm/cm² for air. Denser materials extract energy less rapidly because the shielding effect of the constituent atoms limits distant interactions more than in a less dense medium.

The general form of the equation representing the *primary specific ionization* j_p, which is the average number of collisions per gram per square centimeter that result in the ejection of an electron from an atom, is roughly similar to Eq. (2-16) and Fig. 2-10. Specific ionization is sometimes expressed in *ion pairs per centimeter.* In hydrogen at STP, the minimum primary specific ionization is about 5 ion pairs/cm. An energy of about 30 eV is

expended in producing one ion pair. The *total specific ionization* j_t is the average ionization produced by the primary and all of its secondaries, tertiaries, etc. Equation (2-16) embodies this contribution to the energy loss.

If the energy loss process described by Eq. (2-16) predominates, that is if radiative collisions are negligible, it is possible to predict the amount of matter that a particle with energy E will penetrate. This is called the *range* R. Let us rewrite Eq. (2-16) in its simplest form:

$$-dE/dx = f(E). \tag{2-17}$$

The range-energy relationship can now easily be determined by integration:

$$-\int_E^0 dE/f(E) = \int_0^R dx = R. \tag{2-18}$$

Referring back to Fig. 2-10, it is clear that, when the particle is slowed down to sub-relativistic velocity below the ionization minimum, the rate of energy loss increases very rapidly, and the particle will be stopped in a very short distance. But for relativistic particles, as we have already noted, $f(E)$ is almost constant. Hence, in this case, Eq. (2-18) tells us that the range is proportional to the energy. Figure 2-11 shows a typical range

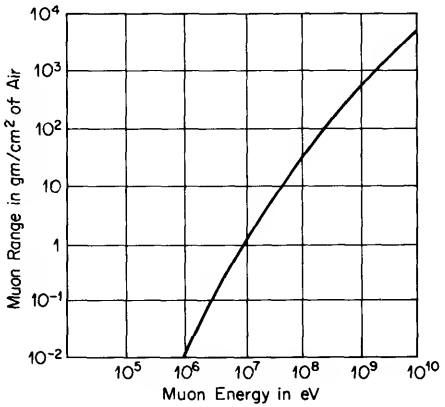

FIG. 2-11 Dependence of range upon energy for μ mesons in air. Note that the slope of the curve is very nearly unity at the upper end.

vs energy curve. Of course, it must be remembered that the computed range is the *total* amount of absorber, no matter how tortuous the route through it, hence, for particles subject to appreciable scattering, the linear absorber thickness that can be traversed may be less than the theoretical range.

The term *straggling* refers to the spread about the average energy loss that arises from statistical fluctuations in the individual processes.

Bremsstrahlung. Radiative collisions involve a still more complicated combination of various probabilities that are subject to extreme fluctuations. These preclude the association of a prescribed range with a given particle. For high energy electrons, the equation for the bremsstrahlung energy loss process is

$$-(dE/dx)_{\text{rad}} = 4\alpha(N_A/A)(Z)(Z+1)(r_0^2)[\ln(183Z^{-\frac{1}{3}})]E, \quad (2\text{-}19)$$

where $\alpha = e^2/\hbar c = 1/137$ is the fine structure constant, and the other symbols are the same as in Eq. (2-16).

We see that the radiation loss varies as the *square* of the atomic number of the absorber, so differences among materials far exceed those in the case of ionization, which varies as Z. Furthermore, there is a strong energy dependence, since $-(dE/dx)_{\text{rad}}$ is proportional to E.

An important feature of the radiation process is not revealed by Eq. (2-19), which holds exclusively for electrons. In contrast with ionization, radiation varies inversely as the *square* of the mass of the incident particle. This happens because a heavier mass experiences a smaller acceleration under otherwise identical conditions. This has important consequences. For example, a proton with a given kinetic energy, expressed in units of its own rest energy, would suffer an energy loss by radiation amounting to only $(1/1836)^2 \simeq$ one three millionths that of a comparable electron! Hence, for the most part, we need consider radiation losses only when we are dealing with electrons. Figure 2-12 shows the rate at which electrons passing through different materials lose energy by radiation, as compared with ionization and excitation.

We can simplify matters by combining the constants in front of E in Eq. (2-19) into a single constant, as follows:

$$1/X_0 = 4\alpha(N_A/A)(Z)(Z+1)(r_0^2)[\ln(183Z^{-\frac{1}{3}})]. \quad (2\text{-}20)$$

If you can persevere through a dimensional analysis of this equation you will find that X_0 has the dimensions of a "length" in gm/cm^2. This quantity, called the *radiation length,* is a characteristic of the medium. The descriptions of radiation phenomena are essentially independent of atomic number when absorber thicknesses are measured in this unit. Typical values of X_0 (and

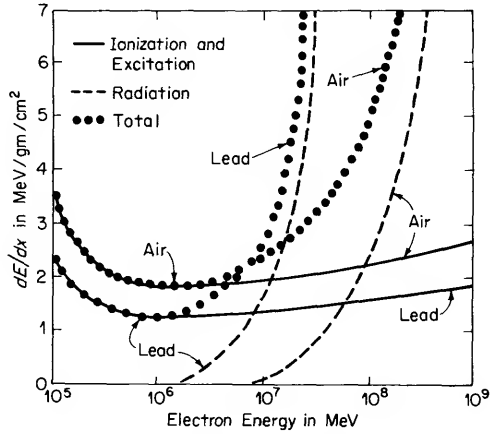

FIG. 2-12 Energy dependence of the rate of energy loss by (1) atomic excitation and ionization, and (2) radiation, for electrons in lead and in air at STP. The sum is also plotted.

some related parameters that we shall define shortly) are listed in Table 2-1. Its physical significance becomes apparent when we look at the simple relationship that results from combining Eqs. (2-19) and (2-20):

$$-(dE/dx)_{\text{rad}} = E/X_0. \quad (2\text{-}21)$$

Suppose the energy of a particle before entering an absorber with radiation length X_0 is E_0. Then, on the average, after penetrating a distance x, its energy, determined by integrating Eq. (2-21), is

$$E_x = E_0 \exp(-x/X_0). \quad (2\text{-}22)$$

So, we see that X_0 is the distance, in gm/cm^2, over which the energy falls to $(1/e)$th (0.368) of the original value. Sometimes,

TABLE 2-1. *Typical Values of Parameters in Radiation Processes.*

	Atomic Number	Atomic Weight	Radiation Length		Shower Unit		Critical Energy	
Substance	Z	A	X_0(gm/cm^2)	X_0(cm)	$l = X_0 \ln 2$(gm/cm^2)	$l = X_0 \ln 2$(cm)	E_c(MeV)	ϵ_c(MeV)
Hydrogen	1	1	138	15×10^5	95.7	10×10^5	940	815
Nitrogen	7	14	45	0.36×10^5	31.2	0.25×10^5	120	103
Aluminum	13	27	26.3	9.69	18.2	6.71	60	52
Lead	82	207.2	5.9	0.517	4.09	0.358	10	7.0

the term *shower unit* $l = (\ln 2)X_0 = 0.693X_0$ is used in referring to the distance in which a fast electron loses half its initial energy (similar to the half-life in radioactive decay).

Another parameter that serves to characterize the effectiveness of a given material as a radiator is the *critical energy*. Unfortunately, this term has two different connotations that, fortunately, are almost equivalent quantitatively: (1) ϵ_c is the energy that a given type of particle would lose by ionization alone, in traversing a thickness of one radiation length, i.e. $\epsilon_c = -\int_{X_0}^{0} (dE/dx)_{\text{ion}}\, dx$; (2) alternatively E_c is the energy at which the rate of energy loss by ionization is equal to the rate of energy loss by radiation, i.e. $(dE_c/dx)_{\text{ion}} = (dE_c/dx)_{\text{rad}}$. It turns out, as Table 2-1 shows, that ϵ_c is slightly less than E_c. Roughly speaking $E_c \simeq 800$ MeV$/Z$ and $\epsilon_c \simeq 700$ MeV$/Z$.

Elastic Scattering. The net angle of scattering of a beam of particles is the statistical sum of many small deflections, in accordance with the Gaussian distribution law. For particles with charge z, momentum p, and velocity v, the mean-square projected scattering angle $\langle\theta^2\rangle$ is approximately given by

$$\langle\theta\rangle^2 = \frac{z^2 E_s^2}{(pv)^2}\frac{x}{X_0}, \tag{2-23}$$

where E_s is a constant ($= 21$ MeV) independent of the mass of the particle and of the nature of the medium.

Thus, the root-mean-square *multiple scattering* angle is proportional to the charge of the particle. It decreases rapidly as the speed v increases, and increases as the square root of the total thickness x traversed, but varies inversely as the square root of the radiation length X_0.

Čerenkov Radiation. For the sake of completeness, we call attention here to another electromagnetic effect that occurs under certain circumstances when a charged particle passes through matter. If the particle speed v exceeds the speed of light in the medium c_m, radiation is emitted in analogy with the bow-wave of a ship, or the shock wave of a projectile moving at supersonic velocity. This *Čerenkov radiation* arises from constructive inter-

ference of electromagnetic waves that are emitted when atoms distorted by the passage of the particle return to their normal positions. How this intriguing and useful effect comes about is illustrated in Fig. 2-13. The light is emitted in a characteristic cone, of angle θ, according to the relationship:

$$\cos\theta = \frac{c_m}{v} = \frac{1}{n\beta}, \tag{2-24}$$

where $n = c/c_m$ is the index of refraction of the medium, and $\beta = v/c$.

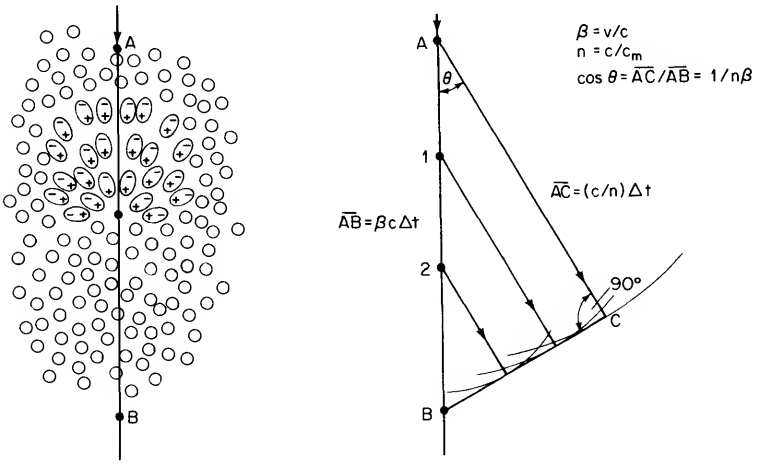

FIG. 2-13 Polarization of a transparent medium by the passage of a charged particle. Wavelets are radiated by the dipole field set up by the moving particle as it distorts the atoms while passing them. Since its speed v exceeds the speed of light in the medium c_m, the particle travels from A to B in the same time that the coherent wave fronts, emitted as it passes the indicated points, reach the line BC. If v is less than c_m, the wavelets radiated from points along the track are not in phase, and hence they interfere destructively.

It must be emphasized that Čerenkov radiation (which is not significant quantitatively as an energy-loss mechanism, amounting to about a thousandth of the ionization-excitation rate) differs from bremsstrahlung in that it involves cooperation among many atoms, rather than a collision with a single atom.

PHOTON ABSORPTION

We have already noted that some γ-ray absorption processes involve the complete elimination of photons in discrete acts. Thus, we cannot talk about either a rate of energy loss, or a range that depends upon energy. We can only determine the attenuation of a beam of photons by calculating the cross section (hence the absorption coefficient) for each process.

Photoelectric Effect. The following equation exemplifies the type of relationship that is derived from theoretical analysis of the process of γ-ray induced photoelectric emission:

$$\sigma_K = 6\pi r_0^2 \alpha^4 Z^5 (m_0c^2/h\nu). \tag{2-25}$$

This gives the cross section σ_K for the ejection of K-shell electrons by very high energy γ rays ($h\nu \gg m_0c^2$).

The cross section for the photoelectric effect is significant only at low energies, such as below 50 keV for aluminum and 500 keV for lead.

Compton Scattering. Although we will not derive the basic Compton effect equations here, we note that the Compton electron never makes an angle of more than 90° from the direction of the incident photon. At grazing incidence, the energy of the electron is zero. If ν_0 represents the frequency of the photon before the interaction, the minimum frequency after scattering is

$$\nu_{\min} = \frac{\nu_0}{1 + 2h\nu_0/m_0c^2}. \tag{2-26}$$

When $h\nu_0 \gg m_0c^2$, the maximum kinetic energy $T_{\max}$ that can be transferred to the directly forward moving electron is

$$T_{\max} = h(\nu_0 - \nu_{\min}) = h\nu_0 \frac{2h\nu_0/m_0c^2}{1 + 2h\nu_0/m_0c^2}. \tag{2-27}$$

In this case, the γ ray is scattered directly back through 180°, with an energy $\simeq \frac{1}{2}\, m_0c^2$.

The cross section for Compton scattering σ_{comp} when $h\nu \gg m_0c^2$ is

$$\sigma_{\text{comp}} = (N_A/A)(Z)(\pi r_0^2)[\ln (2h\nu/m_0c^2) + \tfrac{1}{2}](m_0c^2/h\nu). \tag{2-28}$$

Pair Production. The theoretical treatment of the creation of positron-electron pairs is rather involved. However, the calculations are closely related to the theory of bremsstrahlung, since the processes are essentially inverse. The total cross section for pair production (for a particular set of conditions, i.e. $h\nu \gg m_0c^2$ and neglecting *screening* of the nucleus by outer electrons) is

$$\sigma_{\text{pair}} = Z^2\alpha r_0^2(28/9)[\ln(2h\nu/m_0c^2) - 218/27]. \qquad (2\text{-}29)$$

Compton scattering and pair production predominate in the energy range of γ rays that contribute appreciably to cosmic ray phenomena. The way in which their relative contributions to

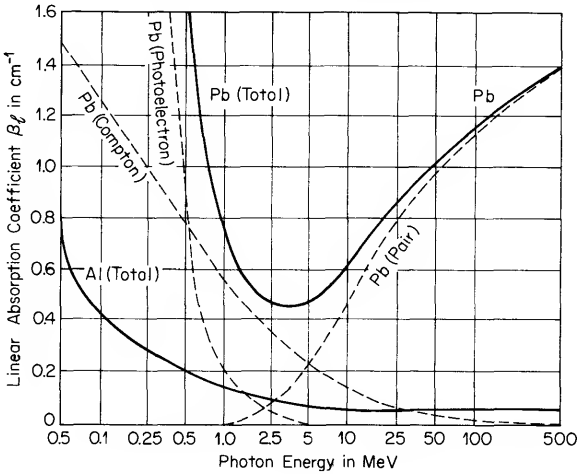

FIG. 2-14 Energy dependence of γ-ray absorption in aluminum and lead, and the separate contributions of photoelectron production, Compton scattering and pair production in lead.

the absorption of γ rays depend upon energy is shown in Fig. 2-14. The total absorption cross section is the sum of the individual ones:

$$\sigma_T = \sigma_{\text{photo}} + \sigma_{\text{comp}} + \sigma_{\text{pair}}.$$

In summary, we note that Eqs. (2-25), (2-28) and (2-29), and Fig. 2-14, reveal the following: (1) at very low energies, where the photoelectric effect predominates, σ_T varies roughly as Z^5, (2)

in the intermediate region (0.05 MeV $< h\nu <$ 16 MeV for Al, 0.5 MeV $< h\nu <$ 5 MeV for Pb), where the Compton effect is most important, it varies as Z; and (3) at higher energies at which pair production takes over, there is a Z^2 dependence.

NUCLEAR INTERACTIONS

Two generations of nuclear physicists have been striving mightily to attain a single objective that can be stated quite simply—understanding nuclear forces.* Thus, it would be both presumptuous and impractical to discuss this subject here in other than quite general terms.

One could digress into a philosophical discourse about what we mean by "understanding," but, suffice it to say that in the present context we are referring to a conceptual framework that would lead to as satisfying and relatively complete treatment of interactions on the nuclear scale as has been carried out on the atomic scale.

A number of nuclear models that appear to fit one or another group of experimental data have appeared over the years. Pictorial nomenclature such as the *liquid drop model,* the *shell model,* the *optical model,* and so on designated different ways of thinking about nuclei through analogies that are susceptible to calculations which can be compared with experimental results. Innumerable theories envisaging different types of fields have been proposed to describe the forces between *nucleons* (proton-proton, neutron-neutron, neutron-proton). In many cases, starting with Yukawa's theory that presaged the π meson, these have predicted new fundamental phenomena. Brilliant analyses based on imaginative, exciting, and challenging new concepts are revolutionizing thinking about this subject.

Fortunately, by following a heuristic approach, we can pursue the cosmic-ray problem without delving into the details of the mechanisms of nuclear interactions.

Nuclear interactions fall into two categories: *weak* and *strong.*

* See MOMENTUM Book No. 8, *Structure of Atomic Nuclei,* by C. S. Cook, Van Nostrand, Princeton (1964).

Table A-1 (Appendix) indicates how the various cosmic ray components behave in this respect.

The topography of the simplest nucleus containing more than one nucleon is mapped in Fig. 2-15. When a strongly-interacting particle collides with a nucleus, that is, when it approaches sufficiently close to experience the nuclear forces, it may become thoroughly integrated, and thus heat up the nucleus as a whole (*nucleon-nucleus collision*). The compound nucleus survives for times of the order of $10^{-16} - 10^{-20}$ second, long compared with

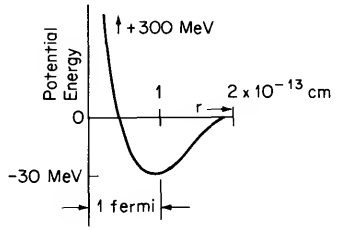

FIG. 2-15 The potential energy of two nucleons at a distance *r* between centers.

the transit time of a nucleon across the nucleus ($\simeq 10^{-22}$ sec). Then fragments—mainly neutrons, protons, or alpha particles—are boiled off, cooling the nucleus down to its normal state. On the other hand, a nucleon may interact much more rapidly ($< 10^{-22}$ sec) with discrete nucleons in passing through the "nuclear matter" creating new particles, or it may pass near the edge in a *stripping* or a *pickup reaction*. The *multiplicity* of a particular interaction specifies the number of particles of a given type that emerge as a consequence of the collision. The interaction of a nucleon with a target nucleus can result in:

1) Evaporation neutrons and protons;
2) Secondary particles, principally pions;
3) Nuclear breakup by:
   a) *spallation* or *fragmentation,* in which nucleons or groups of nucleons, emerge.
   b) *fission,* in which the nucleus divides into two (or more) nearly equal masses.

In addition to inelastic scattering of strongly interacting particles, nuclear forces can give rise to elastic scattering, as, for example, when neutrons collide with protons in billiard-ball fashion.

3 *Experimental Methods*

Did I see it go by,
That Millikan mote?
Well, I said that I did.
I made a good try.
ROBERT FROST

The tools of the trade fall into two general categories—*electrical* and *visual*. The cosmic ray physicist may utilize some type of sensor that, by means of an associated measuring system, responds to one or more characteristics of the radiation flux to which he exposes it. In this case, he may observe an average characteristic by measuring a current, or he may resolve the signals from individual particles, and count pulses. Alternatively, he may employ some method of obtaining pictures of the tracks produced by cosmic rays as they pass through matter, leaving their characteristic signatures. In some cases, both techniques are used in combination.

All detectors have one factor in common—ionization is the *sine qua non* in their operation. However, all the other interactions described in Chapter 2 may be invoked, as appropriate, to serve as handles for identifying particles and determining their properties. The following descriptions of sensors and detecting systems employed in cosmic ray research will be confined to the underlying principles that are relevant for understanding how it is possible to unravel the wide-ranging characteristics of the different components of cosmic radiation. It is unnecessary for us to be concerned here with technological details or with the ancillary circuitry.*

* See, for example, MOMENTUM Book No. 10, *Radioactivity and Its Measurement*, by W. B. Mann and S. B. Garfinkel, Van Nostrand, Princeton (1966).

ELECTRICAL DETECTORS

Included in this family are two genera. The first comprises all species in which an electric field is maintained across boundary electrodes, and the effects of ionization produced by charged particles (which may be secondaries of the particles of interest, as with neutrons is observed. The second includes devices in which light emitted as a result of the passage of cosmic radiation through certain substances is detected by a photosensitive tube.

Ionization Chambers. The classical instrument in cosmic ray research, and the simplest to comprehend, is the ionization chamber. One might have expected that it would have faded into obsolescence long before the passage of more than three-score years. Nevertheless, as we shall see later, important discoveries are still being made with the help of this classical cosmic-ray detector.

Basically, an ionization chamber consists of a gas-filled vessel containing a *cathode* and an *anode* between which a difference of potential is maintained. The current representing the rate of collection of ions produced in the gas by ionizing radiation is measured. The geometrical configuration depends upon the application. The arrangement sketched in Fig. 3-1 and the corre-

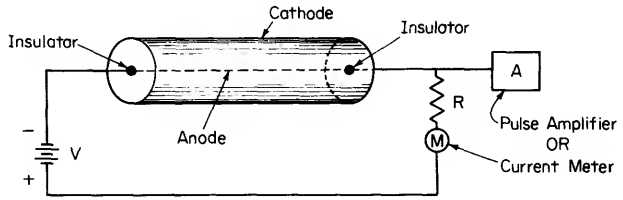

FIG. 3-1 Basic elements of an ionization chamber, a proportional counter, and a Geiger-Mueller counter.

sponding pulse height *vs* applied voltage plot in Fig. 3-2 provide a convenient basis for explaining the action of the three species of the first genus of the electronic detector family.

The central wire or anode is insulated from the cylindrical cathode, and the current is a direct measure of the radiation flux through the chamber. With a constant flux, the ion current rises

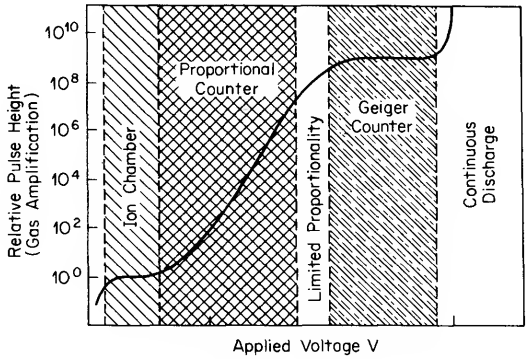

FIG. 3-2 Gas amplification as a function of applied voltage. The abscissa scale and the exact form of the curve depend upon the nature of the gas filling, its pressure, and the dimensions and configuration of the electrodes.

as the voltage V is raised. This is because the tendency of + and − charges to recombine is reduced as their velocity increases with the electric field strength. Finally, when the difference of potential becomes sufficiently high to insure that all of the charges reach the electrodes, *saturation* sets in, and the *plateau* is reached.

We mentioned earlier that the particles can be counted by observing their individual pulses. An ionization chamber utilized in this manner is operated in the *electron collection* mode, to attain shorter time resolution than that associated with the much heavier and therefore slower-moving positive ions. We will refer to the ionization produced by a single particle as its *pulse height*. Thus, in Fig. 3-2, the pulse height on the plateau represents *all* of the energy deposited in the chamber by the particle. As we saw earlier [cf. Eq. (2-16)] the minimum ionization produced by an alpha particle is four times that of a proton. Hence these particles are easily distinguishable through their pulse heights.

Proportional Counters. By increasing the voltage beyond the ionization plateau, the electrons released in the primary ionization process may themselves gain sufficient energy between collisions to ionize the gas molecules, and these in turn produce further ionization, and so on in an *avalanche* process. This *gas amplification* results in an enhanced pulse that is strictly *proportional* to the primary ionization. The multiplication factor is a

function of the difference in potential. The gas amplification of the proportional counter reduces the external circuit requirements as compared with a pulse ionization chamber, although even in this case a high-gain amplifier is required.

An especially important version of proportional counter contains boron trifluoride, BF_3, enriched with the isotope B^{10} as the filling gas. A resonant exothermic nuclear reaction occurs when slow neutrons collide with this boron isotope, which contains 5 neutrons and 5 protons. Thus,

$$_5B^{10} + {}_0n^1 \rightarrow ({}_3Li^7 + 0.9 \text{ MeV}) + ({}_2He^4 + 1.6 \text{ MeV}). \quad (3\text{-}1)$$

The pulses produced by these reaction products, which have a short range in the gas and hence deposit all of their energy as ions, are enormous compared with those from ambient radiations. Neutron-produced pulses can therefore be selected by a *pulse-height discriminator.*

Geiger-Mueller Counters. The application of a still higher voltage pushes the self-limiting avalanche action in the region of *limited proportionality* (where the gas amplification still depends somewhat upon the number of ions produced in the original act) beyond the pale into an explosive response. Instead of remaining localized, the discharge now spreads rapidly along the entire length of the counter, owing to the copious emission of ionizing photons from the highly excited constituents of the gas. Without pursuing the details of the discharge processes that ensue, suffice it to say that only a single ion pair is sufficient to initiate the action. It is as though the voltage across the electrodes were just below the point of spontaneous electrical breakdown. The tiniest spark suffices to trigger off the entire discharge, the extent of which is unrelated to the igniting source. Thus, the *Geiger-Mueller counter* affords no inherent means for distinguishing the properties of the radiations to which it responds. However, the height of Geiger-Mueller counter pulses is uniform and enormous, thereby considerably simplifying the associated electronic equipment.

There are two types of Geiger-Mueller counters. In one, the discharge is *quenched* by external action, essentially by reducing the applied voltage. *Self-quenching* counters contain an admix-

ture of gases or vapors that absorb photons and inhibit processes whereby secondary electrons emitted from the cathode would sustain the discharge in the absence of the quenching mechanism.

Geiger counters were important historically because of their adaptability to being incorporated into systems. To cite only one example, directional resolution can be attained, as we shall show later, by combining Geiger-Mueller tubes into a *coincidence telescope.*

Solid State Detectors. We have already noted that ionization produced in solid materials by incident particles can be measured, hence the useful features of the ionization chamber, notably its linear relation between output signal and energy deposited, need not be limited to gas-filled vessels. Thus, recent advances in solid state technology are creating a new generation of detectors that are significantly extending our capabilities for studying cosmic rays. Aside from purely practical and technical considerations, the principal advantage of solid state detectors resides in the remarkable resolution that can be attained. As the experiments become more and more sophisticated, the importance of examining the fine structure grows increasingly evident. Thus, higher resolution in measurements of the spatial, temporal, energy, and charge distributions of cosmic rays is incessantly being sought to provide answers to old questions as well as to new ones that are continually being generated.

Because solids are so much more dense than gases, semiconductor detectors may be designed to stop certain particles completely, and thereby to measure their entire energy E. On the other hand, they can be made into very thin slabs, that have little effect on E, for determining the rate of energy loss $-dE/dx$. The utility of these features will become more evident later when we discuss detector systems.

A wide variety of semiconductor counters have become available. *Bulk conduction counters* consist essentially of a homogenous material, such as silicon or germanium, appropriately *doped* with impurity centers. *Rectifying junction* counters are the most widely used. These operate by virtue of the properties of the p-n junction. In the forward direction of the rectifier, electrons are driven by an applied field from the n-type material

(carriers normally negative electrons) to the p-type (carriers normally positive holes) and holes from the p-type into the n-type. But in the reverse biased condition, in which the n-type region is held at a positive potential, free charges are removed from the interface of the junction and the surrounding regions.

Actually, there is a built-in voltage even without the application of the external field. This arises from the diffusion of each type of carrier into the other region, leaving excess positively-charged *donors* in the n-type region and negatively-charged *acceptors* in the p-type region. These constitute a charged double layer, which sweeps the carriers from a thin layer at the interface. This carrier-free region, or *depletion layer,* is essentially an intrinsic semiconductor, and electron-hole pairs produced by an ionizing particle that traverses it constitute a detectable current. Its thickness can be increased by applying an external voltage that assists the built-in voltage.

Two general types of p-n detectors are prepared by a variety of processes—*diffused junction* and *surface barrier.* In the former, made with either an n-type or p-type material, a donor or acceptor impurity is introduced to form a depletion layer at the diffusion depth. The latter is made by forming a p-type layer on the surface of n-type material by oxidation, or by creating an evaporated metal-semiconductor interface.

The principal cosmic-ray application of solid state detectors is in studies of the primaries. Detailed information about the magnitude of the primary flux as a function of charge, mass, and energy with hitherto unattainable resolution is being obtained in experiments carried out in space. The observations are now being extended down to lower energies than were accessible heretofore. Because of the nature of the construction of semiconductor detectors, they are amenable to reducing the instrumental threshold for detection far below the limits imposed by the wall thickness of other types of radiation sensor.

Scintillation Counters. The oldest method for detecting individual charged particles was to observe visually the tiny flashes of light that are emitted when small crystals of certain substances, such as zinc sulfide, coated on a screen are subjected to bombardment by radiation. A device utilizing this principle was called

a *spinthariscope*. Tremendous advances in the development of exceedingly sensitive *photomultipliers* that can detect extremely low-level light pulses, coupled with rapid progress in producing scintillators having appropriate characteristics, led to the widespread adoption of this technique in modern cosmic ray research. The basic principle of operation of a scintillation counter is shown in Fig. 3-3.

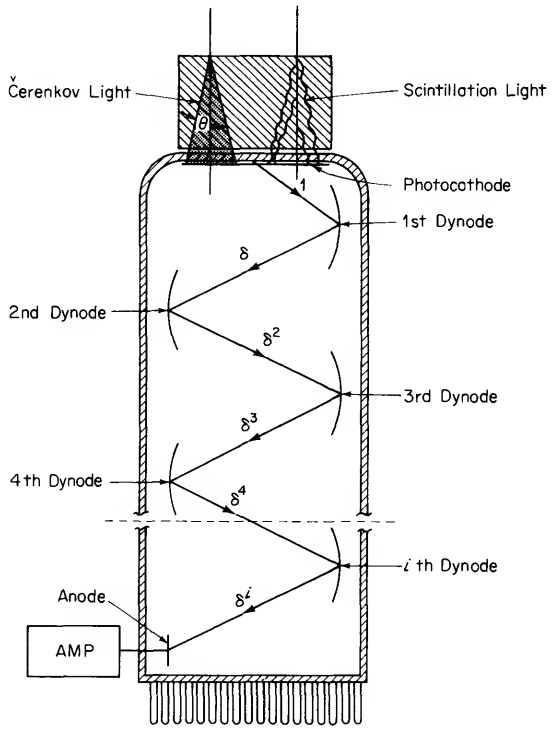

FIG. 3-3 Schematic arrangement of a scintillation counter and of a Čerenkov detector. A typical photomultiplier may have 10 stages ($i = 10$) each with a gain $\delta = 4$, providing an overall amplification of 10^6.

Fluorescent radiation is produced when electrons return to their original lower energy state from which they are excited by a passing charged particle. In some cases, the transition to an intermediate, or *metastable,* state occurs first, causing the emission

to be delayed until the electron is raised back to the excited state by a gain in thermal energy, and then returns to the lower level (*phosphorescence*). This process is inimical to attaining the desired rapid response.

Inorganic and organic phosphors, in solid or liquid form, are employed as scintillators. In some cases, *activators* are added to provide *luminescent centers* having the property that energy of excitation is released as radiation rather than as mechanical interactions. In other cases, these centers occur naturally.

Just as with solid state detectors, scintillation counters can be used for measuring total energy deposited E, or rate of energy loss $-dE/dx$.

Scintillation counters are vastly superior to Geiger-Mueller counters when the detector areas are large. Although trays of Geiger-Mueller counters can accomplish the same purpose, the possibility of producing large plastic slabs of luminescent material has proved to be a great boon to a variety of cosmic-ray experiments on the surface of the earth and underneath. On the other hand, the adaptability of scintillators to small dimensions is a valuable asset in conducting measurements at high altitudes.

Čerenkov Counters. We have already had occasion to introduce the principle upon which operation of this intriguing device is based [see Fig. 2-13 and Eq. (2-24)]. The geometrical arrangement of a *Čerenkov detector* may be quite similar to a scintillation counter setup, hence Fig. 3-3 serves to illustrate the basic elements. In this case, however, the light output corresponding to the same energy loss is very much lower. But this disadvantage is far outweighed by the unique directional and threshold properties of Čerenkov counters. For Eq. (2-24) says that the radiation is emitted in a cone determined by the direction of motion of the particle that induces it. Thus we can easily establish, for example, whether particles are traveling up or down, a matter of considerable importance in carrying out cosmic ray measurements within the atmosphere. Furthermore, Eq. (2-24) tells us that no radiation is emitted if the particle velocity is lower than $\beta_{\min} = 1/n$.

The Čerenkov light output varies as the square of the charge of the particle, just as in the case of ionization. Čerenkov counters

in solid, liquid and gaseous forms are utilized in cosmic ray experiments, and the parallel with the advantages of scintillation detectors is striking.

VISUAL DETECTORS

This family also comprises two genera. The species of one are various devices in which the incident radiation produces visible transitory effects that are photographed for later study. The species of the other are different types of media that incur permanent effects as a result of bombardment. These effects can be seen visually, and can be analyzed to obtain information about the radiation that produced them.

Cloud Chambers. When a gas containing a saturated vapor is suddenly expanded, a state of supersaturation results. This happens because the cooler gas after the expansion cannot normally hold as much vapor as it did when it was warmer. In the case of the earth's atmosphere, the ensuing condensation of supersaturated water vapor on dust particles creates droplets that we recognize as fog. For almost a half century, this principle has been the basis for a most fruitful method for studying cosmic rays by observing their tracks.

As is shown in Fig. 3-4, a dust-free chamber containing a gas and a saturated vapor is expanded adiabatically (without loss or gain of heat), for example by the rapid motion of a diaphragm, to produce supersaturation. Ions created by the passage of charged particles then serve as condensation centers upon which the droplets form. These grow sufficiently large so that, under suitable illumination, they can be photographed.

The specific ionization can be determined by counting the droplets, and interactions in the gas can be studied. In fact, all of the processes enumerated in Chapter 2 (except Čerenkov radiation) can be observed, and the characteristics of the particles determined therefrom. Various absorbers can be inserted in the chamber to reveal the energy losses and ranges of particles, as well as the emergence into the gas of secondaries that they produce in traversing solid materials. Stereoscopic views, obtained by taking two photographs simultaneously from different angles,

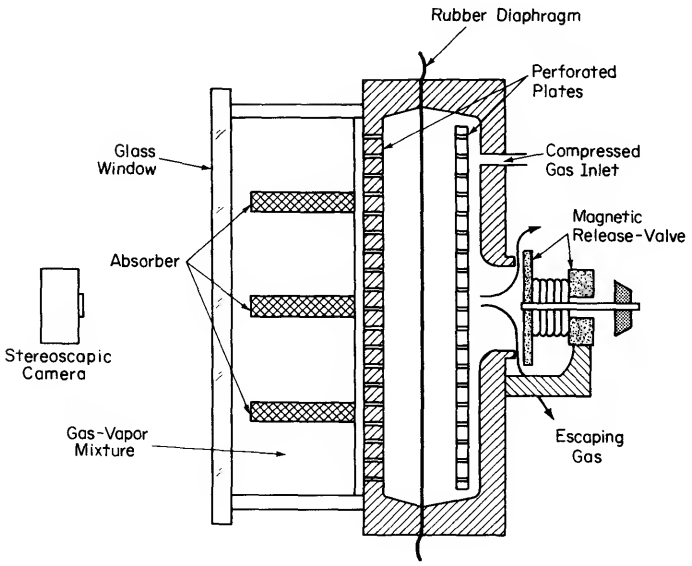

FIG. 3-4 Basic elements of a Wilson cloud chamber. Light sources and GM counters for controlling the expansion are not shown. A magnetic field directed perpendicular to the glass window may be applied for momentum measurements.

provide three-dimensionality. A magnetic field may be applied to deflect the particles, in order to determine charge and momentum.

Finally, and most important, is the advantage that the expansion may be triggered by any of the arsenal of electrical detectors placed inside or outside. Some typical cloud chamber photographs are shown in Plates II and III.

The Wilson cloud chamber is not continuously sensitive, and there is a dead time between expansions in order to allow equilibrium to become reestablished. The *counter-controlled* chamber assures that photographs of the events of interest are obtained, whereas *random expansion* leaves the selection to chance.

A variant of the expansion chamber is the *diffusion cloud chamber,* in which supersaturation is attained by allowing gas containing the saturated vapor to fall under gravity from a warmer to a cooler region. Maintaining a thermal gradient between the top and bottom of the vessel creates a sensitive region

in which conditions are just right for the condensation of vapor on ions. Since this region is shallow, this type of cloud chamber must be operated horizontally. Consequently, although ideal in accelerator experiments for many reasons, including its continuous sensitivity, the diffusion chamber is not used in cosmic ray studies.

Similarly, the *bubble chamber* embodies tremendous advantages in laboratory high-energy physics experiments because of its unique ability to compress a great amount of matter into the visible volume. This device is essentially the inverse of the cloud chamber. In this case gas bubbles form on ions in a liquid when the liquid becomes superheated. To accomplish this, a suitable liquid is heated above its normal boiling point, and pressure exceeding the saturation vapor pressure is applied to maintain it in the liquid phase. Rapid reduction of the pressure, by some means similar to that used for a Wilson cloud chamber, superheats the liquid. Boiling occurs only at the points where there are ions, and the tracks of the bubbles grow to visible size and are photographed.

Spark Chambers. Although the diffusion and bubble chambers did not succeed their parent, the Wilson cloud chamber, in cosmic ray studies, the youngest of the chamber clan has made a very substantial impact because it seems to combine the best of both worlds. It incorporates excellent resolution both in time and space while still retaining visual capabilities, hence it can serve essentially as an electrical counter and a visual detector at the same time.

The *spark chamber* comprises a stack of parallel plates contained in a vessel filled with an atmosphere of a noble gas. Upon signal from controlling counters, a high voltage is very rapidly applied to alternate plates. Electron avalanches quickly start wherever there are ions produced in the gas by any charged particles that were present during the sensitive time. The ensuing bright sparks are photographed.

An ingenious method for handling spark-chamber data in cosmic-ray experiments makes use of the noise produced by the sparks. From measurements of the time for the sound emanating from the spark between each pair of plates to reach suitably

placed tiny microphones, the coordinates of the spark can be specified. Thus, thanks to this true audio-visual aid, the trajectory through the *sonic spark chamber* can easily be reconstructed and the analysis carried out electronically, even in an unmanned balloon flight. Digitized systems, in which a large number of individual spark or glow discharge modules are juxtaposed to define a three-dimensional grid, are also utilized.

Photographic Emulsions. Although the use of photographic emulsions to detect ionizing radiations dates back to the discovery of radioactivity, the renaissance of this technique in its modern form took place only a little more than two decades ago. Then, the range of usefulness was vastly expanded by the introduction of emulsions having sufficient sensitivity to record *any* individual cosmic ray, rather than just heavily ionizing radiations.

A *nuclear emulsion* consists of a high concentration of silver halide crystals embedded in a matrix of gelatin. When a charged particle penetrates this medium, it activates many of the AgBr crystals along its path, just as photons render the grains developable in ordinary photography. These are converted to Ag grains during subsequent processing to form a track that can be studied under a microscope (*cf.* Plate X).

The most sensitive nuclear emulsions respond even to singly charged minimum-ionizing particles. The combination of continuous sensitivity, very high stopping power, and high angular resolution, together with important gains of a practical nature, make them especially suitable for many types of observation, especially at high altitudes. *Stripped emulsions,* or *pellicules,* of thicknesses up to several millimeters are available and, by piling a number of these layers together, *emulsion stacks,* with sensitive volumes up to several liters, have been constructed.

Here again, all of the knowledge about particle interactions summarized in Chapter 2 is brought to bear to interpret the emulsion tracks. From measurements of a number of different track parameters that are related to independent collision processes, all of the characteristics of the particles that produced them can be unraveled.

One shortcoming in some experiments is the absence of a time

scale during exposure. But even this disadvantage has been overcome by moving one emulsion with respect to another at a known speed, and relating the time when a given track was registered to the difference in its coordinates in the two emulsions.

Dielectric Solids. The baby of the visual detector family, paradoxically, is really the granddaddy of them all! Ancient stored tracks of heavily ionizing cosmic rays have been found on meteoritic mineral detectors (Plate IVa) that have been collecting data for eons ($\gg 10^6$ years). In addition to these fossil tracks, isotopes that were not originally present in meteorites arise from nuclear disintegrations produced by cosmic rays. Analysis of the contents of these extraterrestrial cosmic ray meters provides valuable information about both cosmic rays and the meteorites themselves. Although we will hear the fascinating story that the meteorites have to tell later, it is appropriate at this point to recognize the *dielectric solid* detector as an experimental technique.

Particle tracks in solids consist of linear regions that have suffered intense radiation damage from very dense ionization, as a result of which they are preferentially dissolved by a suitable chemical reagent. Meteoritic minerals can be "developed" by solutions of hot ($\geq$200°C) KOH or NaOH. A *latent* track, which is optically invisible but which is revealed by *etching,* is formed whenever the primary specific ionization rate j_p of a slowing down ($\beta \ll 1$) particle exceeds a critical value j_c that is characteristic of the particular solid. The value of j_c is low for materials such as mica, glasses, and various plastics. It is higher in abundant meteoritic materials, such as plivine, hypersthene and diopside.

Plastic sheets can be used as dielectric track detectors for studying the present-day cosmic radiation. When plastic detectors exposed to primary cosmic rays are immersed in a suitable etching bath, the reagent attacks the chemically altered material along the trajectory of the particle, thereby producing a hole which is visible in a microscope.

Plate IVb is a photograph of cosmic ray tracks in a 250μ thick disk of cellulose nitrate exposed for seven days in a polar-orbiting satellite.

SYSTEMS

The seemingly extravagant statement that practically all permutations and combinations of the detectors we just described have been used in cosmic ray experiments may not be too far from the truth. Now, we will cite a few examples of composite systems to introduce certain standard observing apparatus which we will encounter later, and to illustrate the kinds of things cosmic-ray physicists do.

Meson Telescopes. By operating two or more sensors in a *coincidence arrangement,* we can identify events in which both were actuated simultaneously. Of course, the output signal produced by a single detector when it fires persists for a finite length of time. Consequently, it is possible for pulses from the individual counters comprising a coincidence train to overlap fortuitously when they are traversed by unrelated particles that happen to arrive within the instrumental *resolving time.* After taking into account the probability of *chance coincidences* (*accidentals*), a coincident event can be ascribed either to a single particle that triggered each of the detectors, or to associated particles that struck the individual detectors at the same time.

The simplest and oldest such arrangement is the Geiger-Mueller counter telescope. Its principle of operation can be understood by considering the *cubical meson telescope* illustrated in Fig. 3-5. This standardized geometrical arrangement has been adopted by many cosmic ray observatories for continuously recording the intensity of the predominant secondary cosmic-ray component at ground level, the muons. It is clear that to be counted, single particles must arrive within a cone determined by the dimensions of the sensitive areas and the spacing between them. The *opening angle* is 90° in this case. Lead absorber interposed between the trays eliminates most of the electron component, accounting for the name by which the instrument is known.

The analogy with the optical telescope refers only to the restriction of the field of view. Of course, cosmic-ray telescopes can, in principle, be designed with any desired angular resolution, and can be pointed in any direction.

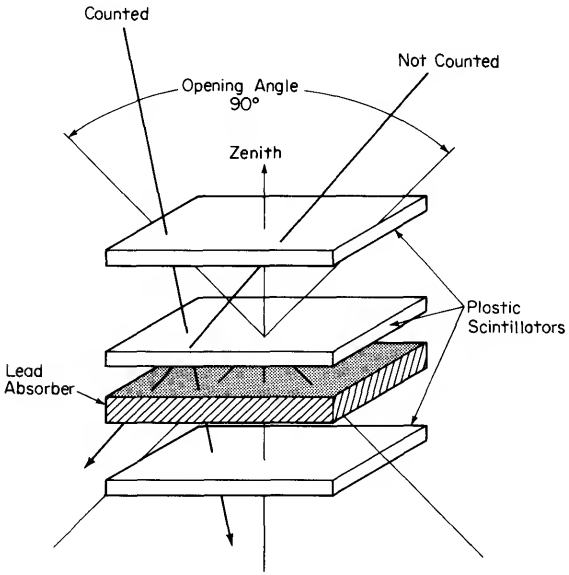

FIG. 3-5 Arrangement of a meson telescope. The cubical configuration has been adopted by many cosmic-ray observatories.

Air Shower Detectors. Suppose you were to spread out a number of counters widely separated from each other in a horizontal plane. What would happen? Would the coincidence counting rate be just what you would predict, knowing the resolving times and the individual counting rates? The perhaps surprising answer is a resounding "no!". The counting rate would be higher than expected from chance coincidences. The hint was dropped in Chapter 2, when the term "shower unit" was casually mentioned. And, by inductive reasoning, one might have concluded from the discussion of energy loss mechanisms for particles and electromagnetic radiation that the inverse processes of bremsstrahlung and pair production could result in the rapid conversion of the energy of a single particle into many other energetic progeny. This does occur (*cf.* Plates II and III), and we shall explore the fascinating consequences of this *multiplication* mechanism later. The resulting phenomenon is called an *extensive air shower,* EAS. The size qualification is added to distinguish an electro-

magnetic *cascade shower,* extending over a large area, from a *local shower,* which is a nucleonic phenomenon that covers a small area.

Extensive air shower detectors run the gamut of size and complexity from a few single counters close together to most elaborate arrays of different types of instruments distributed over extremely large areas. Sometimes, parts of the system may be buried deep below the earth's surface. New techniques for studying EAS are continually being developed, and interest is likely to continue at an accelerating pace, because extensive air showers provide the only available means for studying the very highest energy cosmic-ray primaries.

Calorimeters. Instead of waiting for showers to be produced in the atmosphere, one can create a spatially scaled-down version in dense materials, so that the entire cascade process transpires within a relatively small volume. The total energy dissipated inside the system can then provide a measure of the energy of the incident primary. An instrument that accomplishes this is called a *calorimeter*—for obvious reasons.

Fig. 3-6 shows one such arrangement that has been carried

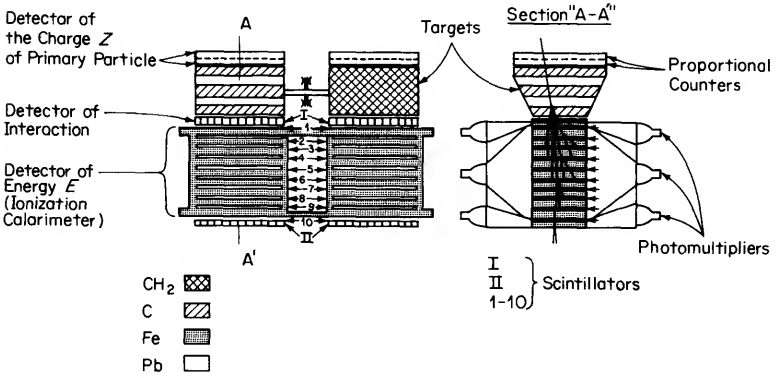

FIG. 3-6 Cosmic-ray calorimeter designed to measure the energy of primary protons in the range $10^{10} - 10^{14}$ eV.

by Soviet "Proton" sputniks. Plastic scintillators are the ionization detectors of the calorimeter. The interaction detectors measure the number of particles in the shower passing through the detector. Two proportional counters measure the charge Z of the

primary. Polyethylene and graphite filters periodically change places during the flight and are removed out of the limits of the instrument solid angle. Measurements of primary protons in the energy range 10^{10}–10^{14} eV are made with this arrangement.

High-Flying Analyzers. Classical detectors, such as Geiger-Mueller counters and ionization chambers, are still being flown aboard balloons and spacecraft. But a myriad of highly specialized combinations of sensors have also appeared on the scene. Their characteristics are continually being improved as experience with the new techniques is gained. Let us look at a few "typical" arrangements just to get a feeling for the infinite variety of possibilities that now exist for examining the fine structure of the primary cosmic-ray beam.

Fig. 3-7 is an idealized view of a dE/dx and E detector. The

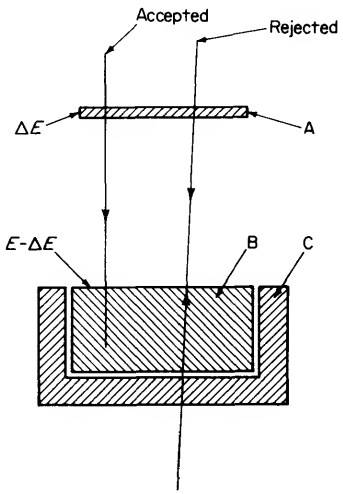

FIG. 3-7 Simplest form of arrangement for measuring the rate of energy loss $-(dE/dx)$ and kinetic energy E with thin and thick scintillators or solid-state detectors.

thin upper scintillator (or semiconductor counter) A measures dE/dx. Particles that stop in the thick lower scintillator (or semiconductor counter) B are identified by *anticoincidence* with the plastic guard scintillator C. An event A + B − C, in which

A and B are activated and C is not, identifies a stopping particle. If A is sufficiently thin, of thickness Δx, the energy deposition is

$$\Delta E = \left(\frac{dE}{dx}\right) \Delta x, \tag{3-2}$$

whereas the energy deposited in C is

$$E - \Delta E \simeq E, \tag{3-3}$$

since ΔE is negligibly small.

Recalling Eq. (2-16) we can write

$$-(dE/dx)_{\text{ion}} = z^2 f(\beta) = z^2 g(E/M_0c^2) \tag{3-4}$$

where the particle speed is $v = \beta c$, E is its incident energy and M_0 its rest mass.

The function $g(E/M_0c^2)$ can be separated:

$$g(E/M_0c^2) = g_1(M_0c^2)g_2(E). \tag{3-5}$$

The rate of energy loss is then

$$dE/dx = [z^2 g_1(M_0c^2)]g_2(E). \tag{3-6}$$

The simultaneous measurement of dE/dx and E determines the value of $z^2 g_1(M_0c^2)$, which uniquely identifies the species of the particle. Actually, the finite thickness of A can easily be taken into account. A typical set of ΔE *vs* $E - \Delta E$ curves for several nuclides is shown in Fig. 3-8. A ΔE *vs* $E - \Delta E$ line exists for each type of stopping particle, permitting its identification. Particles that do not stop in B deposit less energy in *both* B and A than do those that are stopped (Fig. 2-10). The dashed lines represent characteristic energy lines for particles that have penetrated B.

Now, let's consider a different system, in this case one designed for investigating the primary electron component. In Fig. 3-9, vertically incident particles are selected by coincidence between telescope counters T_1 and T_2 (plastic scintillators). An event must also trigger the gas Čerenkov counter C_1 that is sensitive to charged particles with energy $E > 20\ M_0c^2$. The threshold energy for electrons is lower than for protons or alpha particles, thereby making it easy to discriminate against the very large background. A dE/dx measurement is made in counter T_1 and, since all

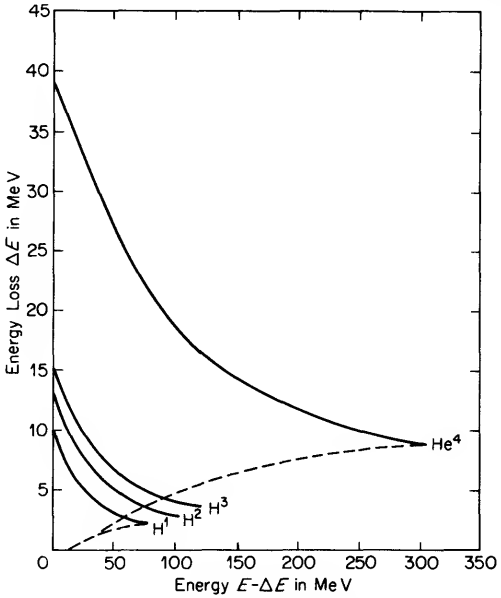

FIG. 3-8 Typical ΔE vs E-ΔE curves. The simultaneous measurement of energy and rate of energy loss yields a data point that falls on one of these characteristic curves, thereby identifying the particle.

accepted particles are relativistic, this sorts the particles according to charge z. An electron will develop an electron-photon shower in the lead glass Čerenkov detector C_2. If the shower is confined to the lead glass cylinder, the total Čerenkov light output is roughly proportional to the energy of the entering electron. G_1, G_2, and G_3 are anticoincidence counters to guard against certain unwanted events that could masquerade as electrons, and S discriminates against certain proton events that might otherwise fall between the cracks.

Neutron Monitors. Important advantages that will become apparent later are gained by observing the *nucleonic component* even though it comprises only a few percent of the total particle flux near sea level. The *neutron monitor* is in some respects analogous to a nuclear reactor, and its front end is called a *pile*. Figure 3-10 shows the geometrical arrangement of the most modern version of this apparatus that is continuously recording the

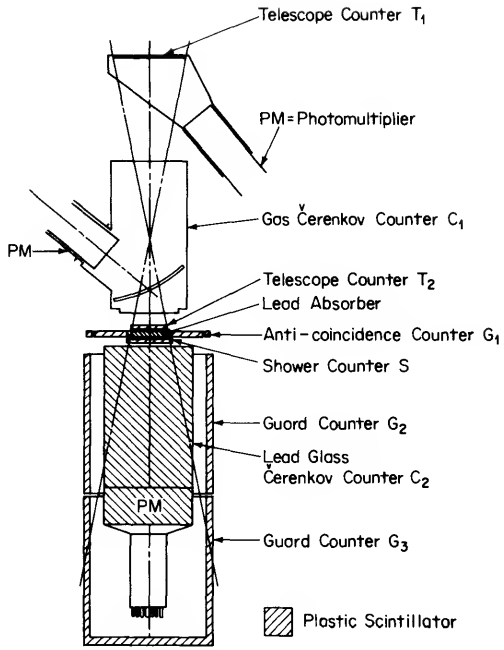

FIG. 3-9 System for investigating the primary electron component.

cosmic-ray intensity at a network of stations which covers the globe and, literally, extends from pole to pole.

A *nucleon* (proton or neutron) incident on the pile has a high probability of causing a nuclear interaction in the lead (the *producer*) thereby yielding a multiplicity of low-energy neutrons (see Fig. 4-16). As these diffuse through the pile, they are slowed down to thermal velocity by elastic (billiard-ball) collisions in the hydrogen-rich material, polyethylene (the *moderator*).

Some of the evaporation neutrons reach the $B^{10}F_3$ proportional counter tubes, and are detected as already explained [see Eq. (3-1)].

LABORATORIES

A discussion of experimental methods would be incomplete without some reference to the many different types of "labora-

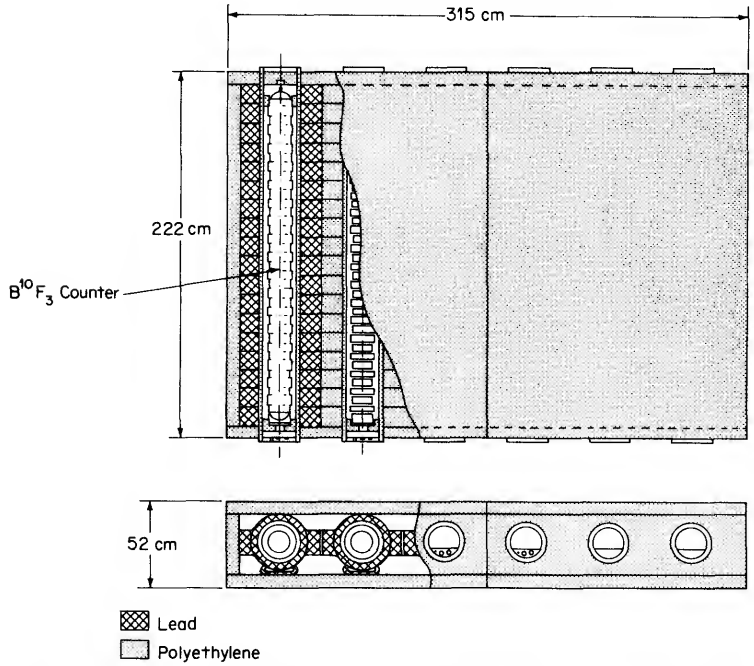

FIG. 3-10 Arrangement of a *pile*, the sensor of an apparatus for measuring the nucleonic intensity. Three identical and independent sections and ancillary equipment comprise a neutron monitor, weighing about 40 tons.

tories" that cosmic-ray instruments are wont to inhabit. A major part of the effort expended in carrying out any cosmic-ray experiment is devoted to transporting the apparatus to the desired location, and making certain that it operates reliably under the usually rigorous environmental conditions. Cosmic-ray research has been historically and traditionally an expeditionary enterprise. Since nature performs the experiments, we must carry out our observations in accordance with her dictates—which generally means in some hard-to-reach albeit perhaps exotic place.

Manned Stations. "Permanent" cosmic-ray observatories are continuously monitoring the cosmic-ray intensity at sites extending from megalopolis to the remotest corners of the earth, at depths or altitudes ranging from deep mines to tall mountain

peaks. Some examples of ground-based cosmic-ray stations are depicted in Plates V and VI. Needless to say, the logistical problems are far from trivial!

Mobile manned stations are also utilized for conducting geographical surveys relating to the effects of the geomagnetic field upon cosmic-ray intensity. Large trucks (Plate VII), ships, and aircraft carry the touring cosmic-ray detectors.

Balloons. The importance of lifting cosmic-ray detectors to great heights should already be evident. Thus, it is no mere coincidence that cosmic ray physicists have been instrumental in the rapid development of ballooning techniques. Plastic balloons (Plate VIII) with volumes of 20 million cubic feet can serve as stable platforms at altitudes of 145,000 feet for payloads of hundreds of pounds.

In an isothermal atmosphere, the pressure p varies with height above sea level h_s exponentially:

$$p = p_0 \exp(-\overline{m}gh_s/kT_K) \tag{3-7}$$

where p_0 is the pressure at sea level, T_K is the temperature in degrees Kelvin, k is the Boltzmann constant, and $\overline{m}$ is the mean molecular mass. $H = kT_K/\overline{m}g$ is the *local scale height,* or the height of the homogeneous atmosphere, that is, the thickness of the atmosphere if the density were constant at the sea level value ($H = 8$ km). Of course, the temperature is not constant throughout a vertical column, hence Eq. (3-7) is an approximation. The so called "standard" atmospheric depth *vs* altitude curve in Fig. 3-11 shows that only 1% of the atmosphere lies above about 100,000 feet, and the residual atmosphere at 145,000 feet is less than 2 gm/cm^2—practically outer space for many purposes, but much too deep for others.

Rockets. For a relatively brief period, before the advent of spacecraft, rockets were employed to boost cosmic-ray instruments to greater heights than could be attained with balloons. Imaginative techniques such as launching the rockets from balloons were developed. Although rockets are still extensively utilized in upper atmospheric physics research (aeronomy) for which they are especially well adapted because they can provide *vertical profiles,* cosmic-ray workers now concentrate upon balloons, satellites

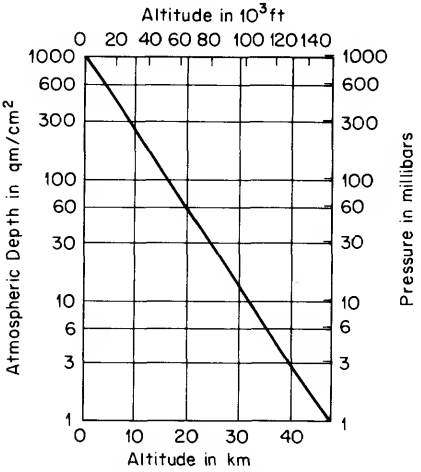

FIG. 3-11 Variation of atmospheric depth with altitude above sea level.

and space-probes, using rockets only for studying energetic particles emitted during distinctive solar events.

Spacecraft. Recognition of the advantages of artificial satellites as vehicles for cosmic-ray experiments initially provided one of the strongest motivations for developing scientific space vehicles. The best known space age discovery bears the name of J. A. Van Allen, who correctly attributed an apparent malfunctioning of his single Geiger counter on Exporer I (Plate IX) to an abnormally high particle flux at the higher altitudes.*

* It is interesting to note that Störmer's calculations (Chapter 4) many years earlier had indicated that charged particles could be trapped in the earth's magnetic field.

4 *Propagation Through the Earth's Magnetic Field and Atmosphere*

Non semper ea sunt quae videntum.
PHAEDRUS

For the soul is dead that slumbers,
And things are not what they seem.
HENRY WADSWORTH LONGFELLOW

The interpretation of any cosmic-ray measurement carried out in the immediate vicinity of the earth requires an understanding of the perturbations introduced by its presence. The effects upon the free-space particle flux of the earth's magnetic field, and of its atmosphere, and of the solid earth itself, must be taken into account. Conversely, these same effects can be exploited to serve useful purposes in our efforts to understand cosmic-ray phenomena. Nature compensates somewhat for the tight control that she exercises over cosmic-ray experiments by providing us with a huge and unique cosmic-ray apparatus—our planet!

The geomagnetic field serves as a vast magnetic spectrometer. One consequence of the deflection of electrically charged particles by magnetic fields is a filtering effect whereby particles that fail to satisfy a certain minimum requirement (depending upon location, etc.) are not admitted. The price of admission, so to speak, becomes progressively lower as the pole is approached, giving rise to the *latitude effect,* as illustrated in Fig. 4-1. Furthermore, the field constitutes a complicated lens which imposes restrictions on the *directions of viewing.*

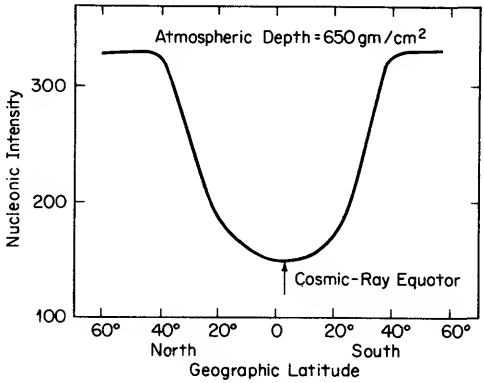

FIG. 4-1 Typical intensity vs latitude plot of data obtained with an airborne neutron monitor. The exact form of the latitude-effect curve depends upon the nature of the detector, the atmospheric depth, the level of solar activity, and the route followed.

An optical or radio telescope detects electromagnetic radiation which, unaffected by magnetic fields, travels from the source to the observing instrument in a straight line. But this is not true in the case of a cosmic-ray telescope. The electrically charged particles to which it responds undergo various gyrations in traveling toward the earth, and the original *direction of approach* far away from the earth may be quite different from the direction in which the instrument is pointing. Figure 4-2 shows the trajectory of one particular proton as it approaches the earth. It is clear that the direction from which it appears to come when it ultimately strikes the earth is not its original direction prior to encountering the geomagnetic field. This quasi-trapped orbit is not necessarily typical, but it serves to indicate the importance of carrying out an elaborate analysis to evaluate the *directional response* of a cosmic-ray detector.

The atmosphere not only transforms the incoming particles into other species, moving in different directions, but it also acts as an absorption filter which, in effect, imposes a certain minimum primary energy requirement, the *atmospheric cutoff*, depending upon the depth in the atmosphere, the nature of the secondary component that is being observed, and the geometry of

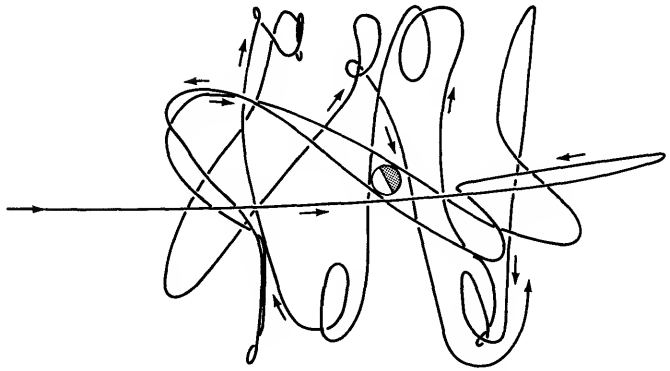

FIG. 4-2 Quasi-trapped trajectory of a proton moving under the influence of the earth's magnetic field after arriving from a distant source. It is clear that if this particle eventually strikes the earth, its apparent arrival direction would not correspond to its original direction of approach.

the detector. This accounts for the *counting rate plateau* beyond the *knee of the latitude effect* in Fig. 4-1.

Thus, the combination of the earth's magnetic field, the atmosphere, and the detector (including any additional superposed absorber, as in the case of underground measurements) comprises a multi-component optical system. Exceedingly complicated analysis with a voracious appetite for computer time must be painstakingly carried out in order to enable us to utilize it effectively for cosmic-ray investigations.

MAGNETIC BENDING

When a charged particle moves with velocity v in a uniform magnetic field **B**, it experiences a force according to the relationship

$$m(d\mathbf{v}/dt) = (ze/c)(\mathbf{v} \times \mathbf{B}). \tag{4-1}$$

In general, v has components perpendicular and parallel to **B**, and the path of the particle is a helix, as is illustrated in Fig. 4-3. The radius r_g is called the *gyroradius* or *cyclotron radius*. If the gyroradius is small compared with the dimensions of the magnetic field, the particle essentially follows a line of force

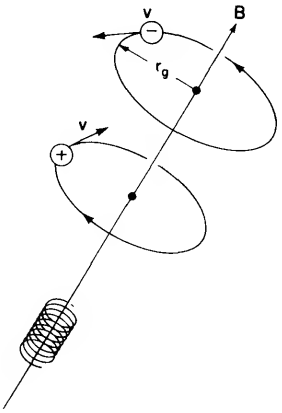

FIG. 4-3 Motion of a charged particle in a magnetic field. If the gyroradius r_g is small, the particle is constrained to follow a line of force.

which defines the direction of motion of its *guiding center*—the point about which the particle executes its cyclotronic motion.

If **B** is perpendicular to **v**, the force is mutually perpendicular to both, and the particle describes a circle. As in the mechanical analogy, the centripetal acceleration is

$$(dv/dt) = v^2/r_g. \tag{4-2}$$

Hence, combining Eqs. (4-2) and (4-1) gives

$$mv^2/r_g = (ze/c)vB \tag{4-3}$$

or

$$Br_g = mvc/ze = pc/ze, \tag{4-4}$$

where p is the relativistic momentum [cf. Eq. (2-2)], e is the charge of the electron, and z is the charge of the moving particle in units of e.

The product of the magnetic-field strength and the radius of curvature Br_g is the *magnetic rigidity* of the particle. After introducing the appropriate conversion factor to keep the units straight, we have

$$p = 300zBr_g ev/c \tag{4-5}$$

where Br_g is measured in gauss-cm.* Thus, the momentum of any charged particle can be determined by measuring its radius of curvature in a known magnetic field.

In discussing the motion of cosmic rays in magnetic fields, it is convenient to characterize a particle by its magnetic rigidity, the quantity $P = pc/ze$ in Eq. (4-4), expressed in volts, rather than by its momentum in ev/c or energy in ev; particles having the same magnetic rigidity P follow identical trajectories, whereas particles with the same momentum p or energy E but different charges ze do not.

Magnetic Analysis. To understand how the earth's field acts as a magnetic analyzer, let us consider the oversimplified situation depicted in Fig. 4-4, before proceeding first to an idealized

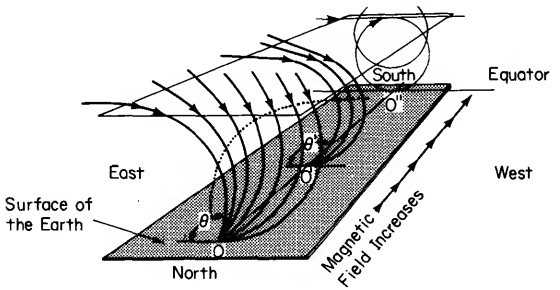

FIG. 4-4 Schematic representation of the concept of allowed directions of arrival. The solid lines are for positive particles. As illustrated by the dashed line, the picture is reversed for negatively charged particles.

approximation and then on to the vastly more complex problem presented by the real field of the earth. Suppose that an observer can measure the particle flux from any direction at any point in the lower plane. As in the case of the earth's surface, no particles come up from below. Between the two planes, there is a magnetic field in the direction indicated by the arrow. The field is uniform over any section parallel to the front of the dia-

* Because the permeability in space is unity, the distinction between magnetic field intensity H (cgs unit-gauss) and magnetic induction B (cgs unit-oersted) may be ignored and the gauss (or *gamma* $= 10^{-5}$ gauss) is often used.

gram, but of increasing strength as shown. The line 0-0″ is like a magnetic meridian in the northern hemisphere, 0″ being at the magnetic equator where the horizontal field is strongest. West is on the right, as marked. Positive particles with a certain magnetic rigidity P are incident on the upper plane uniformly from all angles. Those coming from the eastern horizon reach point 0 at angle θ, 0′ at the more inclined angle, θ', but fail to reach 0″. Only particles with higher magnetic rigidity can reach the regions left of θ, whereas those cosmic rays that are able to reach the region on the right illuminate it uniformly. For incident negatively charged particles, the picture would be reversed, as indicated by the dotted orbit. If particles having only the specified rigidity were present, the observer would find a sharp cutoff in the intensity at some measured angle θ and, knowing the strength and direction of the magnetic field, he could then determine both the sign of the charge and the magnetic rigidity.

Orbits in Dipole Field. The simplest possible model of the earth's magnetic field is the so-called *centered dipole approximation.* In this case, the field is assumed to be the same as that which would be associated with a bar magnet of magnetic moment M located at the center of the earth, and oriented from north to south along the *geomagnetic axis.* The geomagnetic axis is tilted by 11.5° with respect to the geographic axis, so that the *geomagnetic poles* emerge at 78.5°N, 69.0°W and 78.5°S and 111.0°E. Note that the *geomagnetic coordinates* are different from the magnetic coordinates which are plotted on navigational charts, and which represent local magnetic measurements of dip angle, etc.

Störmer addressed himself to the problem of determining the regions of space around a dipole that are accessible to particles of any specified magnetic rigidity. Fortunately, a detailed discussion of Störmer's theory is not essential for understanding the nature of its consequences. But we should note that the analysis involves the solution of the equation of motion [Eq. (4-1) expressed in cylindrical coordinates] of a charged particle moving in the field of a dipole. A simplifying normalization that removes the magnetic moment of the dipole M_D and the particle rigidity

P from the equations is achieved by introducing as a unit of length the so-called *Störmer unit:*

$$C = (300M_D/P)^{\frac{1}{2}} \text{ cm.} \tag{4-6}$$

The Störmer unit has a physical significance: it is the radius of the circular orbit that would be described by a particle of rigidity P volts moving in the equatorial plane of a dipole of magnetic moment M_D gauss-cm. The dipole moment of the earth is $M_D = 8.1 \times 10^{25}$ gauss-cm, and the radius of the earth is $a = 6.38 \times 10^8$ cm. Therefore, on the earth's surface at the equator where $a = C$:

$$6.38 \times 10^8 = [(300)(8.1 \times 10^{25})/P_s]^{\frac{1}{2}}. \tag{4-7}$$

Solving for P_s, we find that the magnetic rigidity of a particle that would just circle the earth at the equator is

$$P_s = 59.6 \text{ GV.}^* \tag{4-8}$$

This is the minimum rigidity which a particle must have to reach the earth from the least-favored direction at the equator, i.e. the eastern horizon for positive particles.

It is probably intuitively obvious that the detailed calculations of allowed and excluded regions at *any* point around a dipole can become rather involved.

An example of the results of Störmer's analysis is shown in Fig. 4-5. Positive particles having a magnetic rigidity $P = 10$ GV cannot reach the geomagnetic equator, but begin to arrive within a narrow cone about the western horizon at some critical latitude. The cone broadens out until, at another higher latitude, it fills the entire hemisphere.

The Störmer treatment does not take into account complications introduced by the presence of the solid earth. Numerical calculations of individual orbits carried out by G. Lêmaitre and M. Vallarta showed that, in fact, not all trajectories within the *Störmer cone* are allowed even in the absence of the earth; there is a *penumbral region* containing a mixture of accessible and inaccessible points. Furthermore, there are some otherwise

* GV = 10^9 volts. This avoids international misunderstanding, as compared with the older use of BV, since in some countries billion means 10^{12}.

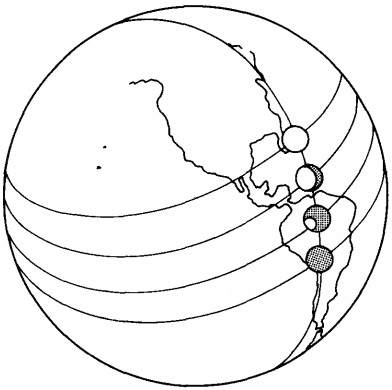

FIG. 4-5 Allowed (light) and forbidden (dark) regions for 10 GV particles.

allowed orbits that intersect the earth. This (obviously) stops the particles, and thereby produces the *simple shadow cone* within the Störmer cone. Figure 4-6 illustrates this effect which is concentrated in the direction of the nearer poleward horizon.

The character of *allowed* (light) and *forbidden* (dark) regions of the sky at an intermediate latitude, 30°N, for positive particles of a given rigidity (10 GV) is depicted in Fig. 4-7. The Störmer allowed cone includes the entire portion of the hemisphere west of the arc that is so labelled. Absolutely no 10 GV

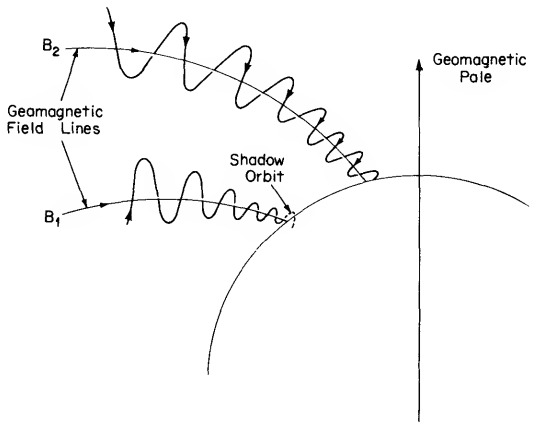

FIG. 4-6 Effect of the solid earth in producing the shadow cone.

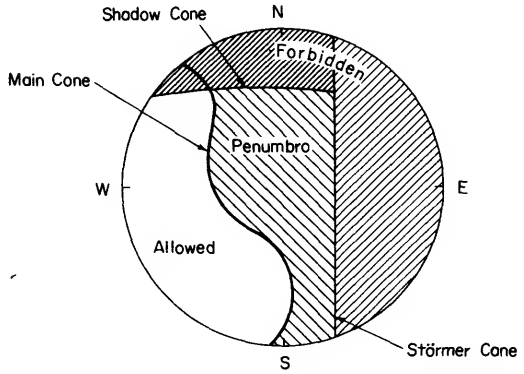

FIG. 4-7 Störmer, shadow, and main cones for 10 GV particles at a middle geomagnetic latitude (30° N).

particles can reach the regions lying outside this cone. Part of the allowed cone lies in the earth's shadow. All of the *main cone,* west of the indicated arc, is accessible to 10 GV particles. Between the boundaries of the main cone and the Störmer cone lies the penumbral region, characterized by alternate light and dark bands.

An important concept in the application of the theory of geomagnetic effects to the interpretation of cosmic-ray measurements was introduced by W. F. G. Swann. He showed that as a consequence of Liouville's theorem, well known in statistical mechanics, the particle flux is the same at all allowed places, and zero elsewhere.

Let us now consider what happens if we look at a particular region of the sky, such as the zenith. From the foregoing considerations, we shall detect *all* particles having rigidities exceeding some lower limit, the *geomagnetic cutoff* or *threshold rigidity.* The flux of these particles will be the same as it would have been if the magnetic field were not present. As our vertically pointing detector is moved toward the pole from the equator, the threshold rigidity decreases, as seen in Fig. 4-8. Here, the vertical cutoff determined by both the Störmer cone and the main cone are plotted. At a given geomagnetic latitude, *no* particle with *less* than the Störmer cutoff can enter in the vertical direction, but *all* particles having rigidities *exceeding* the main cone cutoff

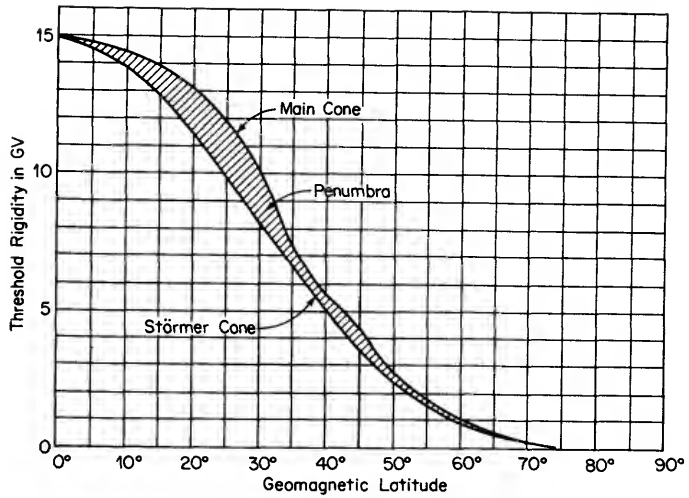

FIG. 4-8 Variation of vertical threshold rigidity with geomagnetic latitude. All particles having rigidities exceeding the main cone cutoff at a given latitude are allowed, whereas all particles with rigidities below the Störmer cutoff are forbidden.

have access. *Some* particles with rigidities between these two limits may enter, depending upon their individual trajectories.

The *Störmer integral,* which is the solution of Eq. (4-1), reduces to a simple expression for the Störmer threshold rigidity for vertically-incident particles P_{s_v}.

$$P_{s_v} = \frac{300 M_D}{4a^2} \cos^4 \lambda_g = 14.9 \cos^4 \lambda_g \text{ GV} \qquad (4\text{-}9)$$

where λ_g is the geomagnetic latitude. Note in Fig. 4-8 that the complicating effects are absent at both the equator and near the poles, as one might expect from symmetry considerations.

Trajectories in Real Geomagnetic Field. Although the validity of the classical approximations based upon the *centered* dipole, or on the *eccentric* dipole shifted 342 km from the geometric center of the earth, were unquestioned for more than two decades, evidence to the contrary then began to accumulate as improved experimental techniques started to provide data of sufficient precision to reveal discrepancies. The realization that the first order representation of the much more complicated real-life

terrestrial magnetic field is insufficient led to a succession of attempts in the last few years to improve the cutoff calculations by correcting for nondipole components of the earth's field in one way or another. Each new model seemed to reduce the discrepancies among the then available data. The nature of successive improvements is illustrated in Fig. 4-9, which shows how intensity measurements recorded in a world-wide airborne survey became progressively better organized by several generations of threshold rigidity calculations.

The culmination of all efforts to predict cutoff rigidities theoretically is the detailed calculation of actual cosmic ray trajectories in the most accurate mathematical representation of the earth's real magnetic field that geomagneticians can derive from the extensive measurements of the magnetic field components all over the globe. This is achieved by a procedure called *spherical harmonic analysis.*

The sound produced by a vibrating string, for example, is the sum of the contributions of the various harmonic frequencies of the higher modes of oscillation that may occur in addition to the fundamental. Analogously, the earth's magnetic field configuration is much more complex than that surrounding a simple dipole, and it must therefore be represented by a sum of a dipole plus higher order terms—that is, contributions by a quadrupole, octopole, etc., must be included. To see what is involved, let us look at a formidable equation that at least suggests the complexity of the computational problem. The magnetic potential, $V(r, \theta, \phi)$, from which the field arising from sources within the earth can be derived is:

$$V(r, \theta, \phi) = a \sum_{n=1}^{\infty} \sum_{m=0}^{n} (a/r)^{n+1}(g_n^m \cos m\phi + h_n^m \sin m\phi) P_n^m(\cos \theta), \tag{4-10}$$

where a = radius of earth,
r = distance from center of earth,
ϕ = longitude, east,
θ = colatitude (90° − geographic latitude),
$P_n^m(\cos \theta)$ = associated Legendre function.

The gauss coefficients g_n^m and h_n^m are constants to be deter-

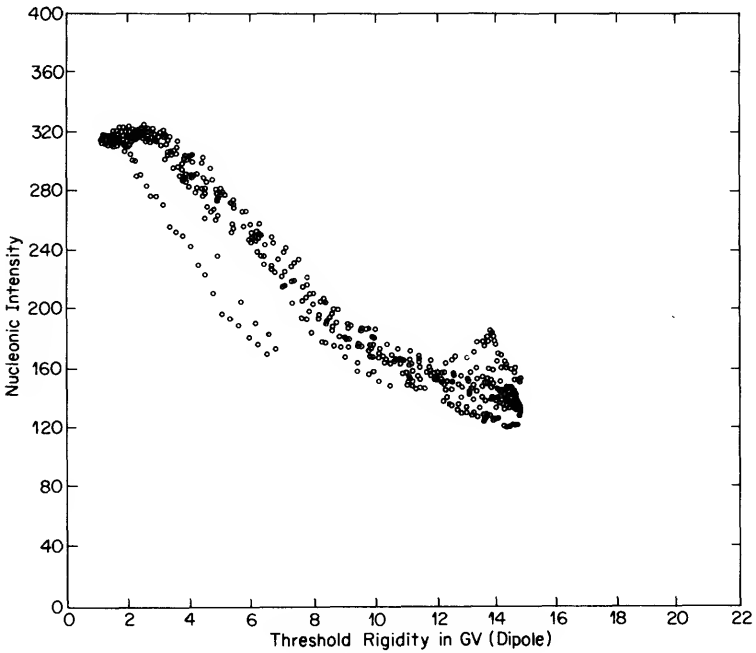
Nucleonic Intensity
400
360
320
280
240
200
160
120
80
40
0
0
2
4
6
8
10
12
14
16
18
20
22
Threshold Rigidity in GV (Dipole)

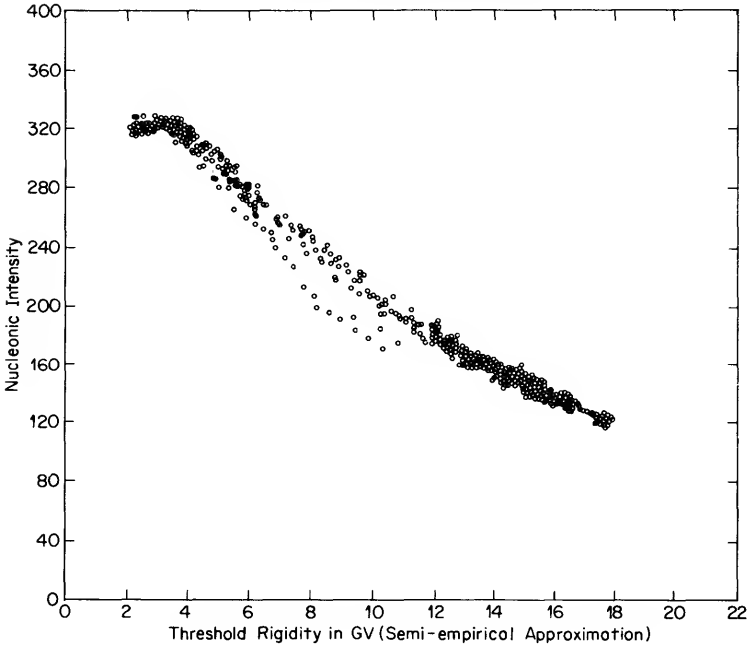
Nucleonic Intensity
400
360
320
280
240
200
160
120
80
40
0
0
2
4
6
8
10
12
14
16
18
20
22
Threshold Rigidity in GV (Semi-empiricol Approximotion)

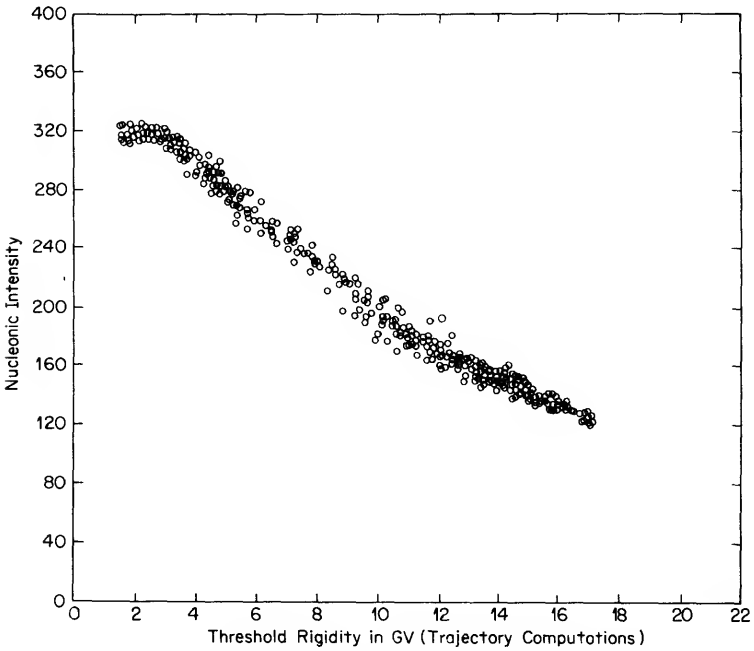

FIG. 4-9 Intensity measurements, obtained with an airborne neutron monitor in a world-wide survey, plotted as a function of geomagnetic threshold rigidity. The abscissas represent three generations of cutoff calculations: (a) dipole field model, (b) semi-empirical approximation to the real field, and (c) interpolation of a world grid of trajectory computations including spherical harmonic terms up to the sixth degree.

mined from the observational data. Field models described by a series of 120 spherical harmonic coefficients that make Eq. (4-10) fit the global magnetic measurements best have been derived.

Needless to say, trajectory calculations having the requisite precision consume a prodigious amount of computer time. Nevertheless, calculations including the spherical harmonic terms in Eq. (4-10) up to the sixth ($n, m = 6$) and, in some cases, the eighth degree field simulation have been carried out. The procedure is to shoot (analytically) from the earth negatively charged particles having various rigidities and to see whether they succeed in escaping to "infinity." Those that do correspond to positive parti-

cles approaching the earth from afar. At a given point on the earth, for a given direction, the lowest rigidity for which the orbits connect with infinity is the geomagnetic threshold. Of course, this method brings out the penumbral effects which make it impossible to define a sharp cutoff at middle latitudes. This is taken into account at least in an approximate way to determine the effective threshold. Figure 4-9 shows the improvement achieved with this ultimate treatment of the problem.

These precise trajectory calculations enable us to make the most effective use of the earth's field as a magnetic analyzer for investigating how various cosmic-ray phenomena vary with rigidity. But they also are prerequisite for studying spatial anisotropies. For this purpose, we need to relate the observed particles to the points on the celestial sphere from which they have actually come—the *asymptotic direction* in Fig. 4-10.

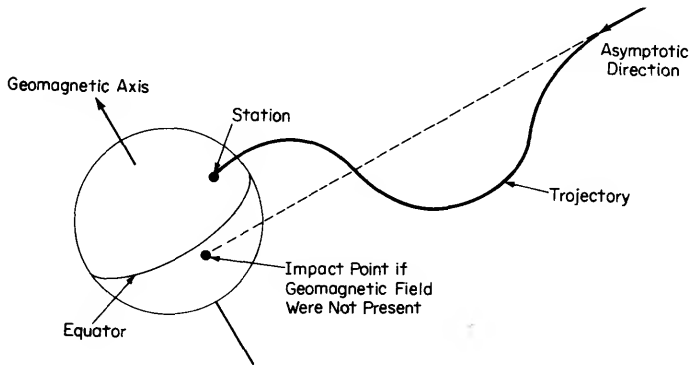

FIG. 4-10 Definition of asymptotic direction. The sketched trajectory is schematic only.

E. Å. Brunberg made the first determinations of asymptotic directions with a sort of analogue computer called a terella.* A movable electron gun is mounted on a model magnetized earth contained in a vacuum system. Electrons are shot at various

* The terella has played an interesting part in the study of the earth's magnetism. See *Magnets* by L. W. McKeehan, MOMENTUM Book No. 16, Van Nostrand, Princeton (1967).

angles from different positions, and their impact points at distances far from the globe are observed by the method sketched in Fig. 4-11.

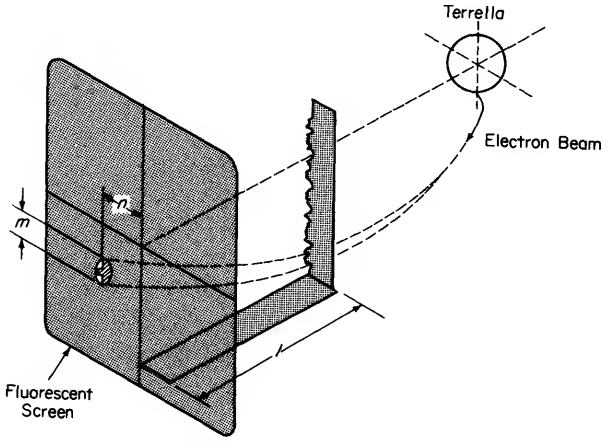

FIG. 4-11 Scheme for determining asymptotic directions with a terrella. Electrons are shot from a scaled magnetized model earth. The shadow of a tooth produced by impact of an electron beam emitted with a given energy and direction appears on the fluorescent screen. The trigonometric relationships among the quantities *m*, *n*, and *l* give the direction of arrival at essentially an *infinite* distance from the earth.

Figure 4-12 shows the asymptotic directions for a couple of stations as determined by trajectory calculations. Each dot represents the point where the only particles of the indicated rigidity that can reach the station in the presence of the geomagnetic field would have hit the earth if the field were absent.

The *asymptotic cone* for a particular cosmic-ray detector is the region of the celestial sphere from which those particles making the principal contribution to its counting rate have come. The position and shape of this *cone of acceptance* depend upon both the primary rigidity spectrum and the details of the coupling between the primaries and the secondaries that are ultimately counted. Figure 4-13 shows some typical asymptotic cones for neutron monitors. This diagram reveals the crucial importance of

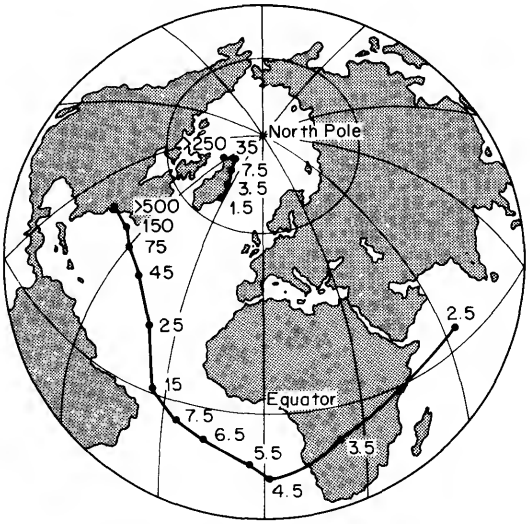

FIG. 4-12 Asymptotic arrival directions for a polar and a middle latitude station. Each dot represents the point on the celestial sphere from which all particles of the indicated rigidity (in GV) that can reach the station must have come.

stations in the polar regions; only at very high latitudes is it possible to observe particles that have come from directions steeply inclined to the plane of the earth's equator. Furthermore, the cones of acceptance of stations even at intermediate latitudes are considerably broader.

These considerations explain why cosmic-ray physicists are inveterate globe trotters, and why they set up shop in such inhospitable places as those pictured in Plates V and VI.

TRANSFORMATIONS IN THE ATMOSPHERE

Having discussed the effects of the earth's magnetic field upon the motion of the incoming primary cosmic rays, we can now consider the next phase in the life of those that are allowed to wend their way into our planetary atmosphere. The fate of a typical cosmic ray when it impinges upon the atmosphere is depicted schematically in Fig. 4-14. The interactions described in

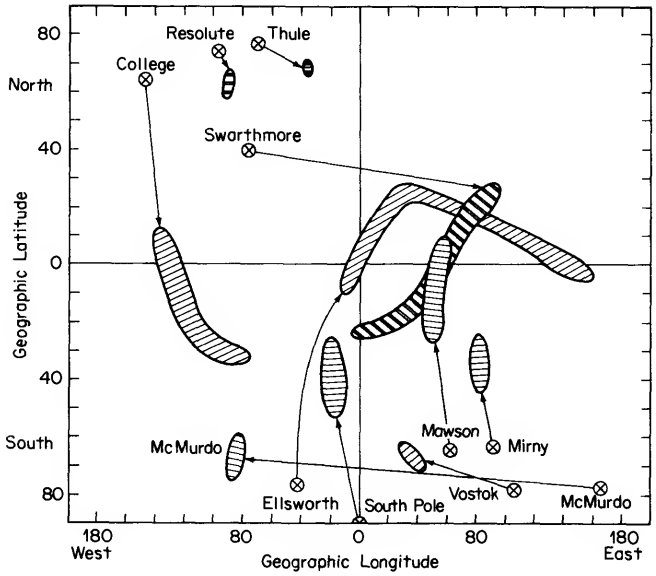

FIG. 4-13 Typical asymptotic cones of acceptance of neutron monitors plotted on the celestial sphere, but with geographic coordinates. The stations are located at the points indicated by x.

Chapter 2 (including ionization, the effects of which are not represented in this diagram) start as soon as an appreciable amount of matter is encountered. Furthermore, the mean free path for nuclear interactions of a very high-energy proton in air is about 80 gm/cm^2. Consequently, direct observation of the primaries necessitates carrying the instruments to balloon altitudes, or even higher if their energies are so low that their ranges are less than the residual atmospheric mass at the ceiling for these vehicles (cf. Fig. 7-3).

There are three modes whereby the energy of the incoming particles is transferred through the atmosphere to sea level and even below: via (1) the *nucleonic* or *nuclear-active* component, (2) the *meson,* or *hard,* component and (3) the *electromagnetic,* or *soft,* component.

Depending upon the magnitude of the energy with which the primary is endowed, one of these three mechanisms for the con-

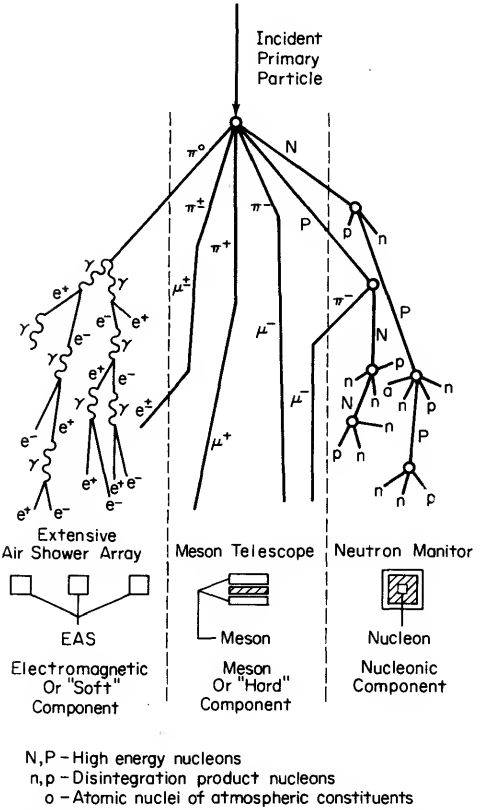

FIG. 4-14 The principal modes whereby the energy of a primary cosmic ray is propagated through the atmosphere.

version of primary energy into a secondary component predominates. The corresponding detectors, in order of increasing energy of response, are: (1) neutron monitor, (2) meson telescope and (3) extensive air shower array.

High energy neutrons and protons, emitted as disintegration products of interactions of the primaries with atomic nuclei of the atmospheric constituents, give rise to the nucleonic component, which then develops in a *cascade* process. Upon reaching the lower atmosphere, the flux of this component decreases rapidly with atmospheric depth (Fig. 4-15), and comprises only a

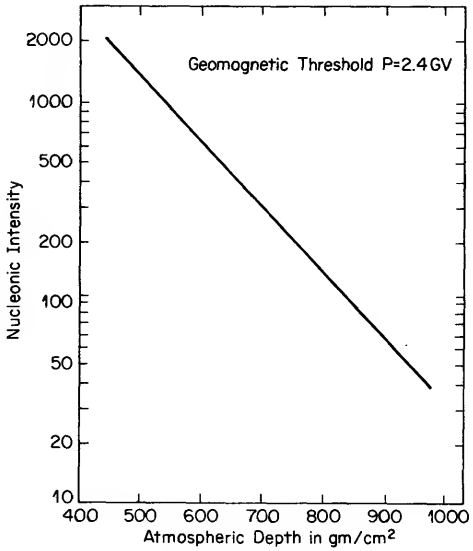

FIG. 4-15 Variation of the intensity of the nucleonic component with atmospheric depth in the lower atmosphere. The slope of the exponential curve depends upon geomagnetic threshold rigidity.

few percent of the total particle flux near sea level. Nuclear interactions of low-energy primaries result mostly in nucleons as disintegration products. A typical event in the chain, called a *star,* is shown in Fig. 4-16. Of course, the evidence for the emerging neutrons is not visible because they do not produce ionization, but they do produce stars.

At higher primary energies, π mesons are also emitted in addition to nucleons. At very high energies, most of the energy is converted into pions in events called *jets,* illustrated in Fig. 4-17. Although every type of so-called elementary particle may be produced in the high-energy interactions, pions play the dominant role in the propagation process. But, referring to Table A-1 (Appendix), we see that the π mesons are unstable, and that they rapidly decay into other particles.

Charged pions turn into muons which carry on the original charge. Although μ mesons are also unstable, Eq. (2-10) tells us that, thanks to relativity, their lifetime is sufficiently long for

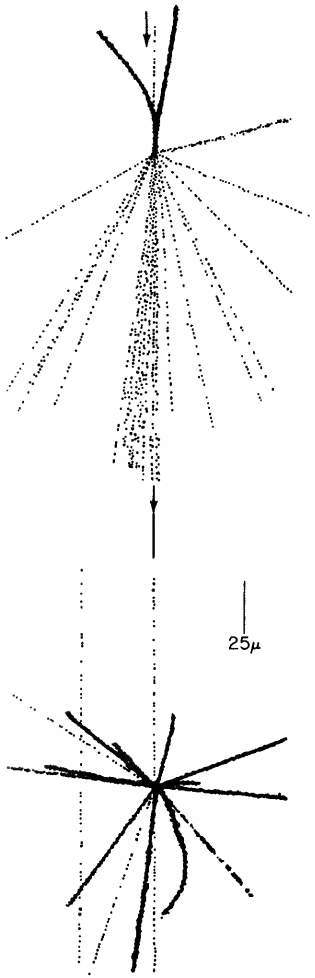

FIG. 4-16 Typical star, in which evaporation neutrons (not visible) and protons (black tracks) are produced when an energetic proton (light track) traveling downward interacts with a nucleus.

some of them to survive the journey to earth. In fact, muons are the most abundant type of cosmic-ray secondary at sea level (note that neutrinos are omitted from Fig. 4-14 because they are virtually undetectable).

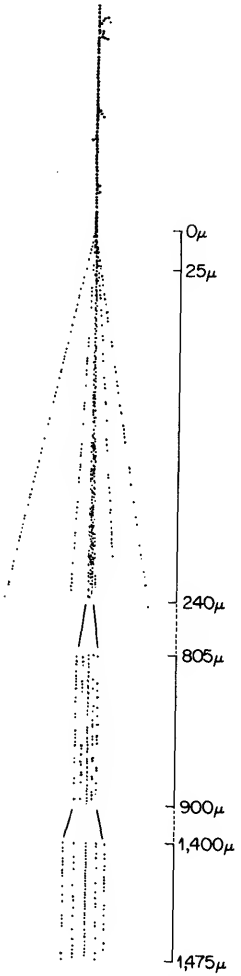

FIG. 4-17 Very high energy interaction, from which, among other products, pi mesons emerge in a narrow angle jet. The primary is multiply charged.

Neutral π mesons decay into γ rays, which, by a succession of electromagnetic processes described earlier, evolve into a great many particles extending over a large area. The number of particles is approximately proportional to the primary energy (*cf.* Fig. 4-18).

Some of the electrons arising from the decay of μ mesons may be sufficiently energetic to initiate showers, and some π mesons may be produced in nuclear interactions of the more energetic secondary nucleons. Furthermore, muons, although weakly interacting, may occasionally produce nucleons. So there is some crossover in Fig. 4-14 that, happily, can ordinarily be ignored.

THE ATMOSPHERE AS A BLACK BOX

Understandably, the detailed analysis of all of the atmospheric processes is exceedingly complex. Fortunately, combinations of theoretical models (sometimes bearing graphic appellations such as *fireball* and *baryon isobar*) with phenomenological treatments have yielded the understanding required for relating observations deep in the atmosphere to the properties of the incident primary particles that the measurements are supposed to represent. Let us consider a few examples.

Suppose we wish to investigate the primary energy spectrum by counting the occurrence rate of extensive air showers at sea level as a function of shower size. By appropriate experimental means, it is possible to determine the number of electrons in a shower. Figure 4-18 shows the theoretically calculated relationship between the number of electrons and the primary energy.

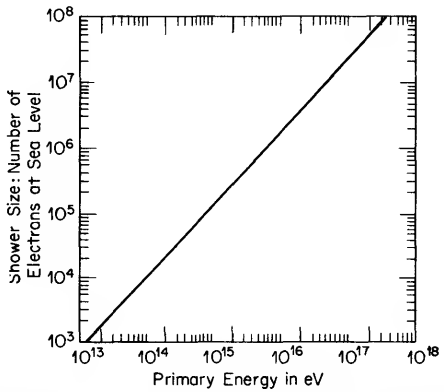

FIG. 4-18 "Calibration" curve of an extensive air shower detector located at sea level. The number of electrons in the shower is plotted as a function of the total energy of the primary that produced it.

Next, let us consider how we can study directly time variations in the primary intensity by observing the counting rate of a ground-based neutron or meson detector. If the total flux of primary particles of type i at time t is $j_i(t)$, the flux of particles having rigidities between P and $P + dP$ is $dj_i(P, t)/dP$; $N_i(P_c\ x, t)$ is the total counting rate of a given detector at a location where the cutoff rigidity is P_c, and the atmospheric depth is x. The corresponding contribution to the counting rate resulting from this increment of the primary spectrum is $dN_i(P, x, t)/dP$. The differential elements of counting rate and primary intensity are related by a factor called the *multiplicity* or *specific yield function* $S_i(P)$. Thus, for a given set of parameters i, x, t, we have

$$\frac{dN(P)}{dP} = S(P)\,\frac{dj(P)}{dP} \tag{4-11}$$

or

$$N(P) = \int_{P_c}^{\infty} S(P)\,\frac{dj(P)}{dP}\,dP. \tag{4-12}$$

$N(P)$ is the experimentally observed *integral response curve,* measured by latitude surveys like the example in Fig. 4-9. From these, one can derive *differential response functions* or *coupling coefficients* for neutrons and mesons. Examples are shown in Fig. 4-19. The differences in the rigidity-dependence of the sensitivity of neutron and meson monitors are clearly evident, as is the downward shift of the energy of maximum sensitivity as the atmospheric depth decreases. The differential primary spectrum $dj(P)/dP$ is determined in balloon-borne or satellite experiments, hence it is also possible, at least in principle, to evaluate $S(P)$.

If we wish to ascribe observed time variations of a secondary component to changes in the primary flux, the atmospheric transducer that couples the primaries to our ground-based detector must remain constant. But it doesn't—the weather affects even cosmic rays! There are two principal meteorological factors that must be taken into account.

First, the total mass of atmosphere above the instrument varies, as is indicated by changes in the barometric pressure. As the mass overhead increases, fewer secondaries reach the detector. The fractional change in counting rate is proportional to the

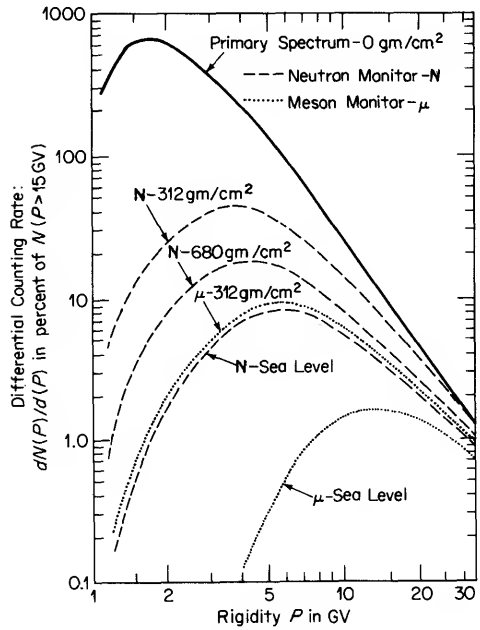

FIG. 4-19 The dependence upon rigidity of the relative responses of neutron and meson detectors at different atmospheric depths.

difference Δp between the ambient pressure and the reference (mean) pressure:

$$\Delta N(P_c)/N(P_c) = -\alpha_i \Delta p, \tag{4-13}$$

where α_i is the *barometric pressure coefficient*. For neutrons, $\alpha_n \simeq 1$ percent per torr, and for mesons $\alpha_m \simeq 0.3$ percent per torr, the exact values depending upon various circumstances. The solution of Eq. (4-13) is

$$N(P_c) = N_0(P_c) \exp [\alpha(p_0 - p)], \tag{4-14}$$

where $N_0(P_c)$ is the counting rate at the standard pressure p_0. This is compatible with the data plotted in Fig. 4-15.

In addition, the meson intensity is influenced in a far more complicated way by the state of the atmosphere. Since muons are unstable, the distance they must travel after their birth to reach the detector determines their chance of survival. Thus, if

we think of them as being produced mainly at the 100 millibar level (which is roughly the *mean* production layer) the number reaching a detector on the ground *decreases* as the height of the 100 mb isobar *increases*. Another effect has to do with the competition between π–μ decay and nuclear capture of π^- mesons. As the temperature of the region between 100 and 200 mb rises, the density falls; consequently more pions decay into muons, since the pion-eating nuclei are farther apart. Because the μ-meson intensity increases in this case, this is a *positive temperature effect*. The situation is actually quite complex but, although radiosonde data are required for making precise corrections, approximate methods often suffice.

5 *Galactic Cosmic Rays*

Seen in the galaxy, that milky way
Which nightly as a circling zone thou seest
Powder'd with stars.

JOHN MILTON

Let us now resume the fascinating story of how our knowledge about the nature of the primary cosmic rays developed after their identity as electrically charged particles had been established. Hopefully, our discussion of Störmer theory pointed to the possibility, at least in principle, of determining their sign by comparing intensities in the eastern and western directions.

This was first investigated by B. Rossi who, in 1931, showed that the preponderance of one sign of charge would give rise to an *east-west asymmetry* in the intensity. But his measurements in Florence, Italy, did not resolve the effect, which under the conditions of his experiment would have been quite small, for reasons that we now understand. However, T. H. Johnson and J. C. Street observed a greater intensity from the west than from the east in experiments on Mt. Washington the following year. This was a surprising result in the light of the general expectation that the primaries were electrons, for which access was easier from the east (Figs. 4-4 and 4-5). It immediately stimulated a great deal of activity, including several expeditions to the equatorial regions where the western excess was found, as predicted, to be appreciably greater (at sea level and zenith angle of 45° the excess was 15% at the equator and 2 or 3% at 50°).

From these experiments, it was concluded that the primaries instrumental in producing effects at sea level were largely positively charged. By a remarkable coincidence, C. D. Anderson discovered the positron in 1932. Hence, there were now two con-

PLATE I Professor Victor F. Hess in the gondola of his balloon in 1912, after a flight in which he discovered the cosmic radiation by carrying instruments up to 17,500 feet. (Courtesy National Geographic Society)

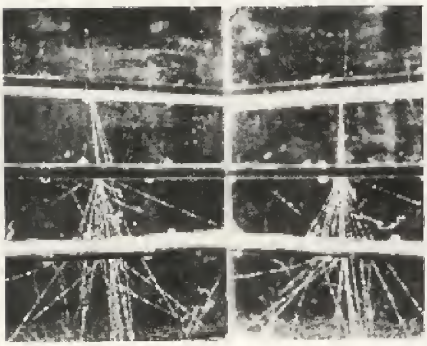

PLATE II Stereoscopic pair of cloud chamber photographs showing the development of a small cascade shower initiated by a single electron (unaccompanied by photons) having an energy of several GeV, entering the uppermost of three lead plates (total thickness $\approx$ 13 cm). Much of the multiplication in the second plate arises from the absorption of photons, which themselves produce no visible tracks, emerging from the first plate.

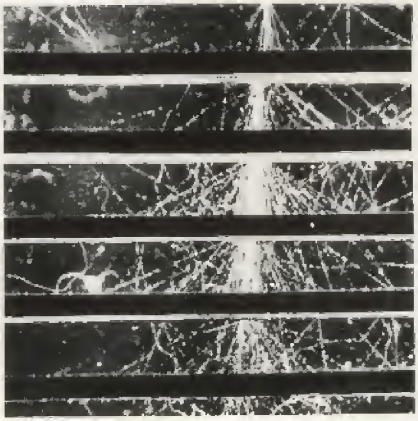

PLATE III Development of photon-initiated cascade in lead plates in a cloud chamber. The maximum number of particles, about forty, is reached after passing through 10 cm of lead, after which the number decreases sharply. The energy of the incident photon is several GeV.

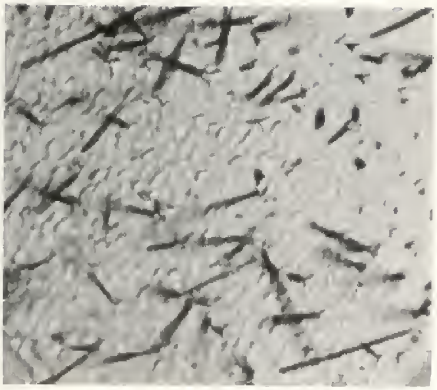

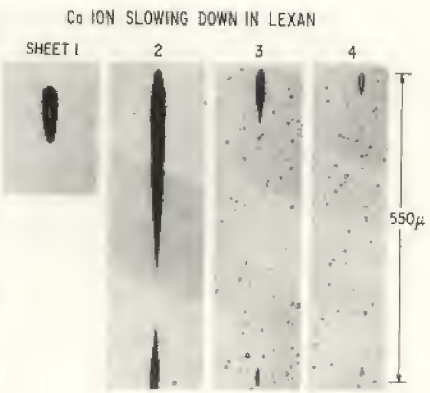

a b

PLATE IV (a) The signatures of cosmic rays in a crystal of hypersthene from the crab orchard meteorite. The abundant, short tracks are from iron group nuclei; the occasional longer tracks are from nuclei of $Z > 28$. (b) Different etched segments of the track of a single cosmic ray nucleus, identified as a calcium ion. The particle has crossed three sheets of polycarbonate plastic (#4, 3, and 2) and come to rest in a fourth sheet (#1). (Courtesy Robert L. Fleischer)

PLATE V Amundsen-Scott Station at the geographic South Pole. Although most of the buildings are under the snow, the cosmic ray laboratory (center) must remain uncovered. (Courtesy National Science Foundation)

PLATE VI The cosmic ray observatory atop the 14,000 ft peak El Infiernillo in the Chilean Andes. (Courtesy Gabriel Alvial)

PLATE VII Mobile cosmic ray laboratory that has travelled extensively throughout North America and Hawaii, at Icaros Naval Base, Acapulco, Mexico.

(Courtesy Hugh Carmichael)

PLATE VIII Release of a 135,000 cu ft cosmic ray balloon at McMurdo Station, Antarctica. Flying similar research vehicles with larger volumes, ranging up to 20 million cu ft, requires somewhat more elaborate launching equipment. (Courtesy Jack Renirie)

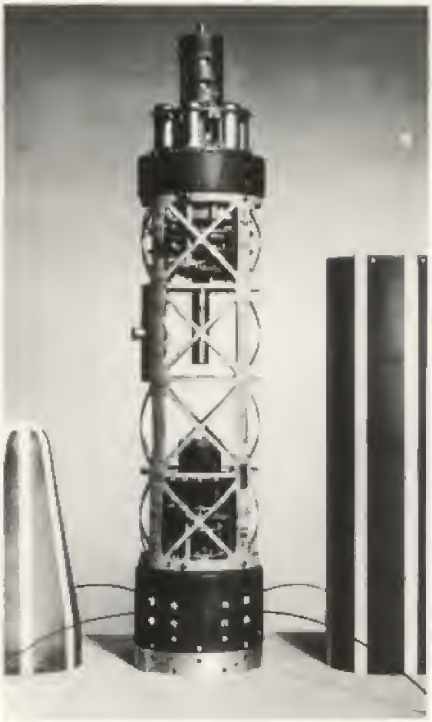

PLATE IX Explorer I, the first U.S. satellite to attain orbit, was launched February 1, 1958. The University of Iowa experiment, designed to study cosmic rays, discovered the radiation belt. (Courtesy James A. Van Allen)

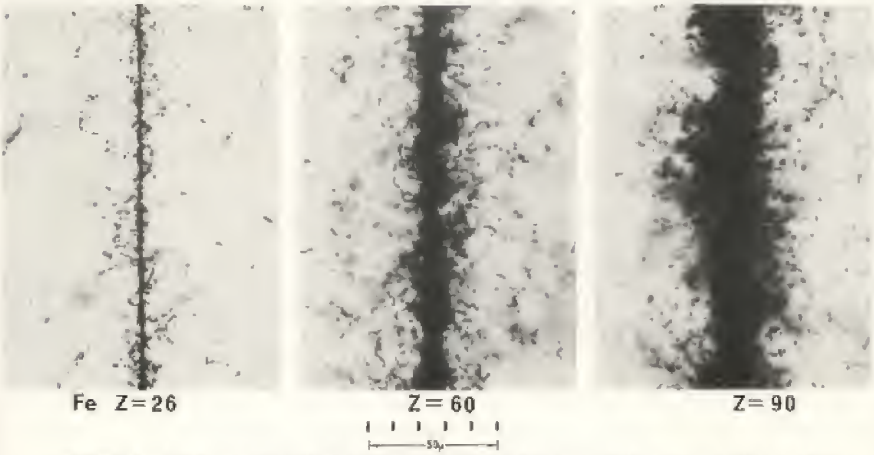

PLATE X Tracks produced in nuclear emulsion by iron and some of the newly-discovered heavier components of the primary cosmic radiation.

(Courtesy Peter H. Fowler)

tenders for the title, and it was an open question whether the incoming cosmic rays were protons or the newly discovered positive electrons. But, as usual, the cosmic ray workers did not quit while they were ahead. The results of further experiments, designed to distinguish between the primaries of the *hard* secondaries that could penetrate large thicknesses of lead, and the *soft* component that was absorbed in a few centimeters, were interpreted as revealing that the latter were equally positive and negative.

The only way to circumvent the dilemma that, it was becoming evident, was inherent in the interpretation of the ground-based measurements was to observe the east-west asymmetry of the primaries themselves with balloon-borne apparatus. In 1939, Johnson and J. G. Barry undertook this experiment in Panama, where the west-east difference was expected to be very large. Unfortunately, again for reasons that are now obvious, their results were not compatible with a predominantly positive primary beam. They concluded that there was a small proton component ($<10\%$), and an electron component balanced with respect to positive and negative charge.

Very soon thereafter, in the early 1940's, M. Schein and his group at Chicago carried out an extensive program of balloon flights with a variety of experimental arrangements. The form of the intensity *vs* absorber thickness curve of the particles at high altitudes, and their lack of a penchant for producing showers as copiously as was expected if they were electrons, led to the almost correct conclusion that all the primaries must be protons.

In 1947, balloon flights with an experimental arrangement designed to have a response that depended drastically upon the charge of the traversing particle were conducted at Swarthmore in collaboration with F. L. Hereford. These revealed that nuclei with atomic number $Z \geq 2$ were present in the primary cosmic radiation. Nuclear emulsions and cloud chambers flown by P. Freier, E. J. Lofgren, E. P. Ney, F. Oppenheimer, H. L. Bradt, and B. Peters the following year showed that elements in the periodic table at least up to the vicinity of iron are members of the primary cosmic-ray family.

It was generally expected that nuclei with still higher charges

would show up some day, but that they would be exceedingly rare. In fact, the first photographic evidence of such particles, with charge as high as $Z \simeq 90$ was reported in 1967 by P. H. Fowler. The photomicrographs in Plate X show how the tracks of relativistic higher Z nuclei compare with those of iron.

Thus was the roster of galactic cosmic radiation essentially completed more than two decades ago—with a notable exception. Contrary to earlier belief, electrons now seemed to be conspicuous by their absence! The search for the surprisingly elusive primary electrons was finally rewarded in 1960 when a counter experiment by P. Meyer and R. Vogt, and a cloud chamber study by J. A. Earl detected this small but significant part of the galactic cosmic-ray population.

The meaningful description of primary cosmic rays entails the quantitative specification of how they are distributed with respect to species, intensity, energy, space, and time. Thus, the intensity *vs* energy relationship—the *energy spectrum*—of each component must be known. Furthermore, the *chemical composition* and even finer details concerning the relative abundances of different isotopes are relevant. Finally, it is important to determine whether the galactic cosmic rays display any directionality and whether their intensity is subject to changes with time.

Tremendous progress has been made during the past two decades in assembling the dossier of the primary cosmic radiation, but the task has been formidable for a number of reasons. The particle fluxes, especially of the nuclei with $Z > 2$, are extremely small. Consequently, statistical uncertainties constitute a major stumbling block. Furthermore, measurements carried out in the atmosphere must be corrected for interactions that break up the primaries or produce a background of indistinguishable secondaries.

For heavy nuclei, estimates of *fragmentation probabilities* have often been quite uncertain. The effects of upward moving protons and electrons—*splash albedo*—add to the already large flux of downward moving atmospheric secondaries in making it difficult to identify singly charged primaries. And even if the detector is arranged to reject the splash albedo, there still re-

mains the problem posed by *reentrant albedo*—outward diffusing secondaries that are trapped by the earth's magnetic field, as predicted by Störmer theory, so that they enter in the downward direction in the other hemisphere.

Finally, even at very high latitudes and altitudes, the atmospheric cutoff imposed by the small but finite residual atmosphere masks out the low energy end of the incident spectrum. Clearly, some of these difficulties are now being circumvented by sending instruments far away from the earth aboard spacecraft. But no single technique can provide all of the answers, and our knowledge about the primary cosmic rays continues to broaden and become more precise as the sophistication and resolution of ground-based, balloon-borne and spacecraft instrumentation increases. All of these experimental approaches supplement and complement each other.

In this and succeeding chapters we can only distill the essence of the intriguing story that is still being written by many workers, using methods that range from classical to ultra modern, all over the world.

ENERGY SPECTRUM

The relationship that expresses how the intensity $j(>E)$ of cosmic rays with energies exceeding a specified lower limit E varies with energy is called the *integral energy spectrum.* The *unidirectional intensity* refers to the flux (cf. page 19) that arrives from a given direction per *unit solid angle,* that is the number of particles per unit area per unit time per steradian. The energy spectrum can be represented by a *power law:*

$$j(>E) = KE^{-\gamma}, \tag{5-1}$$

where K and γ are constants. Taking the logarithm of both sides of this equation, we see that a log-log plot of $j(>E)$ *vs* E should be a straight line with a slope equal to γ. It is striking that, as Fig. 5-1 shows, the value of the exponent does not vary greatly over the entire range of cosmic-ray energies above 10 GeV, extending over more than ten orders of magnitude. We will refer

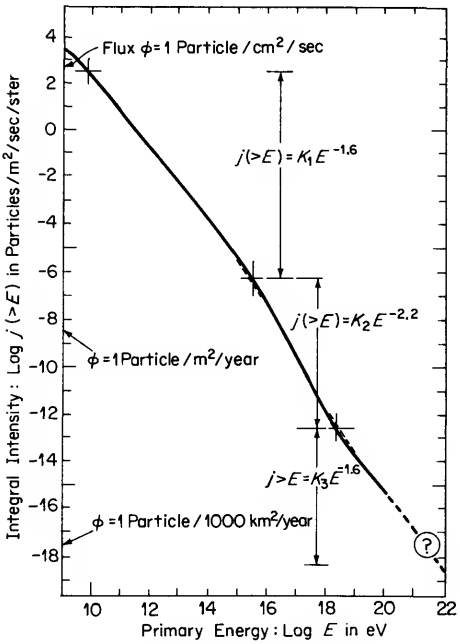

FIG. 5-1 Integral energy spectrum of primary cosmic rays. The abscissas represent total energy, and the ordinates unidirectional primary particle intensity.

later to the small but significant changes in slope at about 10^{15} eV and perhaps at 10^{18} eV, in connection with the origin of cosmic rays.

The flattening of the integral spectrum at the low energy end reflects the shape of the *differential energy spectrum* in that region. Differentiating Eq. (5-1) gives the corresponding differential spectrum, which indicates how the intensity of particles in a specified energy range between E and $E + dE$ (particles/cm^2/sec/steradian/MeV) varies with energy:

$$\frac{dj(E)}{dE} = -K\gamma E^{-(\gamma+1)}. \tag{5-2}$$

Figure 5-2 represents the observed low energy spectra of the various primary components at solar minimum. As we shall see later, these differ somewhat from the true galactic spectra as a conse-

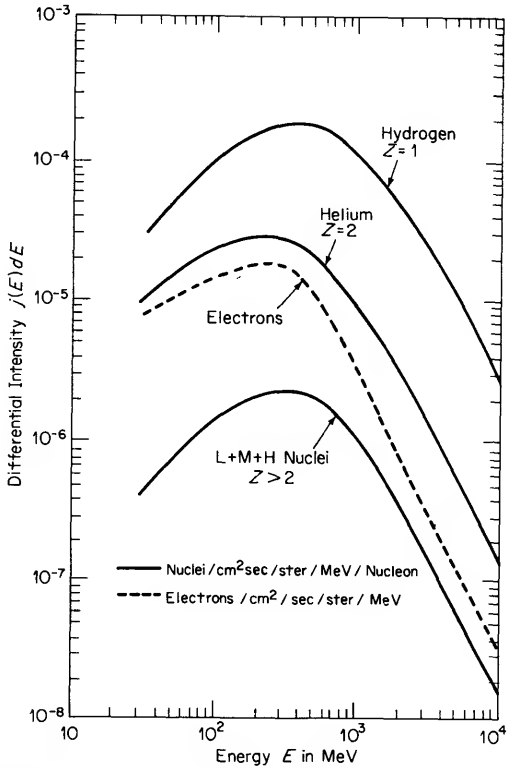

FIG. 5-2 Differential energy spectra of the various species of primary cosmic-ray particles.

quence of solar modulation. After this local effect has been taken into account, the spectra of the galactic protons and the heavier nuclei appear to be quite similar, at least over the low energy region in which the charge can be determined. There are some suggestions that changes in composition may occur at high energies.

Let us now make an order of magnitude estimate of the *energy density* that is represented by cosmic rays. From Fig. 5-1, the unidirectional intensity of primaries with energies exceeding 1 GeV is $j(>10^9 \text{ eV}) \simeq 0.3$ particles/cm²/sec/ster. The corresponding flux in free space is

$$\phi = 4\pi j \simeq 4 \text{ particles/cm}^2\text{/sec} \tag{5-3}$$

and the particle density is

$$N_p \simeq \phi/c \simeq 10^{-10} \text{ cm}^{-3}. \tag{5-4}$$

The average energy $\overline{E}$ is 3×10^9 eV, hence the energy density is $N_p\overline{E} \simeq 0.3$ eV/cm^3. This is an underestimate and, all things considered, the actual value is around 1 eV/cm^3.

COMPOSITION

The relative abundances of the elements in the primary cosmic radiation are listed in Table 5-1. All of these nuclei are completely stripped of their electrons, since charged particles with such high energies become denuded by an inverse ionization

TABLE 5-1. *Relative Abundances of the Elements in the Primary Cosmic Radiation and in the Universe. The Cosmic-Ray Composition Refers to Nuclei Having the Same Energy Per Nucleon.*

Group	Element	Atomic Number Z	Cosmic Ray Abundance *CR* in percent	Cosmical Abundance *CA* in percent	Ratio *CR/CA*
Proton	H	1	93	91	1
Alpha	He	2	6.3	9.1	0.7
L	Li, Be, B	3–5	0.10	4×10^{-7}	3×10^5
M	C, N, O, F	6–9	0.42	0.14	3
H	Ne-K	10–19	0.14	0.014	10
VH	Ca-Zn	20–30	0.04	2×10^{-3}	20
VVH	Ga-U	31–92	2×10^{-6}	10^{-6}	2
SH	>U	≃110	?	?	?

process in traversing a very small amount of matter. The nomenclature for identifying different groups of the *charge spectrum* varies somewhat. For our purposes, we shall use the scheme: *hydrogen* ($Z = 1$); *helium* ($Z = 2$); *light* ($Z = 3$–5), L; *medium* ($Z = 6$–9), M; and *heavy* ($Z \geq 10$), H. Subgroups of the latter are *very heavy* ($Z = 20$–30), VH; and the newly observed, VVH, heavier than Fe group that ranges up to the *super heavy* transuranic elements ($Z \simeq 110$), SH. Sometimes, all multiply charged

nuclei are referred to as heavy nuclei to distinguish them from protons, since they are characterized by a mass to charge ratio $A/Z \simeq 2$, whereas for protons, $A/Z = 1$.

The total energy E of a nucleus is divided among all of its A nucleons, and for comparing energies one would like to have a scale that is independent of the nature of the species, just as magnetic rigidity is. This is accomplished by expressing the energies as *energy per nucleon* E/A, since, roughly speaking, individual nucleons in an assemblage with high energy share the total energy equally, and interact independently as though they were separated. The relative abundances of the different nuclei depend upon whether the tally is made in terms of equal velocity, total energy, energy per nucleon, or rigidity.

In Fig. 5-1, the abscissa represents total energy, since this is the quantity that is determined by EAS measurements, whereas the techniques utilized to obtain Fig. 5-2 yield the energy per nucleon.

The general abundances of the elements in the universe, according to estimates based on the analysis of a variety of astrophysical observations such as stellar spectra, meteoritic composition, etc., are also tabulated. The comparison of cosmic ray and universal abundances has, as we shall see later, important implications with respect to the life history of cosmic rays.

An interesting characteristic of the nuclear abundances that is not shown in Table 5-1 is the relative numbers of nuclei with even charge number Z and with odd Z. Even Z nuclei are more numerous, and in some regions of the charge spectrum, the even to odd ratio is as high as 10 (see Table 7-2).

Concerning the primary electron component, which constitutes a few percent of the incoming particle population, negatively charged particles appear to predominate. At several GeV, the fraction of positrons is only of the order of 10%.

For the sake of completeness, we should recognize here the neutral forms of primary cosmic radiation—γ rays and neutrinos. Understanding of the role they play can be expected to develop as newly available techniques are exploited in the herculean task of determining their characteristics. Indeed, *all* radiations that reach us from beyond the solar system literally comprise the

cosmic radiation. Thus, the newly emerging and highly exciting fields of x-ray, γ-ray, and neutrino astronomy join optical and radio astronomy in their intimate relationship with cosmic-ray physics.

The detailed study of the fine structure in the composition of the primary cosmic radiation provides independent determinations of such salient features in the career of a typical galactic cosmic ray as the amount of matter it has traversed since birth. Thus, for example, calculations based upon the observed relative abundances of the isotopes of helium, $He^3/(He^3 + He^4) \simeq 0.1$, indicate about 3 gm/cm^2. The same result is deduced from the measured fraction $L/(L + M) \simeq 0.2$, by computing how much matter must be traversed for the exceedingly overabundant L group to be produced by the breakup of heavier nuclei.

Alternatively, the Be/B ratio (very roughly <0.3) reflects the *age* of cosmic rays. One of the beryllium isotopes produced by the fragmentation of heavier nuclei is Be^{10}, which is radioactive, decaying into B^{10} with a lifetime of about four million years. Thus, the relative amounts of these two nuclides depends upon the total travel time, which turns out to be in the range of a million to 100 million years. The charge distribution for $Z > 80$ would provide age information by an extension of U-Pb dating. The lifetimes of transuranic elements or their daughter particles span the time scale from 10^4 to 10^{10} years.

SPATIAL DISTRIBUTION

Primary cosmic rays seem to be distributed isotropically throughout our Galaxy, the Milky Way. Except for various well-established local effects produced by solar-controlled mechanisms, and perhaps an extremely small sidereal variation (hundredths of a percent), no true spatial anisotropy has been detected. Such an effect might be expected for exceedingly energetic primaries having such large gyroradii that they would not be appreciably deflected by the galactic magnetic fields which stir up most of the cosmic rays and make them isotropic. However, as Fig. 5-1 indicates, the flux at the high energy end of the spectrum is vanishingly small, hence the statistical uncertainties inherent in

the measurements are very great. The search for discrete cosmic-ray sources in the sky has, thus far, indicated that the distribution of arrival directions is quite uniform. The isotropy has been confirmed to within an experimental uncertainty less than 0.05% at 10^{14} eV, 1% at 10^{17} eV, 10% at 10^{18} eV and 30% at 10^{19} eV.

PREHISTORY

An intriguing question is: "Have cosmic rays been ever thus?" The answer to the query as to whether the intensity of cosmic rays has been constant over a cosmological span of time is to be found in the cryptic messages that they have recorded in meteorites. These fragments of rock and metal contain illuminating information registered by the cosmic-ray bombardment to which they were subjected before plunging close to a fiery death in our atmosphere. The well-preserved nuclear effects wrought by cosmic rays are extremely helpful in studies of the meteorites themselves, just as a host of terrestrial isotopic changes induced directly by cosmic-ray interactions are useful in other disciplines.

The most widely known application of cosmic-ray produced isotopes is the C^{14} *radioactive dating* technique for determining the age of organic matter and archeological artifacts. But many other isotopes are produced by cosmic rays on the earth, and these have been utilized extensively as tracers in studies of the atmosphere, the oceans, the crust and ice caps, marine sediments, and in a variety of other studies in the earth sciences. Figure 5-3 is a schematic representation of the regions and avenues of some of the important isotopic changes which can be observed on the earth.

Cosmogenic changes in a meteorite are produced by nuclear interactions of primary cosmic rays with its constituents in so-called *spallation reactions,* as described in Chapter 2. If the duration of the bombardment is known, one may discover how meteorites were formed and put into the orbits from which they were captured by the earth. Their sizes and shapes before they suffered ablation and often breakup in the earth's atmosphere can be deduced from measurements of the abundance of certain bombardment products as a function of depth.

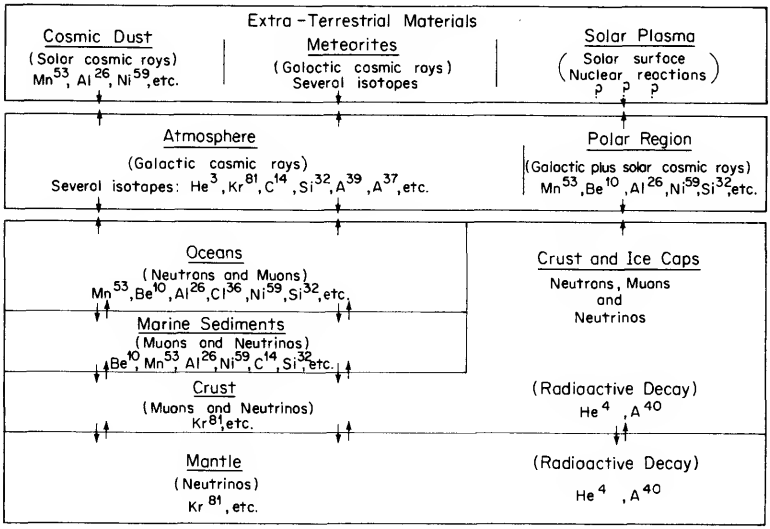

FIG. 5-3 Some of the most important isotopic changes produced by cosmic rays. The direction of motion of matter is indicated by the arrows.

The difficulties inherent in the measurements, which require quite special techniques, are very great. Only about 10^{-7} of the total number of atoms in a meteorite are transmuted, and the yields of some interesting species are less than one per thousand interactions. Terrestrial contamination and other problems are formidable.

Analysis of the cosmogenic stable and radioactive nuclides yields information on the prehistory of cosmic rays. If a meteorite is irradiated by a constant flux of cosmic rays, the radioactive isotopes thus produced build up to a saturation value in a time of about one mean life. On the other hand, the stable isotopes continue to accumulate. Thus, assuming that the present-day cosmic-ray intensity and spectrum prevailed throughout the exposure, the expected rate of production of certain nuclides in an iron meteorite can be calculated. Comparison of the observed and expected concentrations of nuclides with half-lives ranging from a few weeks to millions of years, as shown in Fig. 5-4, establishes the constancy of the flux over several million years.

The *bombardment* or *radiation age* T is defined as the ratio

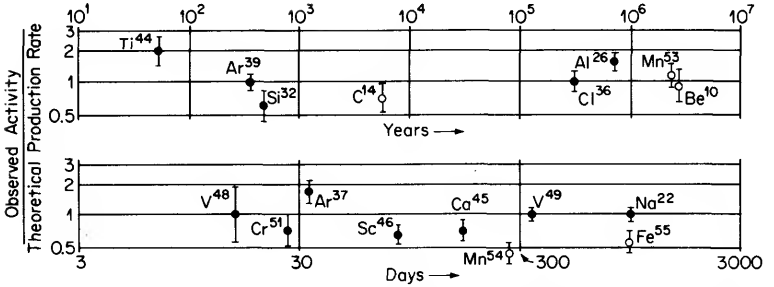

FIG. 5-4 Comparison of observed and expected concentrations of cosmogenic nuclides in an iron meteorite, indicating constancy of the cosmic-ray flux over a period of several million years.

of the total accumulated concentration of a nuclide to its present production rate. For constant bombarding flux, this is the elapsed time between the beginning of the exposure when the meteorite separated from the parent body, and the *meteorite fall.*

The radiation age can also be expressed in terms of the relative concentrations of two nuclides, one of which is stable while the other is short-lived compared with the age, and is thus in *secular equilibrium.* In this case,

$$T = \frac{P_R}{P_S} \frac{C_S}{\lambda C_R}. \tag{5-5}$$

The subscripts R and S refer to the radioactive and the stable isotope, respectively; λ is the decay constant (1/mean lifetime), P is the production rate, and C is the concentration. The ratio P_R/P_S would be equal to unity if the stable species S were produced entirely by the decay of the radioactive species R. Otherwise, its value can be estimated reasonably accurately from spallation systematics.

Measurements based upon these principles have revealed that the average intensity over the last 500 years was the same as that over the past half million years within $\pm 10\%$. Constancy over 10^9 years has been established to within a factor of two. The only available isotope for the longest time determination is K^{40} (half-life $= 1.2 \times 10^9$ years).

Other problems that, in principle, can be attacked by isotope abundance analysis in meteorites relate to the space gradient of

cosmic-ray intensity [Eq. (6-7)], and the prehistoric composition and energy spectra. Finally, the study of fossil tracks in meteoritic crystals by the technique described in Chapter 3 may ultimately make it possible to determine the long-term average fluxes of nuclei with $Z > 20$.

6 *Cosmic Ray Intensity Variations*

The awful shadow of some unseen Power
Floats though unseen among us,—visiting
This various world with as inconstant wing
As summer winds that creep from flower to flower.
PERCY BYSSHE SHELLEY

The search for time variations in their intensity commenced with the discovery of cosmic rays. To determine whether the unknown penetrating radiation came from the sun, Hess made five of his 1911–13 series of balloon flights during the day (including one during a solar eclipse) and five at night, some extending into the following morning.

Thereafter, many further attempts were made with ground-based instruments to detect some dependence of the intensity upon time that might provide a clue as to the source of the radiation. For example, in 1923, measurements by Kolhörster and G. v. Salis with an ionization chamber atop the Jungfrau seemed to indicate an increase in intensity as the Milky Way passed overhead. Contradictory results were subsequently obtained by many workers who hoped to confirm this effect, some finding variations over the sidereal day up to 15%, others finding none at all. More than four decades later the reality of an exceedingly small ($<.05\%$) *sidereal variation* is still being debated!

The first report of a variation with local solar time was made by G. Hoffman and F. Lindholm in 1928. The maximum intensity occurred in the early afternoon, and the minimum at night. The amplitude was less than 0.5%. This happens to be in the right ballpark!

But the meteorological factors described in Chapter 4 intro-

duced periodic intensity variations, including the widely studied *seasonal* changes, that caused confusion and controversy. Real progress in sorting out periodicities not associated with the atmosphere had to await the evolution of the requisite understanding of the nature of these disturbing effects, and the development of analytical procedures for minimizing their contributions.

A major step in providing a firm footing for studies of cosmic ray intensity variations was the establishment by S. Forbush in 1936 of a "permanent" network of reliable continuously recording ionization chambers (see Fig. 1-2). After more than three decades, these instruments are still in operation at Godhavn (Greenland), Cheltenham (now Fredericksburg, U.S.A.), Huancayo (Peru) and Christchurch (New Zealand). Through a combination of exceedingly careful work, keen analytical insight and resourcefulness, together with infinite patience, Forbush has discovered most of the known time variations in the cosmic-ray intensity. The most recent, a wave in the amplitude of the diurnal variation with a period of two solar cycles, was reported in 1967.

The analysis of the data recorded during the first ten years of operation at the four locations provided a most convincing demonstration of the existence of a significant *solar daily variation* that was not of meteorological origin. The amplitude at mid-latitudes was about 0.15% with a maximum at approximately 3:00 P.M. local time.

At about the same time, K. Malmförs discussed some results that had been obtained with an ingenious method that H. Alfven and he had devised five years earlier. The idea was to point one inclined meson telescope toward the north, and one toward the south, and then to compare the measured diurnal variations. Since, for the same angle of inclination, the particles arriving from both directions have passed through the same amount of atmosphere under approximately the same conditions, the difference should represent the real diurnal variation.

Suppose, at latitude 45°, the telescopes are inclined at 45° from the vertical. The north-pointing telescope looks along the earth's axis, hence any periodic daily variation that it sees must be caused by atmospheric effects. The south-pointing telescope scans the equatorial plane, and sees the sum of the atmospheric

plus nonatmospheric variations. Thus, the S−N difference represents the intensity presumably unaffected by meteorological fluctuations. H. Elliot and D. Dolbear later extended the method to include measurements with inclined telescopes pointing in the eastern and western directions. In this case, the two telescopes scan the same part of the sky in succession as the earth rotates.

In 1933, W. Messerschmitt observed that the cosmic-ray intensity decreased during a magnetic storm. The worldwide extent of this effect was demonstrated by Forbush in 1937, whence any sudden intensity reduction has since been called a *Forbush decrease.** The other type of transient intensity change, also discovered by Forbush, is the *solar-flare increase,* a phenomenon with which we will be concerned in the next chapter.

The first evidence for a *27-day recurrence tendency* was obtained by A. T. Monk and Compton in 1939. This was related to the 27-day rotational period of the sun with which, as was well known, the level of geomagnetic disturbances is closely correlated. Several different manifestations of the return to the visible disk of active solar regions during successive rotations of the sun have since come to light.

The 27-day variation had clearly connoted the influence of individual centers of activity on the sun upon cosmic-ray intensity. The corollary of this conclusion is that the intensity varies with the number and magnitude of the active centers. This effect was ultimately demonstrated by Forbush. In 1957, he showed that the cosmic-ray intensity is *inversely* correlated with sunspot numbers. H. V. Neher had also been observing the *long-term* or *solar-cycle variation* with balloon-borne ionization chambers in a continuing series of annual flights at Thule, near the geomagnetic pole. His measurements bespoke the presence at solar minimum of a large flux of slow protons that seemed to diminish as solar activity increased. Taken together, these observations led to the conclusion that low-energy particles are subjected to much greater variations than are higher-energy particles.

Except for the problematical sidereal effect, all of these periodic and transient time variations in intensity represent spatial aniso-

* Forbush has now become resigned to this, although he winces when people replace the word *decrease* with *decline!*

tropies in the cosmic-ray intensity arising from solar phenomena. We are just beginning to understand some of the subtleties of the mechanisms that come into play.

Let us now summarize the present state of our knowledge about the spatial anisotropies and the *modulation* mechanisms that produce them, but defer until the next chapter further discussion of time variations attributable to the local production of cosmic rays by the sun. Before attempting to understand the role played by the sun in all of these matters, we should digress for a brief review of the relevant solar physics. Fortunately, for the present purposes, we need not be armed with a complete picture of the sun and of the fantastic and, for the most part, little-understood modes of energy transformation that occur on our nearest star. Rather, it will suffice to focus our attention on the means whereby the sun exercises control over the electromagnetic conditions in interplanetary space and the immediate environs of our planet.

THE SUN AND THE INTERPLANETARY MEDIUM

A brand-new scientific discipline, *solar-terrestrial physics,* embraces the study of the sun and its emissions, of the interplanetary medium, and of the earth's environment. Research in this field falls into two general categories. Essentially steady-state conditions characterize the so-called *quiet sun,* a term which, of course, implies only relative calm. Superposed upon this base are disturbances, or storms, that collectively comprise *solar activity,* the distinguishing feature of the *active sun.*

The Quiet Sun. Four concentric regions can be delineated. The *interior,* from which radiant energy does not escape directly, consists of the *core,* the sun's thermonuclear power house, surrounded by the *convective envelope* that extends about one hundred thousand kilometers to just below the visible exterior.

The *photosphere* is the apparent surface. This thin layer, only a few hundred kilometers in depth, is the origin of the visible radiation which, roughly speaking, corresponds to that from a black body at a temperature of almost 6000°K. Under high resolution, structural details called *granules* can be seen.

The *chromosphere* is a dynamic transition region, about 10,000–15,000 km thick, between the "cool" photosphere and the "hot" corona. It is the seat of shortwave radio frequency radiation, ultraviolet light, and x rays. Complex and inhomogeneous, it is characterized by rapid temperature changes and a high level of excitation. A sort of prairie-fire effect is produced by the motions of close-packed *spicules*—jet-like prominences, with lifetimes of several minutes and velocities of about 20 km/sec, that can reach heights of 10,000 km.

The *corona* is the tenuous outer highly ionized gaseous atmosphere of the sun. Although the corona is usually represented in eclipse photographs as extending outward to a distance of several solar radii, in reality the earth is immersed in the corona, which continues out to even much greater distances from the sun. Although the intensity of coronal light is only about a millionth of that of sunlight, processes corresponding to temperatures of millions of degrees occur. The corona is also a source of x rays and radio-frequency radiation.

The Active Sun. Solar activity is the manifestation of the occurrence on the solar surface of a number of discrete, local perturbations, or *active regions,* with individual lifetimes that, typically, may range from one day to three months. Some live almost a year. A *solar-activity center* develops in an area about one-tenth of the solar disk. Its development is accompanied by the appearance of a number of features that distinguish the active sun from the quiet sun. These active regions characterize *solar cycles,* the duration of which is 10 to 14 years. Their frequency of occurrence, average size, and lifetime first increase and then decrease until they eventually disappear entirely. New-cycle active regions may appear as long as 30 months before the old cycle has ended. No adequate physical picture of the solar-cycle variation has yet been developed. In point of fact, the solar cycle connotes much more than a variation of sunspot numbers. However, systematic data on this index of the level of solar activity extends over more than two and a half centuries, and some recorded observations date back to the time of the discovery of sunspots by Galileo in 1610.

With only one exception, all of the features related to the active

sun, including the shape of the corona, follow the solar cycle, but to a widely varying extent. No clear variation in the integrated visible light output has been measured as yet.

Sunspots are dark regions that are 1000°–1500° cooler than the surrounding photosphere. Their sizes range from hundreds of kilometers (*intergranular dark spots*) to 10^5 km (areas of a billion square miles!), and their lifetimes, roughly correlated with size, are as long as many months. Strong magnetic fields up to about 3000 gauss and perpendicular to the surface may develop before the spot becomes visible, and may persist afterwards. Sunspots rarely occur at latitudes above 35° or 40°. Spots in a new cycle appear at the higher latitudes, and drift toward the equator as solar maximum approaches. They often occur in pairs of opposite polarity (*bipolar* spots). The polarity orientations (sign of leading and following members) in the two hemispheres are consistently opposite, and reverse in alternate 11-year cycles.

Faculae, as seen in white light, or monochromatic *plages,* are areas that are brighter than their surroundings because, in general, they are several hundred degrees hotter. Somewhat larger than granules, they can appear at higher latitudes, and may cover 10% of the solar disk. They surround all spots and spot groups, but their lifetimes are longer. These features are always associated with magnetic fields.

Prominences look like projections of the photosphere into the chromosphere, and their form and pattern are varied. Typically, the longest dimension is 10^5 km. They are cooler, denser, and more opaque than the surrounding coronal material, and may move at velocities of hundreds of kilometers per second. Their lifetime is several weeks. They may disappear catastrophically, and then reappear in the original form, repeating this behavior several times. Prominences seem to be shaped by the local magnetic field. High-resolution photographs reveal a fibrous or webby fine structure. They are often associated with sunspots although they may occur at high heliographic latitudes where there are no sunspots.

Filaments are thin or blade-shaped prominences that are observed in *spectroheliograms,* photographs with light in a very narrow wavelength band. They are projections, viewed from

above, of stable prominences lying across lines of force at the top of an arch connecting two magnetic regions of opposite polarity, supported like a hammock. *Flocculi* are wormy-looking bright or dark short filaments.

Flares, or sudden chromospheric eruptions, are catastrophic events that can have almost immediate repercussions at the earth. We shall have occasion to describe in detail the characteristics of these most violent of all solar phenomena in discussing solar cosmic rays.

The Solar Wind. Although correlations between certain geophysical effects and sunspots had been known for many years, the nature of the sun-earth links was a long-standing and challenging mystery. Perhaps the first inkling of the solution struck Störmer when, as was noted earlier, he considered the possibility that the aurora is produced by low-energy electrons emitted by the sun.

The foundations of our current understanding of the subject were the theoretical studies started by S. Chapman in 1927. These came to fruition in calculations published by Chapman and V. C. A. Ferraro in 1931. They attributed a number of observable geomagnetic effects to the impact on the earth of a jet of ionized but electrically neutral gas that swept past the earth roughly a day after being emitted by the sun. This type of highly conducting particle stream is, in fact, now called a plasma, and the study of its properties falls within the domains of *magnetohydrodynamics* and *plasma physics.**

The next milestone was the recognition in 1951 by L. Biermann that the large acceleration of Type I comet tails, which could not be accounted for by the radiation pressure of sunlight, could be caused by a rather intense flux of low-energy protons blown outward from the sun. The fact that these tails persisted even when there were no magnetic storms, and when comets moved outside of the ecliptic plane, seemed to suggest a continuous ejection in all directions from the sun.

In 1954, Chapman proposed a static model of the solar corona,

* See MOMENTUM Book No. 11, *Plasmas—Laboratory and Cosmic,* by F. I. Boley (1966) and MOMENTUM Book No. 18, *Magnetohydrodynamics,* by N. C. Little (1967), Van Nostrand, Princeton.

envisaging the earth as being located inside it, in which the charged-particle density was about 300 electron-proton pairs per cubic centimeter at the earth's orbit. However, certain difficulties stemmed from the differences between the observed temperature distribution at the sun and that required to transfer energy from the coronal base by thermal conduction.

The great breakthrough came in 1958, when E. Parker proposed a theory in which hydrodynamic streaming of plasma continuously ejected by the sun is the energy transport mechanism. The outwardly expanding coronal gas moves at hypersonic velocity. In analogy with the propagation of supersonic acoustic waves in which the wave velocity exceeds the velocity of sound in the medium, $(\gamma p/\rho)^{1/2}$, in this case the particle velocities exceed the analogous *Alfven velocity*, $(B^2/4\pi\rho)^{1/2}$. Parker christened the radially streaming plasma the *solar wind*. His predictions concerning its properties have been borne out in detail by both *in situ* measurements by spacecraft and ground-based observations. Furthermore, investigations by Parker and a number of others, of the cosmic-ray intensity modulations produced by the solar wind, have provided a general understanding of the mechanisms that cause the different intensity variations. The search for new phenomena to which the solar wind might be expected to give rise is still in progress.

The average characteristics of the solar wind in the vicinity of the earth are listed in Table 6-1. It is remarkable that such profound effects can be wrought by this minute concentration of

TABLE 6-1. *Average Characteristics of the Solar Wind Near the Earth's Orbit. Values in Parentheses Represent Typical Ranges.*

Composition	Protons, electrons, and a few percent α particles
Flux	5×10^8 particles/cm^2/sec
Velocity	500 (300–600) km/sec
Density	10 (1–20) particles/cm^3 (of each sign)
Thermal Energy	10 eV
Temperature	10^5 °K
Mean Free Path	1 AU
Proton Energy	1 keV
Electron Energy	10 eV
Magnetic Field	5 (3–15) $\times 10^{-5}$ gauss
Conductivity	100 (ohm–cm)$^{-1}$

matter in an otherwise perfect vacuum (except for 10^{-5} cometary dust particles per cm^3)! The special abilities of the solar wind to push charged particles around reside in the magnetic field that it transports. For magnetic fields rooted at the sun are literally pulled out into space like taffy and carried along by the outgoing plasma.

To understand how this happens, we must recall Lenz's law, according to which a good conductor tends to resist any change in its internal magnetic field. Any alteration of the field produces an electromotive force, in accordance with Faraday's law, and this emf produces a current, the associated field of which opposes the magnetic field change. Ordinarily, these currents would damp out rapidly because of the finite resistance of the conductor. But the conductivity of the interplanetary medium is so high that the current does not die out, with the result that the solar plasma transports the magnetic field away from the base of the corona. This *frozen-in magnetic field* remains with the plasma, even though the lines of force may become kinked.

The solar wind continues to blow until it reaches a distance from the sun r_0 at which the energy density of the solar magnetic field $B_s^2/8\pi$ ergs per cubic centimeter has decreased to that of the galactic magnetic field $B_g^2/8\pi$ ergs per cubic centimeter.

An interesting twist is introduced by the rotation of the sun. Since the plasma is accelerated radially outward from the sun, the interplanetary field lines would also be radial if the sun were fixed. But the sun rotates with uniform angular velocity Ω as illustrated in Fig. 6-1. Particles emitted with velocity v from points 1–4 at successive equal intervals of time Δt reach points 1′–4′ at time $4\Delta t$. The distance that each particle has traveled in each Δt is marked on the radial line that traces its path. The frozen-in field, firmly anchored to the sun, follows the heavy line, an *Archimedean spiral,* exactly like the stream of water emerging from a rotating lawn sprinkler. The *stream angle* or *garden hose angle* is given by:

$$\tan \xi = \frac{\Omega r}{v}. \tag{6-1}$$

Since $\Omega = 1$ rev/27 days $\simeq 2.7 \times 10^{-6}$ radians/sec, and at the

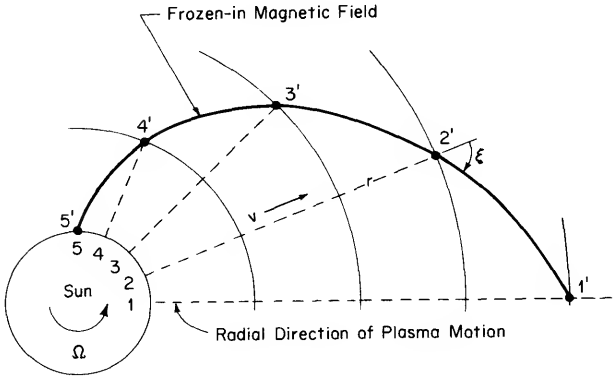

FIG. 6-1 Archimedes spiral configuration of magnetic field lines frozen into plasma moving radially outward from the rotating sun. At the earth's orbit, the garden-hose angle ξ is about 45°.

orbit of earth $r \simeq 1.5 \times 10^{13}$ cm, we find that the garden hose angle corresponding to $v = 400$ km/sec is about 45°.

Another important feature of the interplanetary magnetic field is the observed sector structure. As is indicated schematically in Fig. 6-2, the field points predominantly toward the sun for a period of 6 or 7 days, and then in the reverse direction for a similar interval. Of course, when the sun is active it is not possible to trace sectors for more than one solar rotation.

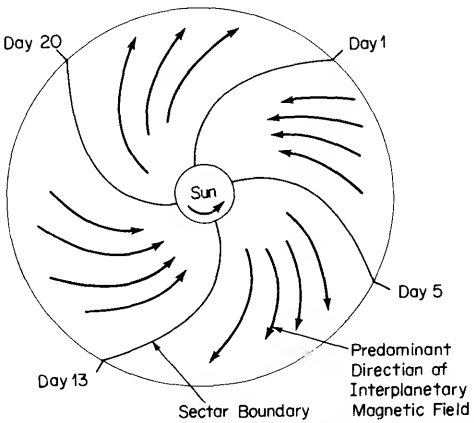

FIG. 6-2 Sector-structure of the interplanetary magnetic field.

Needless to say, this is an oversimplified picture, although it describes the gross features of the interplanetary magnetic field rather well. Effects of changes in the plasma velocity and the magnetic field polarity, or of hydrodynamic shock waves, can introduce small-scale irregularities into the otherwise *ordered field,* or may produce a large-scale *disordered field.* All the different characteristics of the interplanetary magnetic regime in one way or another affect most of the cosmic rays that reach the inner solar system.

The effectiveness of each of the modulation processes is determined by the detailed structure of the interplanetary medium. Thus, for example, the distribution of the scale sizes of magnetic irregularities and the mean distance between them are significant factors. Clearly, the mode of scattering when a particle encounters a clump of twisted and tangled magnetic field lines depends upon whether its gyroradius is small or large compared with the linear dimensions of the scattering center. To see this, we need only note that, roughly speaking, the angular deflection θ of a cosmic-ray particle having a radius of gyration r_g in passing through a field of length x is $\theta = x/r_g$.

MODULATIONS AND ANISOTROPIES

Spatial anisotropies are studied with ground-based instruments by relating observed time variations in the intensity to directions in space via the procedures described in Chapter 4. With the advent of the space age, it has also become possible to observe asymmetries directly by measuring the unidirectional intensities of particles with known characteristics as a function of the spatial orientation of the detector. In general, these two methods are complementary, since they cover different energy ranges.

In utilizing cosmic rays as space probes for investigating both the gross and detailed properties of the interplanetary medium, one attempts to deduce various physical parameters by comparing the data with the predictions of theoretical models. For example, it is possible to determine the mean free path between the scatterings that occur when a particle collides with small-scale magnetic irregularities. Needless to say, untangling all of the rele-

vant factors poses a complex problem, but, fortunately, relatively simple models can often be invoked to yield an understanding of the underlying physics.

An important characteristic of any modulation process is its dependence upon magnetic rigidity, since the interactions of particles with interplanetary magnetic fields are the root cause of the anisotropies. The relationship between the fractional change in intensity $\Delta j(P)/j(P)$ and the rigidity P is called the *variational spectrum*. One form of the spectrum of variation is

$$\frac{\Delta j(P)}{j(P)} = KP^{-\gamma}. \tag{6-2}$$

Thus, $\gamma = 0$ connotes equal attenuation of the intensity of particles of all rigidities.

Diurnal Variation. Figure 6-3 shows the average daily variation, as observed by a particular neutron monitor. The percentage deviation of the counting rate from the mean is plotted as a func-

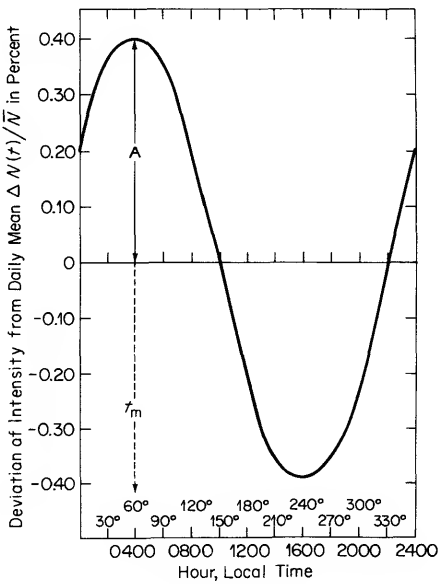

FIG. 6-3 Twenty-four hour variation in the cosmic-ray intensity.

tion of local time. The *amplitude* $\overline{A}$ and *time of maximum* t_m are indicated.

A periodic variation can most conveniently be represented by a vector of length proportional to the amplitude, and pointing toward the direction (or time) of maximum intensity. This vector completely describes the spatial anisotropy.

The observed diurnal variation can be split up into its *harmonic components* by a *Fourier analysis.* Let us consider just the *first harmonic* or *24-hour wave* plotted in Fig. 6-3. $\Delta N(t)$, the deviation of the counting rate at time t from the daily mean, is given by

$$\Delta N(t) = a \cos t + b \sin t, \tag{6-3}$$

where t is expressed in degrees. Since 360° represents 24 hours, an hour is equivalent to 15°. This equation can be put into more convenient form by a simple transformation. Let

$$\begin{aligned} a &= \overline{A} \sin \epsilon, \\ b &= \overline{A} \cos \epsilon. \end{aligned} \tag{6-4}$$

Then

$$\Delta N(t) = \overline{A} \sin (t + \epsilon). \tag{6-5}$$

According to this equation, $\Delta N(t)$ attains its maximum value $\overline{A}$ at time t_m, where $(t_m + \epsilon) = \pi/2$. Now let us construct a vector that represents both amplitude $\overline{A}$ and time of maximum t_m. We can plot this vector in polar coordinates on the *harmonic dial* shown in Fig. 6-4. The virtue of this *clock diagram* is that the vector **A** points directly toward the time of maximum t_m, since $\epsilon = (\pi/2) - t_m$. The Fourier coefficients given by Eq. (6-4) correspond to the components a and b of the vector **A** in the two directions at right angles.

A similar analysis can be carried out to determine higher harmonics that may also be present. Attention has generally been limited to the first two harmonics. In the case of the *second harmonic* or *semi-diurnal variation,* the vectors are plotted on a 12-hour clock.

The diurnal variation vectors may fluctuate appreciably from day to day. This is illustrated in Fig. 6-5, where the dots repre-

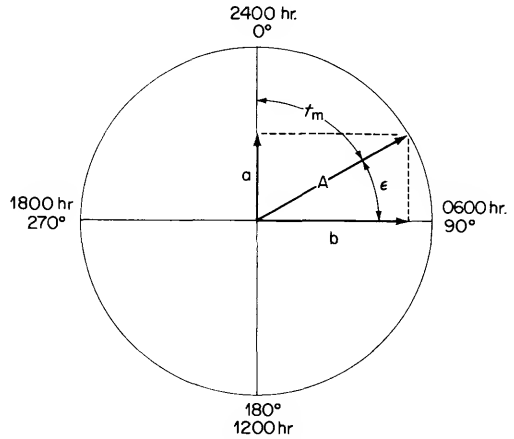

FIG. 6-4 Harmonic dial representation of the diurnal variation.

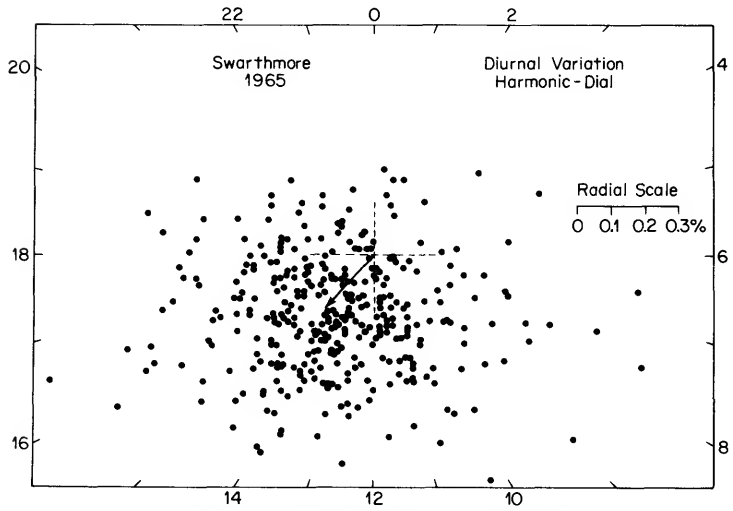

FIG. 6-5 Daily variation vectors (from origin to dot) on individual days during an entire year. Arrow represents the annual mean.

sent the heads of the individual daily vectors determined from observations extending over an entire year. The arrow is the annual mean.

The striking feature is that, despite the great scatter, the

average amplitude and direction of the diurnal vector is quite persistent. We can see this by adding the monthly mean vectors for the same year, as in Fig. 6-6.

Next, in Fig. 6-7, we note that the direction of the diurnal anisotropy is rather constant from year to year. However, after realistically evaluating the uncertainties, which is no easy chore, we find that the amplitude is not constant. The reality of this effect is confirmed by Fig. 6-8, which shows the solar-cycle vari-

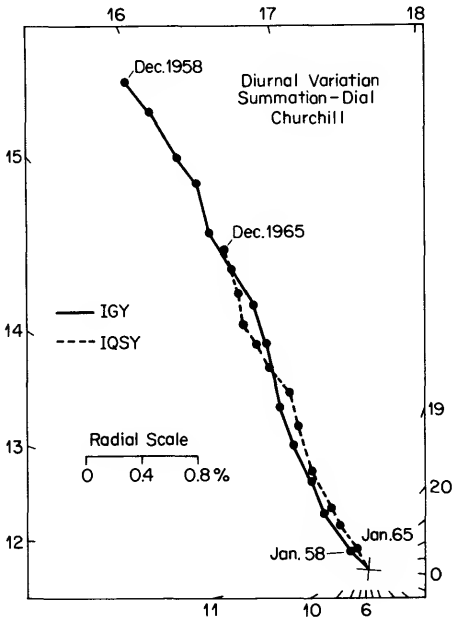

FIG. 6-6 Summation dial. Each vector, added to the preceding one, represents the monthly mean diurnal variation.

ation in the amplitude of the daily variation as revealed by analysis of the "long-playing records" of the Carnegie ionization chambers.

Thus far, we have been referring to the time of maximum, or the *phase* of the diurnal variation, in terms of the local solar time of the observing station. To determine the direction in space of the apparent source of the maximum intensity, we recall that it

is necessary to correct for *geomagnetic bending* of the primary particles to which the detector responds. This is accomplished by the procedures already outlined in Chapter 4. The arrows in Fig.

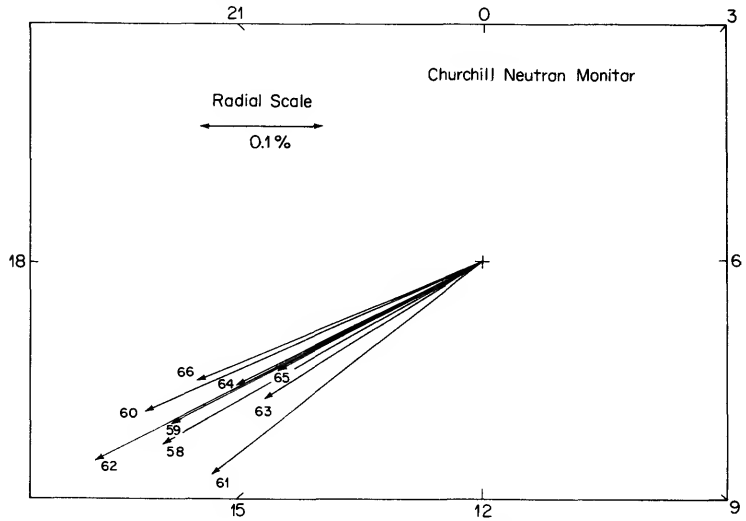

FIG. 6-7 Annual mean daily variation over a complete solar cycle.

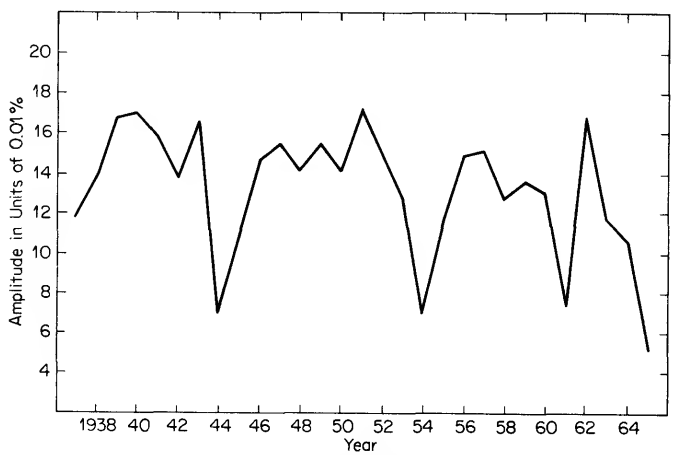

FIG. 6-8 Amplitude of the solar daily variation of the meson intensity as determined from ionization chamber records extending over nearly three decades.

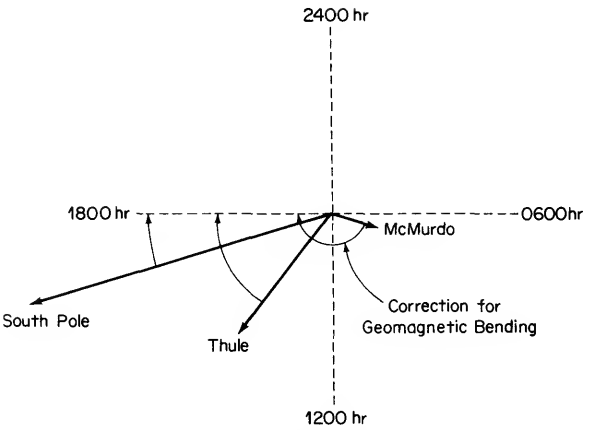

FIG. 6-9 Diurnal variation at several stations as observed in local solar time, and the calculated corrections for geomagnetic bending.

6-9 are the mean vectors at several different stations before correction for bending. The arcs indicate how far each vector must be rotated, according to calculations of the asymptotic cones, to make it point toward the real time of maximum. It is indeed comforting that the vectors derived from the observations at different locations all line up, and the amplitudes differ as they should.

Figure 6-10 suggests why the maximum intensity is seen at 1800 hours local solar time. The spiral interplanetary magnetic field co-rotates with the sun, more or less as though it were a rigid structure. Thus, the isotropic cosmic-ray "gas" is stirred around by the great paddle wheels, imparting to it a velocity of a few hundred kilometers per second. Since this is faster than the velocity of the earth along its orbit, the intensity coming from the direction 90° East of the sun-earth line is enhanced, whereas that arriving from the opposite direction, 90° West, is reduced. Calculations based upon this model predict roughly the observed amplitude. Furthermore, the expected amplitude varies as the cosine of the latitude, in accordance with the observations.

On the average, the variational spectrum of the daily variation is of the form of Eq. (6-2), with $\gamma \simeq 0$, up to a limiting rigidity, P_u, above which the diurnal anisotropy disappears. Thus,

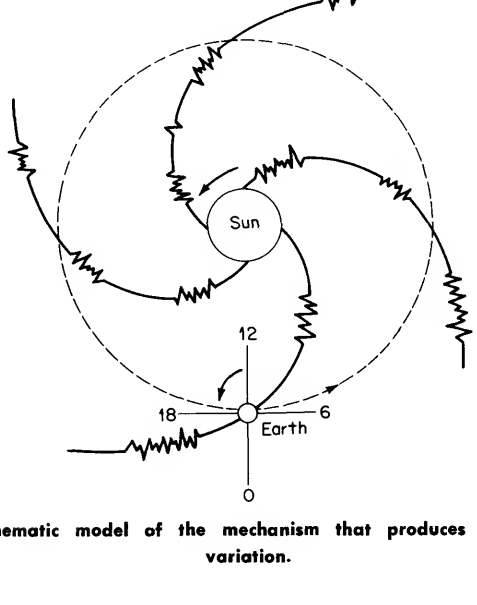

FIG. 6-10 Schematic model of the mechanism that produces the solar daily variation.

$$\frac{\Delta j(P)}{j(P)} = K \qquad P < P_u,$$

and

$$\frac{\Delta j(P)}{j(P)} = 0 \qquad P > P_u. \tag{6-6}$$

P_u changes during the solar cycle, and may range from as low as 55 GV at solar minimum up to 100 GV at solar maximum. Of course, as the scatter of the vectors in Fig. 6-5 suggests, short term fluctuations in the spectrum may be quite large.

The study of the 24-hour periodicity, with a mean amplitude of several tenths of a percent, poses an exceedingly challenging problem. Even with the newest techniques, and despite their capabilities for providing greatly reduced statistical uncertainties, many difficulties remain, and definitive results are not easy to come by. Since the upper limits that have been determined for the magnitudes of semi-diurnal and sidereal variations are appreciably smaller, it goes without saying that discussion of their implications is somewhat more speculative.

The amplitude of the semi-diurnal variation is less than 0.1% and the intensity seems to be maximum in both directions along the line 135° west of the earth-sun line. This is more or less perpendicular to the direction of the interplanetary magnetic field. The spectral index (Eq. 6-2) is $\gamma \simeq 1$ up to $P_u \simeq 100$ GV. The presence of the second harmonic appears to imply the existence of a cosmic ray *density gradient,* that is perpendicular to the equatorial plane.

The apparent sidereal variation is only a few hundredths of a percent. It is, indeed, the proverbial needle in the haystack. Questions about its reality are still being raised on several counts. To appreciate the nature of the difficulty, one need but recall that the sidereal day differs from the solar day by only four minutes, which amounts to just one day per year. Consequently, the shadow of spurious variations generated by the solar wave looms ominously as a major source of uncertainty.

Forbush Decrease. In contrast with the diurnal variation which is a *local-time* effect, the other types of modulation are *universal-time* effects. This means that their repercussions are felt all over the world almost simultaneously, even though, in some cases spatial anisotropies can produce temporary asymmetries. Thus, the Forbush decrease is essentially a universal-time phenomenon, although small differences in *onset time,* or other features can occur.

A Forbush decrease is a very sudden reduction in the cosmic-ray intensity, followed by a much slower recovery, as is illustrated in Fig. 6-11. Typically, the counting rate of a neutron monitor drops as much as 5% within a few hours, although this can stretch out to as long as two days. The *recovery* to pre-decrease level may extend over an interval of several days to several weeks. The superposition of several Forbush decreases, as in Fig. 6-12, is called a *cosmic-ray storm.*

Transient intensity decreases often occur in association with magnetic storms, but there is not a one-to-one correspondence. Either phenomenon may happen without the other. Both of these effects are often observed one or two days after a solar flare. This delay corresponds to the transit time of plasma ejected toward the earth in the explosion.

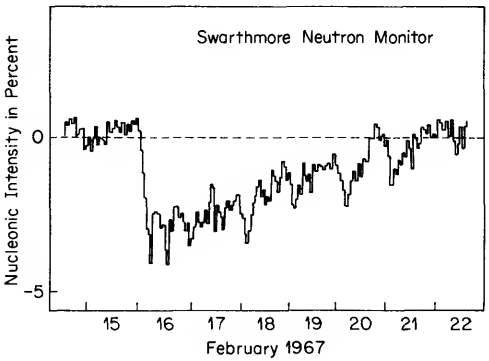

FIG. 6-11 Typical Forbush decrease.

Because of the apparent correlation between geomagnetic disturbances and cosmic-ray intensity, Forbush decreases were first ascribed to effects localized at the earth itself, such as time variations in the magnetic field. However, the fact that they were observed at polar stations, where the cutoff is atmospheric rather than geomagnetic, coupled with other arguments pointed toward a more far-reaching phenomenon. Observations with deep-space probes have since revealed that, in fact, the scale size of these events is greater than 0.1 AU, and may well exceed 1 AU.*

A Forbush event may display a great deal of fine structure. There is sometimes a precursor which manifests itself either as a *pre-increase* or a *pre-decrease*. Spatial anisotropies can also occur. This is illustrated in Fig. 6-13, which is especially interesting because it was the first example of a north-south asymmetry, an effect that has been very elusive. Furthermore, the magnitude of the intensity drop usually depends upon latitude since the typical variational spectrum (Eq. 6-2 with $\gamma \simeq 1$) is an inverse dependence upon rigidity. Finally, trains of enhanced diurnal variation, with amplitude even exceeding 1%, are sometimes observed, as is shown in Fig. 6-14.

As are all cosmic-ray intensity modulations, the Forbush de-

* AU is the abbreviation for *astronomical unit*, the mean distance of the earth from the sun $= 1.496 \times 10^8$ km.

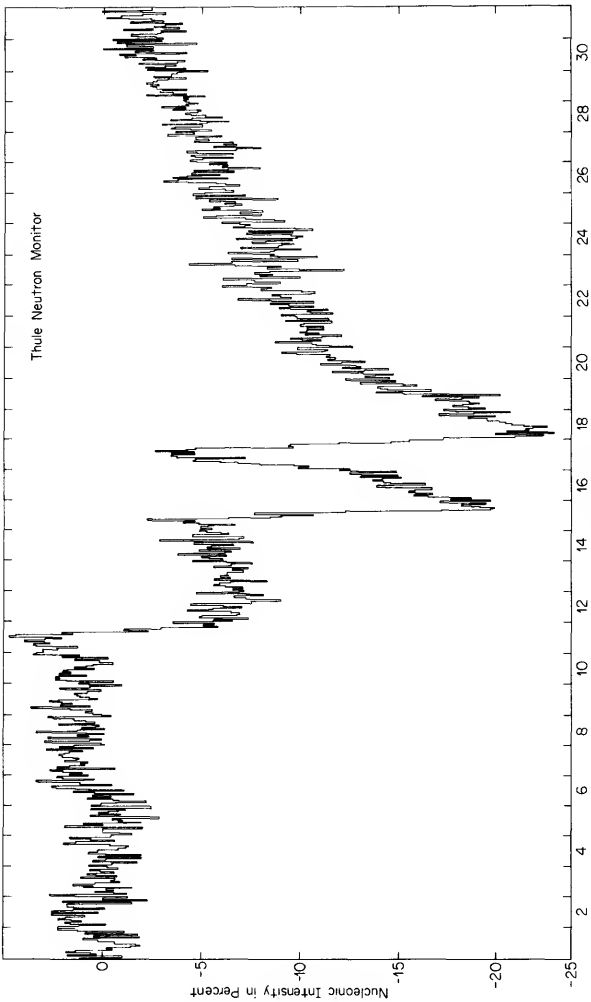

FIG. 6-12 Outstanding cosmic-ray storm.

crease is a solar-wind phenomenon. The magnetic plasma cloud ejected by a solar flare at a velocity greater than that of the plasma which preceded it causes a *blast wave* as in Fig. 6-15. This sweeps particles away as it expands, leaving the volume in back of it partially depleted of cosmic rays. This effect can also be visualized as a *magnetic tongue* or *bottle* that, as in Fig. 6-16, excludes some galactic cosmic rays from its volume. Thus the bubbles of solar plasma can act as cosmic-ray shields.

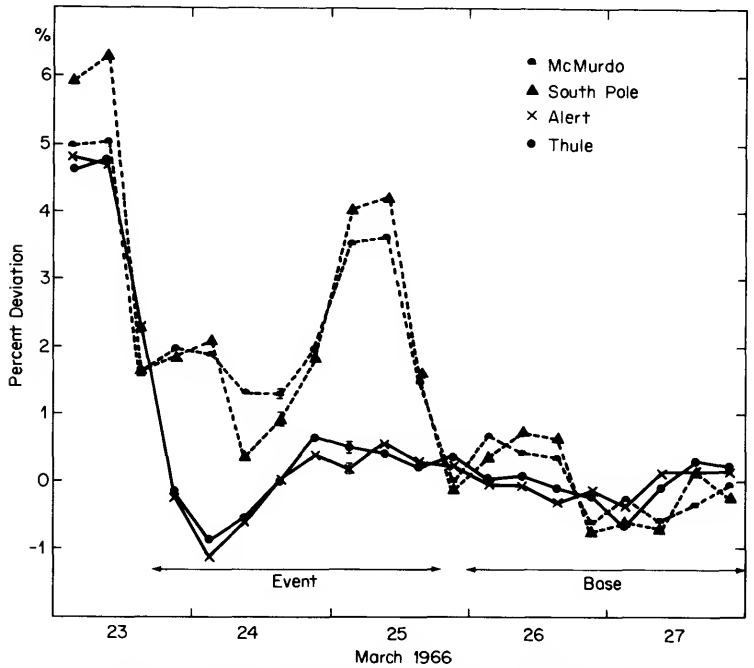

FIG. 6-13 Forbush decrease exhibiting a north-south asymmetry, indicative of a spatial anisotropy perpendicular to the plane of the earth's orbit.

27-Day Recurrence Tendency. Forbush decreases tend to recur at intervals of 27 days, the synodic rotation period of the sun, just as do geomagnetic storms which stem from the same cause. In fact, diminutive versions of the Forbush decrease may recur many times.

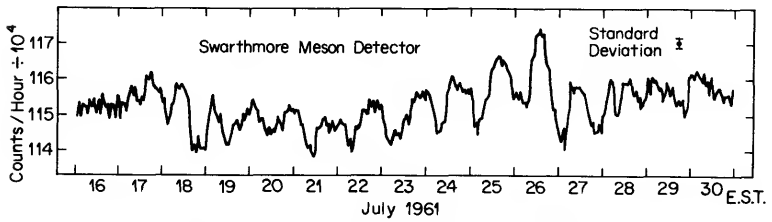

FIG. 6-14 Train of enhanced diurnal variation.

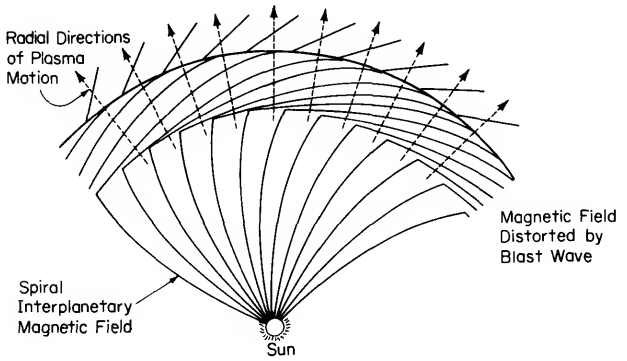

FIG. 6-15 Schematic representation of blast wave mechanism that can produce a temporary reduction in the cosmic-ray intensity.

One technique for investigating recurrence tendencies is the method of *superposed epochs* or *Chree analysis.* Suppose we choose as *zero* day, $N = 0$, those days that show a particular feature, such as appreciably higher than average (or lower than average) intensity. We then write down the intensity for the *following* days, $N = 1, 2, 3 \ldots n$ and the *preceding* days $N = -1, -2, -3 \ldots -n$. The average value for each of these $(2n + 1)$ days is then plotted against N, as in Fig. 6-17. Statistical procedures, such as *autocorrelation* or *power spectrum* analysis, are also useful for investigating recurrent phenomena.

Long Term Variation. The solar wind blows unceasingly. But the electromagnetic conditions in the *solar magnetic cavity* that it carves in space reflect the changes in the level of solar activity, and respond to discrete outbursts on the sun. Thus, the interplanetary weather can be quite stormy. And it is not surprising that, in addition to individual storms, there are "seasonal" changes in the average characteristics during the solar-activity cycle. All of the transient and periodic intensity variations that have already been described evidence these changes. As Fig. 6-18 testifies, even the variations vary over the 11-year period! But, in addition, there is one other exceedingly important process, the *long-term modulation,* that transcends all the other temporal changes.

Fig. 6-19 shows the change in intensity during the most recent

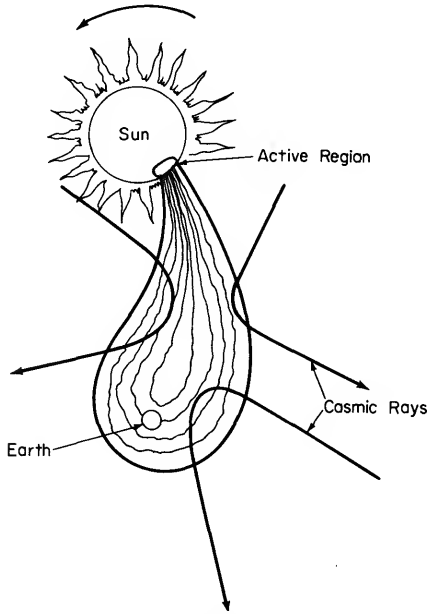

FIG. 6-16 Magnetic bottle model of the modulation of cosmic-ray intensity during a Forbush decrease.

solar cycle, as observed with a high latitude neutron monitor. Of course, the magnitude of the change depends upon the nature of the detector and the range of solar activity. Typically the total reduction from solar minimum to solar maximum is about 20% for nucleons, and 5% for mesons. These figures suffice to expose what is happening. As solar activity increases, more and more galactic cosmic rays are being denied admission to the inner solar system. Furthermore, the lower the rigidity of a particle, the less chance it has to reach the earth's environs.

This implies that the observed primary spectrum differs from the unabridged galactic spectrum that prevails beyond the boundary of the solar magnetic cavity. Until recently, it was generally believed that the spectrum measured at solar minimum would closely resemble the bona fide galactic spectrum. But, Fig. 6-20 reveals how drastically our views on this subject have changed.

Just as the solar wind theory was successful in predicting the

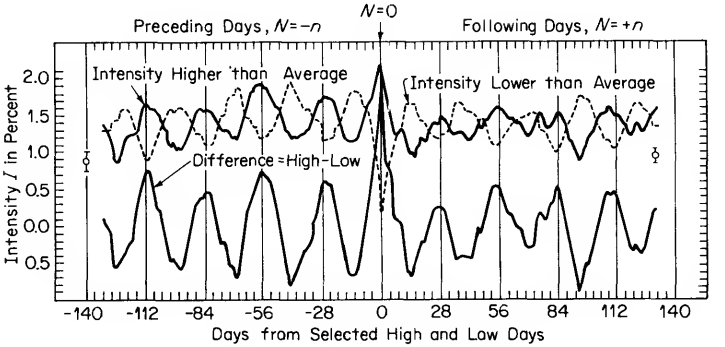

FIG. 6-17 Method of superposed epochs for investigating recurrence tendencies. The 28-day separation of the peaks corresponds to the sun's rotational period.

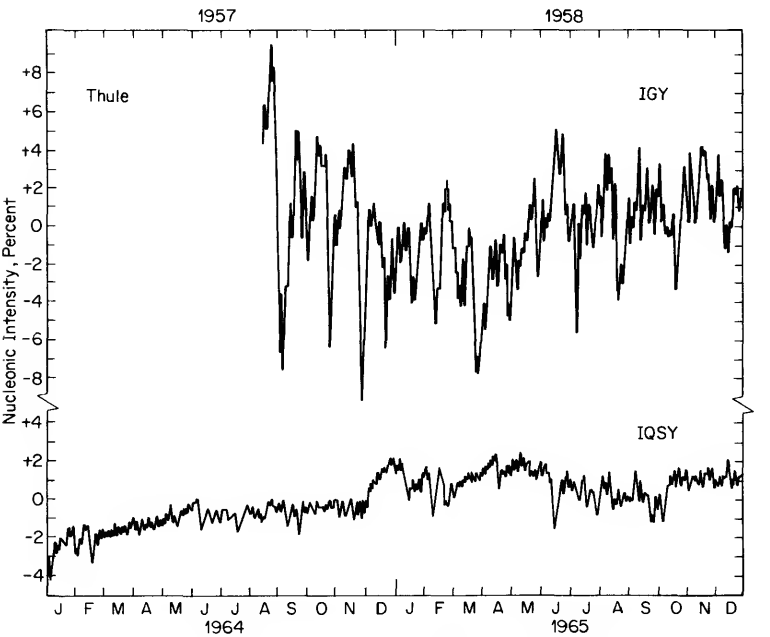

FIG. 6-18 Neutron monitor data recorded during a period of maximum solar activity (IGY = International Geophysical Year) and minimum solar activity (IQSY = International Years of the Quiet Sun). The two scales are the same. In each case, the ordinates represent deviations of the daily mean intensity from the mean over the entire corresponding period.

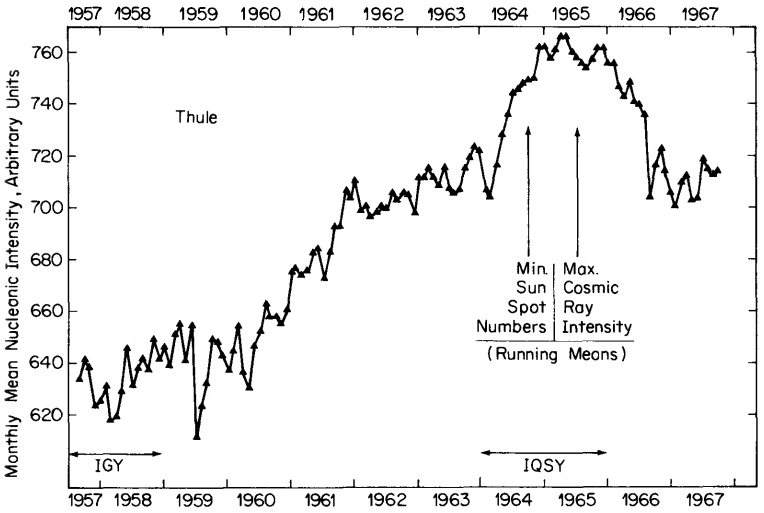

FIG. 6-19 Intensity of the nucleonic component at a high latitude station during one solar cycle.

properties of the interplanetary medium and in accounting for the other cosmic ray modulations, it has also explained the solar-cycle variation. The basic mechanism is the *convective removal* of galactic cosmic rays by encounters with the magnetic field irregularities carried outward from the sun by the "steady state" solar wind. The cosmic ray density in the inner solar system represents a balance between outward convection and inward diffusion. This implies that, even at solar minimum, the cosmic-ray spectrum observed at earth is not the galactic spectrum. The latter must be unfolded from the experimental data with the help of a theoretical model.

The form of the rigidity-dependence of the long-term modulation is of paramount importance, since it is crucial in extrapolating the observations out into the galaxy. Because of the action of the outward-blowing solar wind, the flux of cosmic rays is progressively reduced as the sun is approached. In other words, there is a density gradient, and diffusion theory tells us that the fractional change in the cosmic-ray density N (Eq. 5-4) per unit radial distance from the sun is

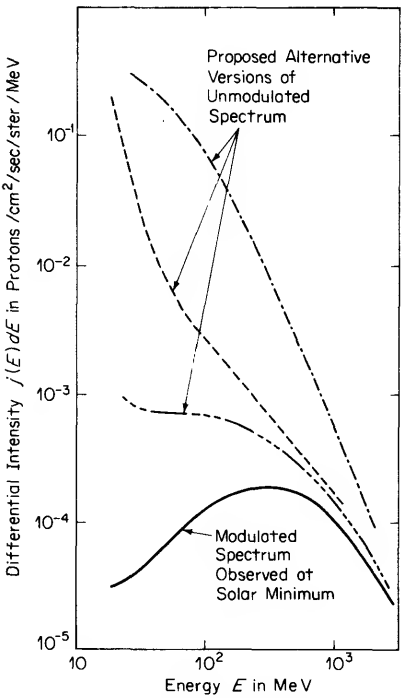

FIG. 6-20 Galactic cosmic-ray spectrum according to several different evaluations of the effects of solar modulation. The curve nearest to the spectrum observed during the most recent solar minimum epoch now seems to be the most reasonable.

$$\frac{\partial N}{N\partial r} = \frac{3v_w}{v_p\lambda_i}, \tag{6-7}$$

where v_w is the solar wind speed, v_p the particle speed, and λ_i is the mean free path for collisions between a cosmic-ray particle and a scattering center. Integration gives the ratio of the observed density N_r of cosmic rays with rigidity P at a distance r from the sun to the density N_{r_0} beyond r_0, the boundary of the region of solar modulation. In its simplest form, this can be written

$$N_r/N_{r_0} = \exp(-K_v/D), \tag{6-8}$$

where D is the diffusion coefficient describing the motion of the particles in the solar magnetic fields that permeates interplane-

tary space. K_v is a quantity related to the bulk outward speed of the solar plasma, and to the extent of the region of modulation about the sun. D depends upon the rigidity and species of the particle, and can be evaluated from experimental data. K_v is independent of these parameters, and its absolute value (and hence the total modulation) has not yet been determined experimentally. Fig. 6-20 shows that there have been some differences of opinion as to the correct evaluation of D, and the best estimate of K_v.

Details such as the energy losses (and gains) suffered by the incoming particles as a consequence of deceleration (and acceleration) processes, also need to be taken into account. Nevertheless, the basic principles underlying this model seem to be borne out by most of the available experimental data, which, in turn, show how the theoretical model needs to be refined in the next approximation.

Returning to Eq. (6-7), if we insert the values $v_w \simeq 500$ km/sec, $\lambda_i \simeq 0.05$ AU, and $v_p \simeq c$, we find that, near the orbit of the earth, the *space gradient* for particles with rigidities in the GV range should be about 10% per AU. Although measurements by deep space probes, extending over about 0.4 AU, seemed to be consistent with expectation, there is considerable dispersion among the conclusions of different experimenters.

Earlier estimates of r_0, the distance at which the momentum density of the solar wind decreases to the point at which it is stopped by the interstellar magnetic field, were based upon the time interval between sunspot minimum and cosmic-ray maximum (Fig. 6-19). If one argues that this lag is the travel time required for the solar wind to reach its outer boundary, then, since $r_0 = v_w t$, with $v_w \simeq 500$ km/sec and $t \simeq 8$ months, the boundary would be at about 70 AU.

Measurements of the space gradient have suggested that the solar magnetic cavity is actually much smaller, and may extend out to only 5 or 10 AU. Furthermore, there is no *a priori* reason for regarding sunspots, a photospheric phenomenon, as a precise index of the relevant solar-wind parameters, which represent the state of the corona. This is borne out by the virtual disappearance of the lag when the intensity of the 5303Å coronal green

line in the solar equatorial region is substituted for sunspot numbers.

It is interesting to note that, since the gyroradius of a 10^{12} eV cosmic ray in a magnetic field of 5×10^{-5} gauss is of the order of 5AU, the interplanetary field dominates the motion of particles with energies below this limit. These particles constitute 99.9% of the cosmic radiation.

Many details are now being subjected to close scrutiny through definitive experiments in space. For example, the comparison of the modulation experienced by different species, especially at very low energies where the effects are greatest, provides sensitive criteria for deciding upon the validity of various models that have been proposed.

An alternative explanation of the modulation in terms of an electrostatic field had been suggested earlier, but was subsequently shown to be inconsistent with the more recent observations. However, the electric field produced by the time variations of the electromagnetic field associated with the fluctuating solar wind, and analytically resembling a heliocentric field, provides the basis for a somewhat different and useful theoretical approach.

In any case, theoretical and experimental studies of the cosmic-ray intensity modulations are being pursued vigorously. The final answers may not be forthcoming until deep-space probes are able to reach regions that lie far beyond the present limits of accessibility. Until journeys to great heliocentric distances and extended excursions from the ecliptic plane become feasible, local cosmic-ray measurements are likely to provide the only clues as to what it's like out there.

7 *Solar Cosmic Rays*

The kindly shine of summer, when tracked home with the scientific spy-glass, is found to issue from the most portentous nightmare of the universe—the great conflagrant sun: a world of hell's squibs, tumultuary, roaring aloud, inimical to life.

ROBERT LOUIS STEVENSON

It is ironic that, for thirty years after the discovery of cosmic rays, the sun cleverly concealed her ability to spawn her own breed of energetic particles. She protected her secret by endowing most of her offspring with a quota of energy that was not quite enough to enable them to propagate their effects through the earth's atmosphere.

Only on very rare occasions, less than once a year on the average, does she give them the price of a ticket to the earth's surface, so that, through their progeny, their arrival can be heralded by ground-based cosmic-ray instruments. Somewhat more frequently, perhaps ten times as often, they are permitted to penetrate a smaller distance, into the upper atmosphere—the stratosphere where often they are detected by balloon-borne apparatus, and the ionosphere where they produce radio effects that are observed by ground-based equipment. And it now seems that solar particles with such low energies that they can be observed only with interplanetary space probes are being born practically all the time.

All of these *solar energetic particles* differ from the constituents of the solar wind in that they do not engage in the collective motions that characterize the much lower-energy particles comprising the solar plasma. On the other hand, except for their birthplace, they are identical with their counterparts in the galactic cosmic radiation. Consequently, they are generally called

solar cosmic rays. As we review the early history of the study of solar cosmic rays, it will become clear that this seemingly paradoxical terminology is really quite appropriate.

For the first six years after Forbush had fired up the Carnegie ionization chamber network, the only spectacular world-wide intensity fluctuations were all sudden decreases. Then, in rapid succession, came the first two *solar flare increases* shown in Fig. 7-1. Over a span of more than three decades, there have been only three other events with a measurable flux of particles having sufficiently high energies to affect meson detectors. On the other hand, neutron monitors have detected cosmic-ray intensity enhancements at a long term average rate of about one per year.

As is already evident in Fig. 7-1, the magnitude of the deviation from the pre-flare level falls off rapidly with decreasing latitude, indicating that the energy spectrum of solar particles is quite steep. In fact, only on one occasion, the all-time record-shattering event of February 23, 1956, has there been a clear indication of a flux enhancement at the equatorial station, Huancayo, where the geomagnetic threshold is 13.5 GV.

In the early 1950's balloon flights at Swarthmore showed that some solar flares produce only low energy particles which are rapidly absorbed near the top of the atmosphere, and hence do not affect ground-based cosmic-ray detectors. But the time was not yet ripe to see the connection between these lower energy but less rare solar cosmic rays and an ostensibly remote radio phenomenon. For a long time, ionospheric effects related to solar disturbances had been noted at high latitudes. Understandably, observers thought that they were intimately associated with auroral phenomena and geomagnetic storms, as indeed they are.

Finally, in 1957, D. K. Bailey showed that the radio-wave attenuation accompanying the event of February 23, 1956, could not be considered merely as a special case of *auroral absorption.* The following year, K. Anderson's balloon flight at Fort Churchill, Canada, provided the first direct confirmation that the particles responsible for the intense absorption of radio waves at high latitude were mainly protons.

Thereafter, studies of radio-signal intensity records by a number of workers revealed that widespread radio blackouts were

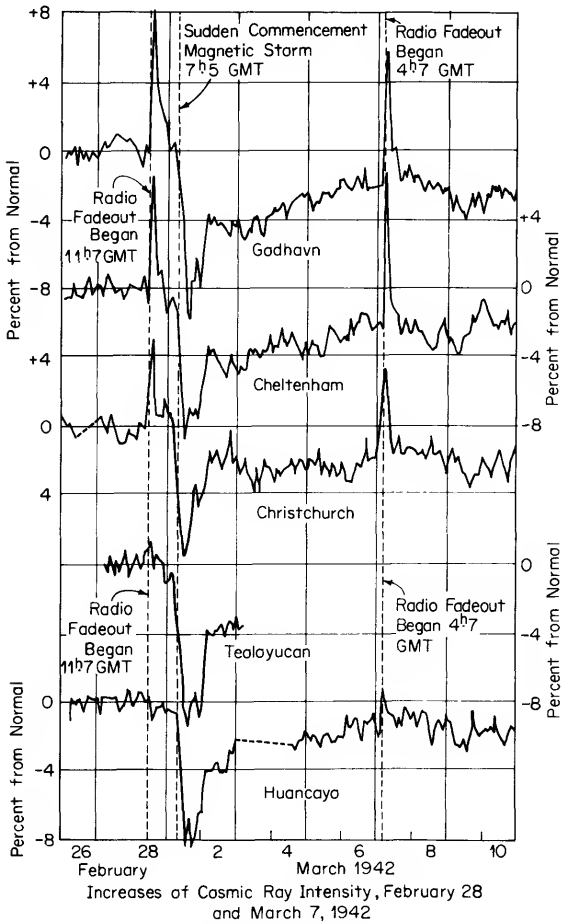

FIG. 7-1 First recordings of solar cosmic rays. Similar occurrences of an increase in the meson intensity have been exceedingly rare.

caused by the arrival of low-energy solar protons throughout the polar regions in *polar cap absorption* (PCA), or *solar proton* events.

The technique of continuously monitoring low-energy solar cosmic rays by making rf signal intensity measurements with radio receivers on the ground facilitated their detailed study by

balloon and rocket-borne instruments. By launching these high altitude research vehicles at appropriate times either while PCAs were in progress or on the basis of predictions (or educated guesses!) of impending solar activity, a great deal of information has been amassed about solar cosmic rays.

Sporadic outbursts on the sun transpire explosively, hence, as might be anticipated, the energy, charge, space, and time distributions of solar cosmic rays vary significantly from one event to another, and even at different times during a single event. Consequently, the generalizations that we shall have to make in order to convey some notion of what happens are subject to notable exceptions. Of course, this is the reason for the unabated interest in studying solar cosmic rays. For each event tells us something new about the sun and the interplanetary medium. Furthermore, spacecraft are continuing to provide new opportunities for definitive experiments, especially by opening up for investigation the extremely low-energy segment of the solar particle population. Indeed, we can learn much about some of the "less dramatic" but more common cosmic acceleration processes by watching them in action on a more or less typical star—the only one whose distance is measured in light minutes rather than in light years.

MORPHOLOGY OF A SOLAR PARTICLE EVENT

Before summarizing some of the salient features of solar cosmic rays, let us consider the sequence of consequences of a solar flare. Figure 7-2 shows the temporal relationships among all of the phenomena that *may* follow a great explosion on the sun. It must be emphasized that most flares produce only some of the indicated effects. Furthermore, the shape of the individual traces depends upon the characteristics of the detector, and other considerations. With these qualifications, this picture can be regarded as typical of a *ground-level event,* that is, one in which enhancement of the particle flux at sea level is observed.

Electromagnetic Emissions. To observe flares visually, the solar disk is viewed through a narrow-band optical filter in the light of $H\alpha$ (hydrogen alpha, the first line in the Balmer-series, 6563Å).

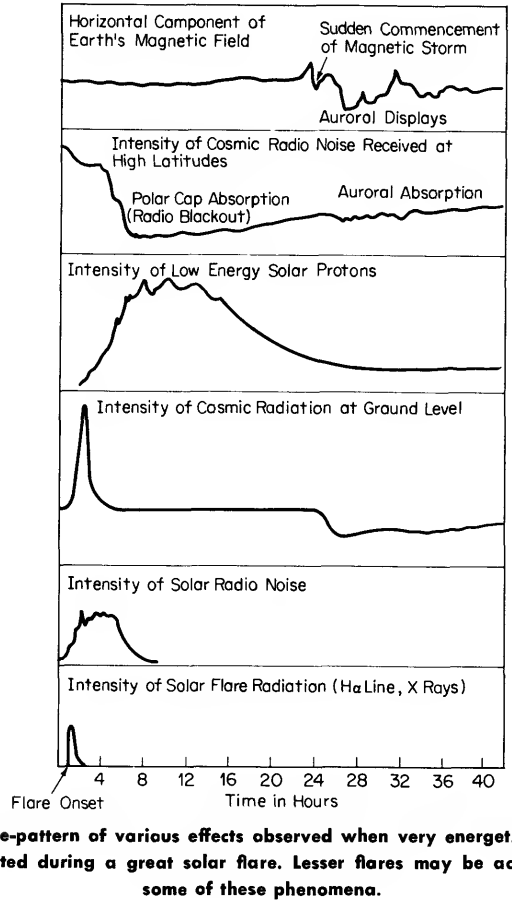

FIG. 7-2 Time-pattern of various effects observed when very energetic solar cosmic rays are emitted during a great solar flare. Lesser flares may be accompanied by some of these phenomena.

Following the notation of Table 7-1, a flare is rated according to *area* and *brightness*. The ground level events observed thus far have, for the most part, been associated with the more violent eruptions that are assigned Importance 3 or 4B, or slightly less. But sometimes even a relatively minor eruption can produce a small PCA.

Typically, the duration of a great flare is an hour or two. The *flash phase,* during which the Hα intensity rises rapidly to a maximum, may last for only a minute. Accompanying the visible

TABLE 7-1. *International Astronomical Union Scheme for Assigning Solar Flare Importance Ratings.*

"Corrected" Area in Square Degrees	Relative Intensity Evaluation		
	Faint (f)	Normal (n)	Brilliant (b)
≤2.0	Sf	Sn	Sb
2.1– 5.1	1f	1n	1b
5.2–12.4	2f	2n	2b
12.5–24.7	3f	3n	3b
>24.7	4f	4n	4b

brightening of the chromosphere are all the other electromagnetic products of the energy-transformation processes that comprise the awesome explosion. These include ultraviolet light, soft and penetrating x rays, and γ rays on the one hand, and a broad range of radio emissions on the other.

Ionospheric Effects. Photoionization by x rays promptly increases the electron density in the earth's upper atmosphere, thereby causing a *sudden ionospheric disturbance,* or SID. This reaction to the arrival of electromagnetic radiation may involve the *D-region* extending from about 50 to 90 km, the *E-region* from 90 to 160 km, and the *F-region* beyond.

There are several possible manifestations of an SID depending upon how the different layers of the ionosphere are affected. These include *shortwave fade-outs* (SWF) of radio transmission, *sudden phase anomalies* (SPA), *sudden enhancements of atmospherics* (SEA) and *sudden cosmic noise absorptions* (SCNA).

The arrival of charged particles after a delay that depends upon their travel time from the sun to the earth (see Fig. 7-3) produces a massive increase in the ionospheric electron density. Inasmuch as low energy protons have access to high latitudes [Eq. (4-9) and Fig. 4-8], and since they are heavily ionizing in the lower ionosphere (cf. Figs. 7-3 and 2-10) they are especially efficacious in absorbing both man-made and cosmic radio signals.

The first PCA was recorded (but not recognized) in the early 1950's with a high-powered arctic communications network employing a mode of radio wave propagation discovered by Bailey and called *ionospheric forward scatter.* Although the detailed scattering mechanism is not understood, it can be ascribed to

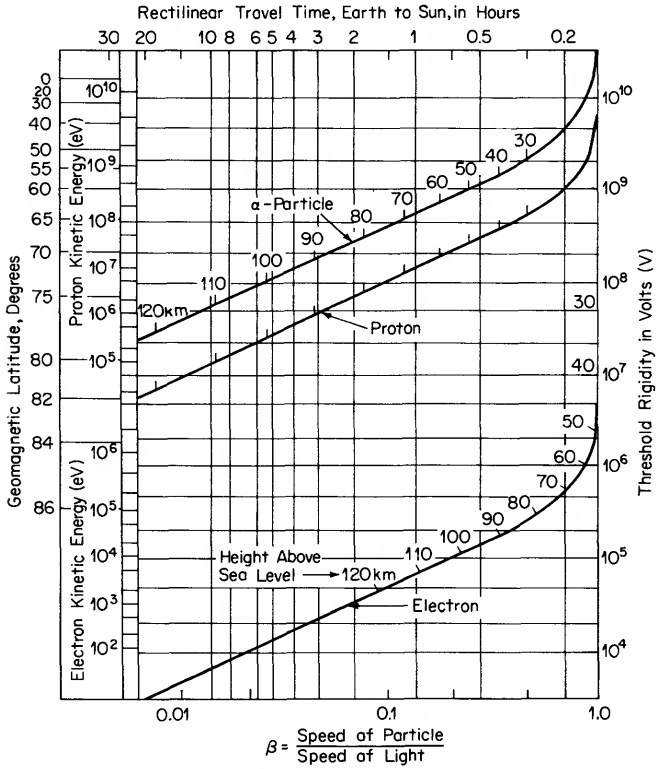

FIG. 7-3 Relationships among energy, rigidity, depth of penetration, lowest latitude of arrival and rectilinear sun-earth transit time for various particles.

irregularities arising from wind shear and turbulence in the mesosphere at a height of 70–75 km during daylight hours and about 85 km at night. A very small fraction of a VHF signal with a frequency exceeding the limit for the well-known garden variety of ionospheric reflection is returned to earth from a thin ($\simeq$5 km) scattering stratum. The antenna patterns intercept the scattering layer at the mid-point between transmitter and receiver which, typically, may be 1000 km apart.

The received signal intensity in decibels is directly proportional to the logarithm of the ambient electron density in the region of the scattering inhomogeneities. Thus, if the electron

density in the scattering layer is greatly increased, the signal intensity increases. On the other hand, if most of the abnormal ionization lies below the principal scattering level, the signal intensity decreases, because absorption is proportional to the electron density along the path traversed by the radio wave. During daylight, when the increase in electron density during a PCA is very great, the *absorption* effect dominates the *enhancement* effect, and the signal shows a net decrease. After sunset, however, *night-time recovery* is caused by electron attachment to O_2 molecules owing to the cessation of *photodetachment*. Then, the enhancement effect dominates. Both of these effects are dramatically evident in Fig. 7-4 which shows the forward scatter record during the spectacular 1956 event.

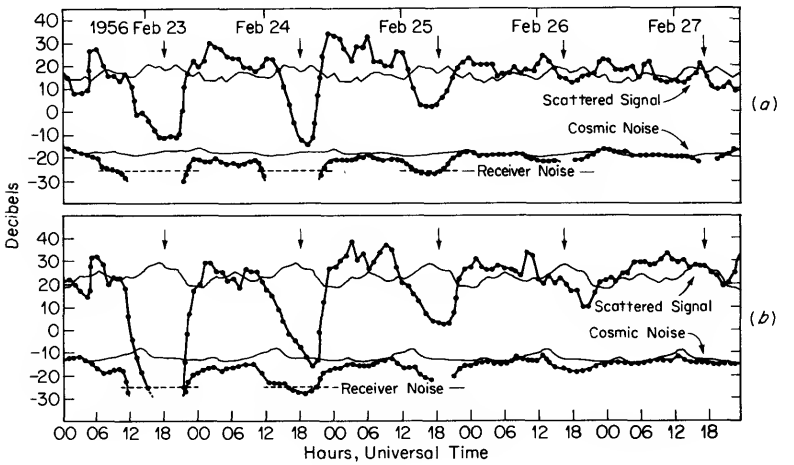

FIG. 7-4 Intensity of ionospheric forward scatter signal and background cosmic noise during the great solar particle event of February, 1956. (a) Thule to Søndre Strømfjord, Greenland (b) Goose-Bay, Labrador to Søndre Strømfjord.

The *riometer* (*r*elative *i*onospheric *o*pacity *meter*) is a radio receiver with a wide-beam vertically pointing antenna. It measures the *total* absorption of cosmic radio noise in its passage through the entire ionosphere. This instrument, first used by G. Little and H. Leinbach in 1958, observes SIDs, and auroral absorption that is frequently produced in the auroral zone by

the localized precipitation into the E-region of low energy electrons (tens of keV—see Fig. 7-3), as well as PCA events.

Comparison of radio wave absorption and *in situ* measurements by rocket-borne instruments has made it possible to determine quantitatively the fluxes of solar particles from the observed signal attenuation. Figure 7-5 shows the calibration curve

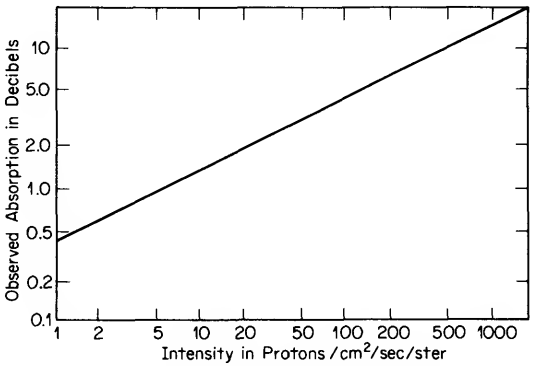

FIG. 7-5 Cosmic noise absorption as a function of proton flux for a 30 Mhz riometer.

for a 30 megahertz riometer. The absorption in decibels varies approximately as $1/(\text{frequency})^2$, and, for a given incident spectrum, it is very roughly proportional to the square root of the particle intensity.

Neutron Monitor Time Profile. Each ground-level event seems to exhibit its own distinctive features. The magnitude of the counting-rate increase may range from barely perceptible ($\simeq 1\%$) to staggering. Fig. 7-6 shows the February 23, 1956, solar cosmic ray event as recorded at Chicago. The nucleonic intensity at some stations reached a maximum of 40 times the pre-flare level. Fig. 7-7 is an example of a complicated sequence of events that was observed by the world-wide network of neutron monitors in November, 1960.

The *rise time* to maximum may range from less than an hour to several hours, after which the intensity usually decays exponentially, returning practically to the background level in a few

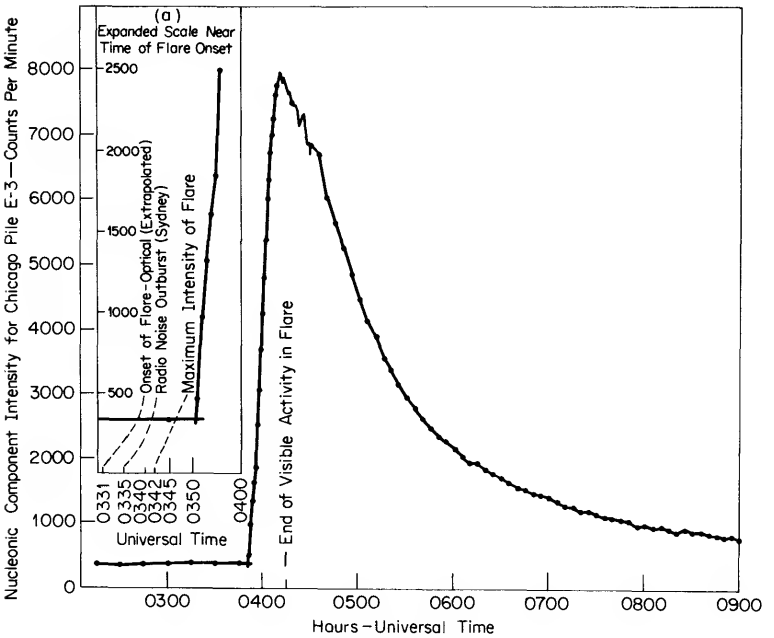

FIG. 7-6 Chicago neutron monitor observations on 23 February, 1956.

hours, or longer, depending upon the magnitude of the increase.

The enhancement always exhibits a marked altitude and latitude dependence because solar particle spectra are steep—the flux falls off very rapidly with increasing energy. Furthermore, there may be a geographic asymmetry indicative of guiding center motion of the particles traveling from the sun to the earth along the spiral interplanetary field lines. This anisotropy does not occur when the propagation is controlled by a diffusion mechanism.

ENERGY SPECTRUM

Our old friend, the power law spectrum, encountered earlier in the discussion of galactic cosmic rays also usually fits the solar cosmic rays, at least over limited ranges of energy. Thus, the data at a specified time t have often been represented by the follow-

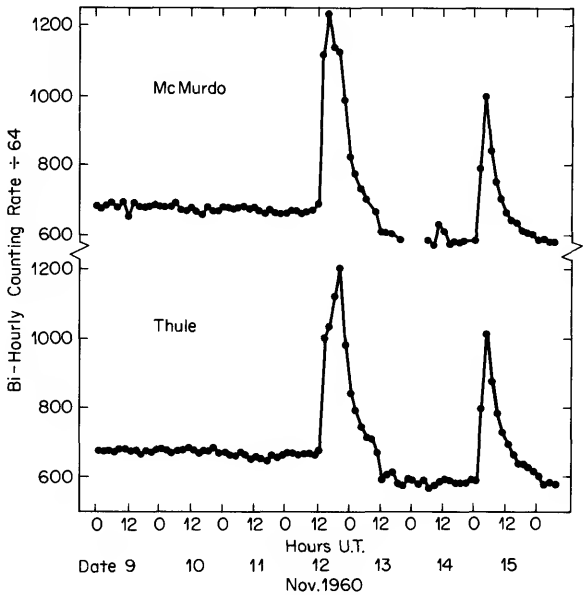

FIG. 7-7 Observations in bi-hourly intervals at polar neutron monitor stations during November, 1960. An unusual double-peaked structure on 12 November, 1960 is resolved when the time scale is expanded (15 minute intervals).

ing relationship in terms of energy, or a similar one in terms of rigidity:

$$j(>E) = K(t)E^{-\gamma(t)}. \tag{7-1}$$

As exemplified in Fig. 7-8, the value of the exponent $\gamma(t)$ (which ordinarily ranges from 3 to 7) is appreciably higher than it is for the galactic cosmic rays. Furthermore, the power law applies in the low-energy region below the maximum of the observed galactic differential spectrum (cf. Fig. 5-2). Thus, whereas the observed galactic differential intensity below about 1 GeV *decreases* toward lower energies, the solar particle flux *increases*.

An alternative representation that usually covers a wider range quite well, as illustrated in Fig. 7-9, is

$$j(>P) = j_0(t) \exp\left[-P/P_0(t)\right]. \tag{7-2}$$

The steepness of the spectrum is determined by P_0, the *e-folding*

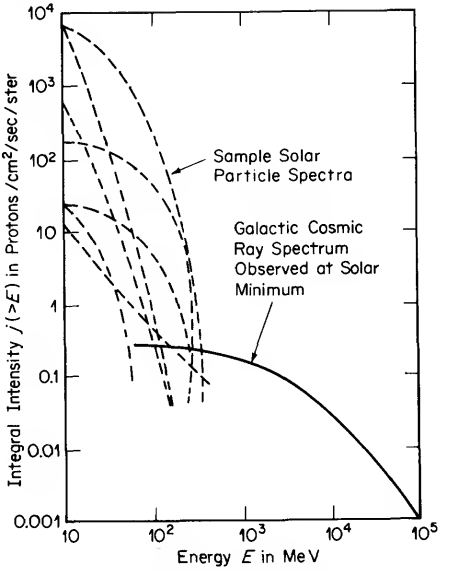

FIG. 7-8 Comparison of power-law representations of energy spectra during several solar cosmic-ray events with the galactic proton spectrum.

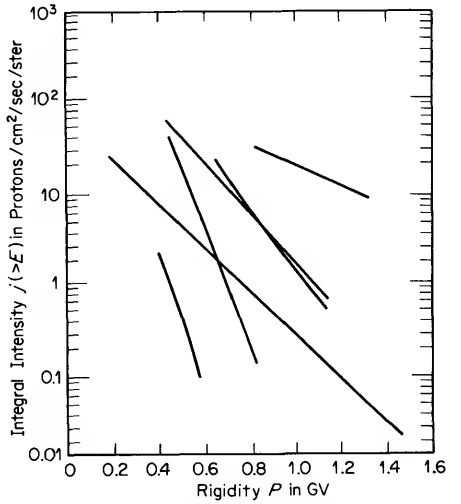

FIG. 7-9 Exponential representation of the integral rigidity spectra of solar protons during different events.

rigidity which ranges from roughly 40 MV (steep) to 400 MV (flat). Values of j_0 are from about 2 protons/cm^2/sec/ster to 8×10^3 protons/cm^2/sec/ster.

The spectrum generally steepens with time, that is, the relative number of high-energy particles falls off rapidly compared with the lower-energy component.

The flux of energetic solar particles is frequently thousands of times greater than the galactic cosmic-ray flux of about 4 particles/cm^2/sec, and peak fluxes of protons with energies above 10 MeV as high as $\simeq 10^5$ particles/cm^2/sec have been observed. The integrated flux in a single event may exceed a billion particles/cm^2!

This obviously represents a big bundle of energy. We can make a crude guess about how much of its energy the sun imparts to solar cosmic rays in one of the largest events by multiplying (integrated flux at the earth) (average energy) (the area of the surface of the sphere at 1 AU):

$$(10^9 \text{ cm}^{-2})(10^7 \text{ eV})[4\pi(1.5 \times 10^{13} \text{ cm})^2]$$
$$= (2.8 \times 10^{42} \text{ eV})(1.6 \times 10^{-12} \text{ ergs/eV}) \simeq 10^{31} \text{ ergs.} \quad (7\text{-}3)$$

This is comparable with the energy of about 10^5 hydrogen bombs. Although this back-of-the-envelope type of calculation involves some glaring but compensating over- and under-estimates, it is in the right league. Calculations based on a diffusion model lead to the same result.

COMPOSITION

As in the galactic cosmic-ray beam, protons predominate, and alpha particles are also present. However, there is a most puzzling wide variation in the proton to helium ratio. Their spectra, expressed in rigidity, seem to be similar, but the ratio of protons to helium nuclei in the same rigidity interval may vary from 1 to 50.

Fig. 7-10 shows how this ratio has varied with energy per nucleon in several events. Above a fixed energy, it may vary from 10 to 100.

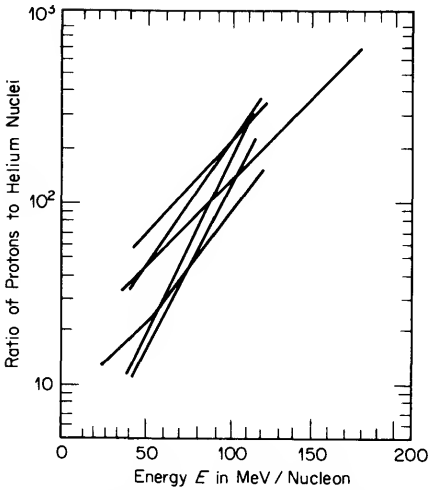

FIG. 7-10 Solar proton to helium ratio as a function of energy per nucleon at various times.

Heavier nuclei are also present, although they are less abundant than in the galactic cosmic radiation. Unlike hydrogen, whose relative abundance is variable, the charge spectrum of the multiply charged nuclei remains constant, and is independent of energy. As Table 7-2 shows, the relative abundances reflect the chemical composition of the sun.

The distinctive solar radio emissions that characterize all solar cosmic-ray events clearly manifest the acceleration of electrons in the flare region. Radio astronomers designate solar rf events as Types I to V. Type IV *continuum radiation*, a continuous, steady "burst" that may cover the entire radio spectrum, invariably accompanies the emission of solar energetic particles.

But, unlike the heavier particles that, at least when certain unknown conditions prevail, manage to escape from the regions in which they are accelerated, most of the electrons remain trapped in the strong local magnetic fields. Here, those that attain relativistic velocity lose much of their energy by emitting *synchrotron radiation* in the radio-frequency region of the electromagnetic spectrum.

TABLE 7-2. *Relative Abundances of the Elements in Solar and Galactic Cosmic Rays, and in Solar and Galactic Matter in General, Normalized to the Base Value 10 for Oxygen.*

Element	Atomic Number Z	Solar Abundances		Galactic Abundances	
		Cosmic Rays	Matter	Cosmic Rays	Matter
He	2	1000	(4500)*	500	1500
Li	3	—	$<10^{-4}$	2	$<10^{-4}$
Be	4	<0.1	$<10^{-4}$	6	$<10^{-4}$
B	5				
C	6	5	5	18	3
N	7	2	1	8	2
O	8	10	10	10	10
F	9	<0.3	.01	1	$<10^{-3}$
Ne	10	1	(1)*	3	3
Na	11	—	.02	2	0.02
Mg	12	0.4	0.3	3	0.4
Al	13	—	.02	0.6	.04
Sc	14	0.3	0.4	1	0.4
P-Sc	15–21	0.6	0.3	1	0.2
Tc-Nc	22–28	<0.2	.05	3	0.3

* The number in parentheses represents the relative abundance of this element in the corona rather than in the photosphere.

Nevertheless, some electrons do escape. But, just as their galactic cousins, they eluded observation until recently. High-energy (GeV) solar electrons appear to be virtually absent. However, a large number of low-energy solar electron events have been observed with instruments aboard spacecraft. As the detector thresholds are pushed down to lower energies, both solar electrons and protons are detected more frequently, until eventually ($\simeq$1 MeV) they seem to be present even when they cannot be attributed to specific solar active regions.

One might expect that, in the great holocaust, some of the protons accelerated during the flare would plunge deep into the solar atmosphere producing, among other things, a neutron albedo. Even when conditions are quiet, the fantastic nuclear furnace would seem to be a prolific source of neutrons. The sun-earth transit time of a 10^8 eV neutron (same as for a proton in Fig. 7-3) is roughly equal to its mean lifetime against decay, $\sim$17 minutes (cf. Table 2-1). Nevertheless, neutrons do not appear on the roster of solar cosmic rays. It's a puzzlement!

PROPAGATION

It goes without saying that solar cosmic rays are basically anisotropic, since their source is in our own backyard. But even though the rectilinear distance is short compared with galactic dimensions, there is sufficient stuff between the sun and the earth, especially when the sun is hyperactive, to isotropize the solar cosmic rays sooner or later during a flare event. The extent and duration of the initial anisotropy depends upon the position of the flare on the solar disk.

Fig. 7-11 reveals that flares in the sun's western hemisphere

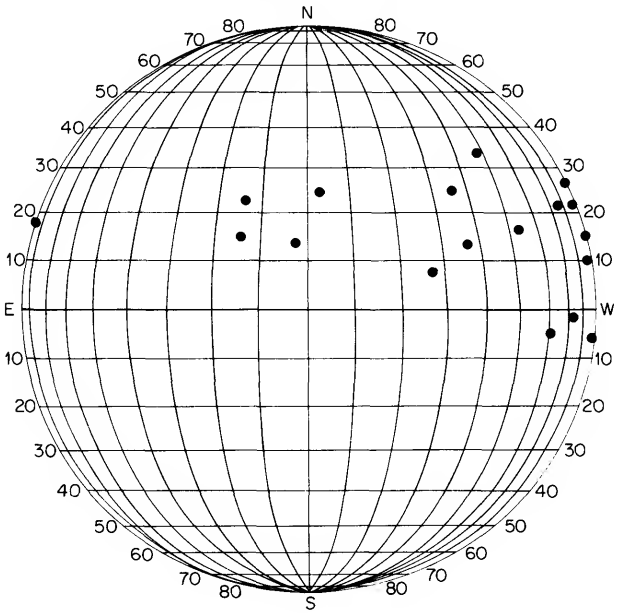

FIG. 7-11 Position on the sun's visible disk of observed flares that have produced solar protons with energies exceeding about 500 MeV (ground level event).

are more likely to produce solar particles that can reach the earth.* The reason for this heliographical favoritism is illus-

* The northern hemisphere also appears to be favored, but this is a consequence of the unexplained fact that, for some time, there has been a prepon-

trated schematically in Fig. 7-12. The spiral magnetic lines of force guide the solar particles, and tend to funnel them from the sun to the earth. There is easy access from the western limb, whereas particles originating in the eastern sector have to cross the field lines. Thus, in the latter case, they diffuse toward the earth, following a more tortuous path than do the particles that

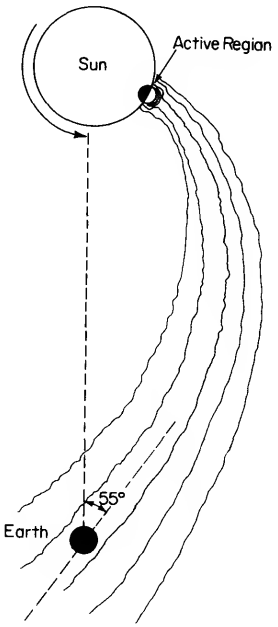

FIG. 7-12 Schematic representation of the sun-earth turnpike—the route that affords easier access from the sun to the earth for solar particles emitted from the western segment.

can flow through a magnetic tube. Consequently, eastern hemisphere flare events are *slow risers* compared with the more favored western hemisphere events which are characterized by a rapid onset after the flash phase of the flare. But, in all cases, diffusion

derance of the more prolific active centers in this half of the sun. Another interesting point not brought out by Fig. 7-11 is that a "fixed" region on the sun appears to have been the seat of most of the energetic solar particles for some time.

eventually sets in, and even if the propagation is very anisotropic during the initial stages (*direct radiation*) many particles that did not start their journey on the sun-earth turnpike finally reach the earth later (*indirect radiation*).

Fig. 7-13 reveals how far solar protons may actually travel before arriving at the earth. The observed relative intensity is plotted as a function of the distance traveled, computed for each

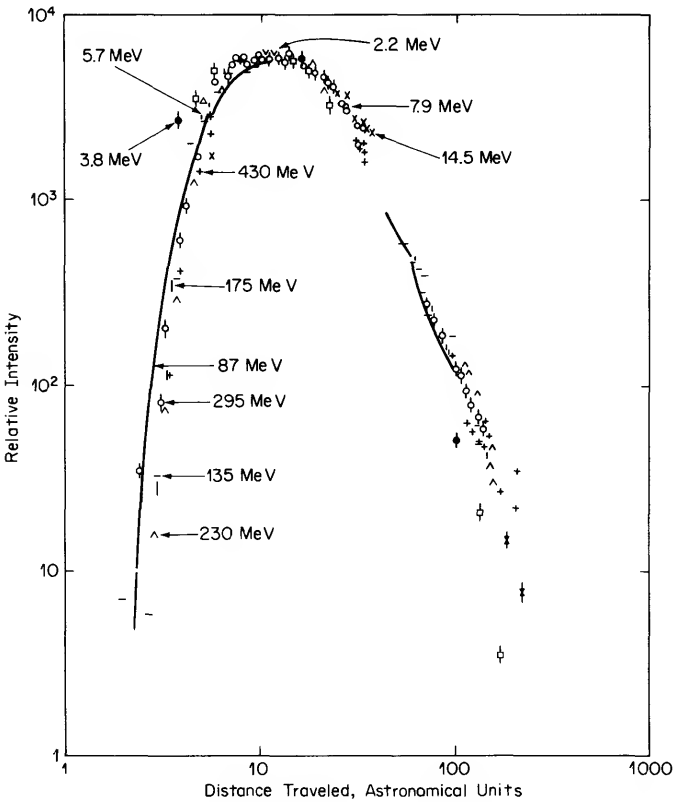

FIG. 7-13 Normalized differential intensities of solar protons as a function of the total distance traversed while enroute from the sun to the earth. The abscissas are obtained by multiplying (1) the elapsed time between the flare and the arrival of each energy group at the earth by (2) the velocity corresponding to the observed energy.

indicated energy component by multiplying the corresponding particle velocity by the elapsed time from event to observation. Most of the particles in this case traversed more than ten times the rectilinear earth-sun distance.

The mean free path typically is of the order of 0.1 AU. Since memory of their initial directions is erased by scattering with magnetic irregularities (i.e. the particles *random walk*), we would expect that, at least occasionally, some products of a flare on the far side of the sun should reach the earth. But until very recently, there were no known events in which this happened. The first example of the arrival of solar cosmic rays originating on the invisible disk is shown in Fig. 7-14. The extremely slow rise to maximum, the isotropy throughout the event, and the quantitative features as analyzed in terms of diffusion models for the propagation of the particles, all connote the unseen source. But

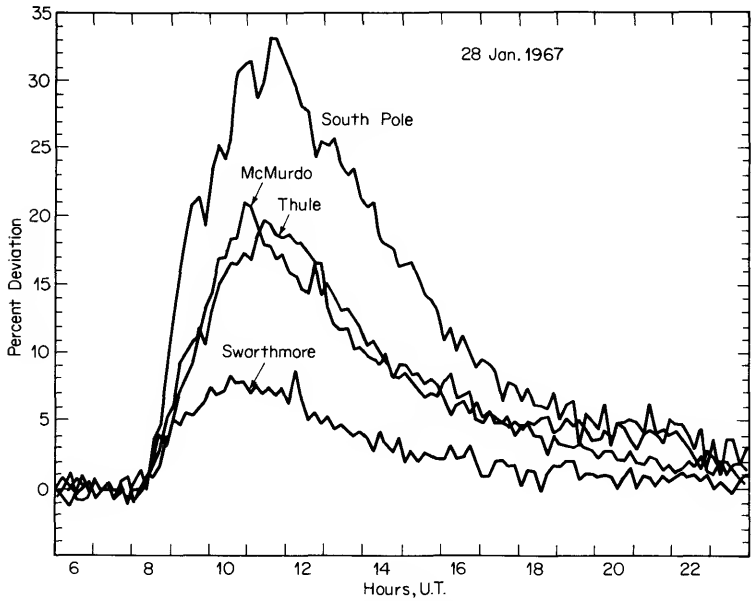

FIG. 7-14 First example of the arrival of very energetic solar cosmic rays from the far side of the sun.

the burning question persists. Why doesn't this happen more often?

Fig. 7-12 clearly fits into our picture of the spiral structure of the interplanetary magnetic field. It is instructive to consider an example of how this model can be deduced from cosmic-ray observations alone. Fig. 7-15 is a snapshot of the "flat" world dur-

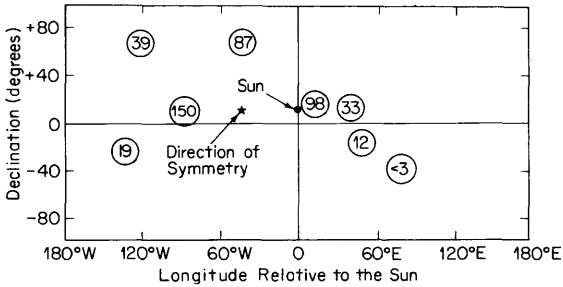

FIG. 7-15 Example of the variation in the neutron monitor counting rate increase above the pre-flare level in percent (numbers in circles) with asymptotic direction of viewing of a number of stations (circles).

ing a particular solar flare event. It shows the dependence of the percentage intensity enhancement upon direction of viewing of a number of neutron monitor stations. The direction in space about which the solar cosmic-ray flux was symmetrical, as well as the position of the sun at that time, are marked. We see that, in accord with Fig. 7-12, the apparent source was 55° west of the sun.

In Fig. 7-16, the same neutron monitor data are plotted as a function of the angle δ between the axis of symmetry and the asymptotic direction in space from which the solar particles to which the detectors responded came. No station was looking directly at the source, but the intensity was presumably maximum from the direction $\delta = 0$, *i.e.* 55°W of the earth-sun line and 10°N of the ecliptic. Although the individual directions viewed by the different stations surround the direction $\delta = 0$, all the data fall along a single curve.

Spacecraft measurements show how strongly low-energy ($\lesssim$ tens of MeV) solar cosmic rays can be collimated along interplanetary field lines. The particle streams sometimes exhibit a filamentary

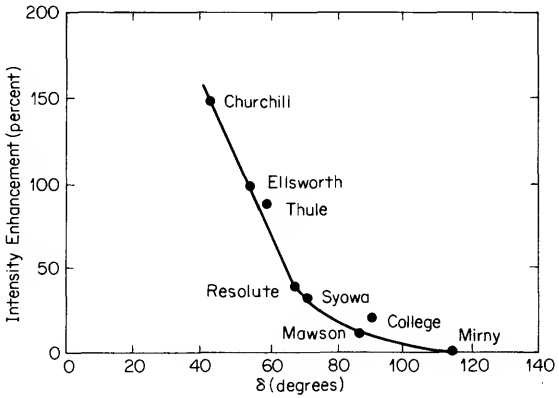

FIG. 7-16 Data from Fig. 7-15 plotted as a function of the angle between the indicated axis of symmetry and the asymptotic direction of viewing.

structure because they are constrained to move through frozen-in magnetic tubes which guide the particles even though they twist like spaghetti, in the manner depicted in Fig. 7-17. The entire intertwined bundle co-rotates with the sun in the general Archimedes spiral configuration.

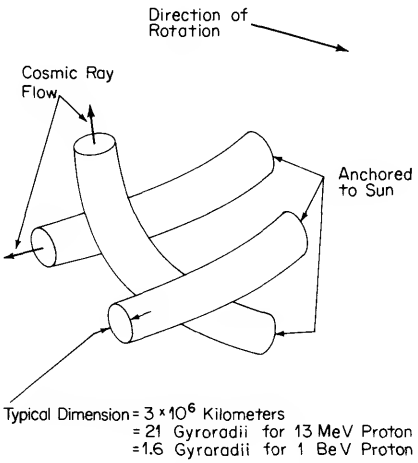

FIG. 7-17 Spaghetti-like tubes of force through which low-energy solar cosmic rays may flow.

ACCELERATION PROCESSES

Although considerable progress has been made toward understanding how solar cosmic rays propagate, the mechanisms whereby they acquire their energy and are stored at and escape from the sun are still mysterious. All of the processes that have been proposed to describe the acceleration of solar cosmic rays are also relevant to the problem of galactic origin. Since we shall have occasion to discuss this subject in detail later, we need only identify them here.

The *Fermi* mechanism* involves collisions of particles with moving magnetic scattering centers. In *betatron* acceleration,* charged particles are energized by a time-varying magnetic field. Dynamical *plasma pinches* and *hydromagnetic instabilities* are very complicated processes, for which theoretical calculations do not lead to complete conclusions, but require unattainable observational guidance. Unfortunately, the acceleration processes take place in regions that cannot be observed directly. Perhaps several different mechanisms are operative. They may even cooperate as, for example, in the case of *magnetic pumping,*** which is a combination of betatron action and scattering by magnetic irregularities. In any case, the time in which the acceleration and/or the ejection of particles into space is accomplished seems to be extremely short, perhaps of the order of minutes, roughly corresponding with the explosive phase of the flare.

As an alternative to regarding the flare as the mother of the energetic particles, one may speculate that the optical phenomenon is the offspring of trapped energetic particles that suddenly precipitate into the photosphere. This is, in fact, quite analogous to the relationship on earth between the Van Allen belts and aurora.

Actually, asking the question "How do the solar particles derive their energy from the flare?" is really tantamount to asking "What makes the flare happen in the first place?" Vast amounts

* See p. 160.
** See p. 164.

of energy, adding up to as much as 10^{33} ergs, are suddenly released in the largest eruptions. This exceeds the entire thermal energy stored up in the whole corona and chromosphere! And, as we have noted, sometimes a few percent of this energy, of the same order as the fraction appearing as H_α light, is transferred to solar cosmic rays. In seeking an explanation, one recourse is to look to the solar wind as the key to this problem. Somehow, plasma must slowly store magnetic energy, and then release it catastrophically. Let us examine this possibility quantitatively.

The energy density associated with a magnetic field of intensity B gauss is given by

$$\rho_B = B^2/8\pi \text{ ergs/cm}^3. \tag{7-1}$$

The largest flares occupy a volume of about 10^{29} cm^3, which means that, for an associated sunspot field of $\simeq$1000 gauss, the magnetic energy is $\simeq 10^{33}$ ergs. The annihilation of this field could provide all of the energy that is released in the flare.

SPACE RADIATION DOSES

In addition to its purely scientific importance, a detailed knowledge of the properties of solar cosmic rays and of the conditions that presage a solar cosmic-ray event has immediate practical application to space activities. Exposure to excessive doses of radiation in the space environment could produce serious radiobiological effects in astronauts. Since solar cosmic rays pose the prime radiation hazard in man's ventures beyond the magnetosphere, especially on extended missions, it is appropriate to comment briefly on this problem. However, although it is possible to make some remarks about potential dose rates on the basis of past experience, it must be remembered that evaluating the effects of a given exposure constitutes a profoundly difficult biological problem.

The basic unit for measuring radiation is the *roentgen* (r) which is defined as the quantity of radiation required to produce 1 esu of charge per cubic centimeter of air under standard conditions. The *roentgen equivalent, physical* (rep) denotes an energy absorption of 93 ergs per gram, which is the amount of

energy absorbed by 1 gram of soft tissue exposed to 1 r of x rays. The more modern unit, the *rad,* is defined as the radiation required to produce an energy absorption of 100 ergs per gram.

The biological effects produced by 1 rad of different types of radiation can vary, although the energy absorption is the same. To take this into account, a factor called the *Radiation Biological Effectiveness* (RBE) has been introduced to relate the radiological consequences of other radiation to that of x or γ radiation. The *roentgen equivalent man* (rem) is equal to the product (RBE) (rad).

At solar minimum, when the galactic flux is about 4 particles/cm^2/sec, the integrated daily rate is 3.5×10^5 particles/cm^2, and the yearly rate is 1.2×10^8 particles/cm^2. The corresponding doses are 20 millirad per day and 7 rad per year. Individual solar events can produce much higher doses over short periods, although excluding the very large eruptions, the yearly dose of solar cosmic rays is not alarmingly greater than that of galactic cosmic rays, and is easily handled with 3–4 gm/cm^2 of shielding. However, the largest events have generated doses in the hundreds of rads. In one case, a surface dose of almost 1500 rad would have been encountered behind a 1 gm/cm^2 shield.

Orbital electrons are dislodged and molecular bonds are severed when ionizing radiation is absorbed in matter. When this occurs in living cells, subcellular processes are disrupted, and the normal functioning of the cell is impaired. In particular, damage to deoxyribonucleic acid (DNA) which is involved in the fundamental control of the genetic and functional activities may appear. Radiation damage in complex mammalian organisms consisting of billions of cells grouped into systems and organs may be *somatic* and *genetic.* Somatic effects are manifested directly in the tissues of the organism, and may occur *early* (minutes to weeks) or *late* (months or years). Radiation effects are a probabilistic function of many factors. Thus, the responses to individual solar flare events could range from nil through immediate symptoms that could affect the safety of the mission and even to death.

Many considerations, including the shielding and the individual, would determine the outcome of exposure to a particular

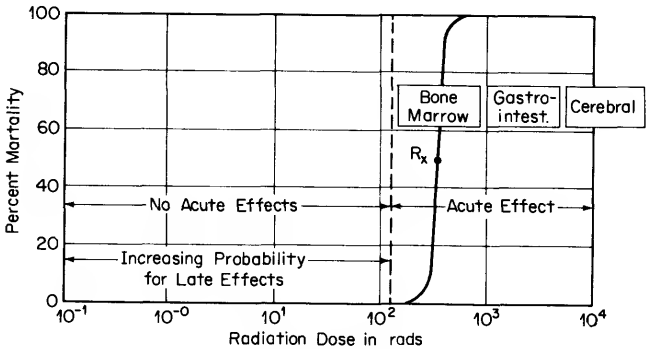

FIG. 7-18 Radiobiological effects produced in humans by penetrating energetic particles. For low energy particles, the dose tolerances may be an order of magnitude higher.

solar cosmic-ray storm. Fig. 7-18 roughly represents the radiobiological effects suffered by humans exposed to energetic particles. Somewhat larger skin doses of soft radiation can be tolerated, and the *percent mortality* curve is shifted appreciably to the right in this case. On the average, 125 rads should not produce significant disease symptoms in man, and the skin can probably absorb ten times as much before affecting astronauts acutely. Fig. 7-19 shows, for one of the larger solar flare events, how the tissue surface dose would have been reduced by the addition of

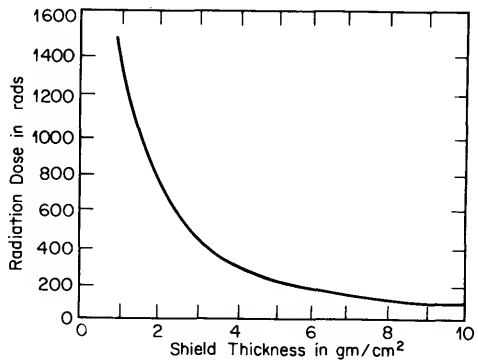

FIG. 7-19 Variation of tissue dose that would be sustained during a large solar flare event with the thickness of a protective aluminum shield.

shielding. Needless to say, all of these factors are taken into account in planning manned missions.

Many studies have been directed toward the development of criteria for predicting the occurrence of cosmic-ray flares, and the sun is being maintained under continuous surveillance by a wide variety of observing instruments. Centers of activity are watched closely for symptoms suggesting that a proton flare may be imminent.

Since we have not yet completely mastered the art of predicting the weather here on earth, it is perhaps not surprising that, even though remarkable strides have been made in forecasting the solar weather, there is still plenty of room for improvement.

8 *The Origin of Cosmic Rays*

There was a star danced, and under that was I born.
WILLIAM SHAKESPEARE

The difficulty in deciding upon the origin of cosmic radiation lies not so much in inventing hypotheses, but rather in verifying whether or not they are representative of what occurs in nature. Ever since their discovery, speculation about where and how cosmic rays are born has been rife. In this revolutionary new era of astronomy that started with the discovery of cosmic radio noise, processes that are capable of giving rise to cosmic rays have been found to be necessary causes or consequences of other astronomical phenomena. But even proposals based upon observationally established physical principles must be examined not only qualitatively, but also quantitatively. The detailed knowledge that now exists concerning the cosmic rays themselves, on the one hand, and galactic structure and stellar evolution on the other, places rather severe restrictions upon theories concocted to answer the key questions that completely define the cosmic ray origin problem:

1. *Where* were they produced?
2. *How* were they accelerated?
3. *When* were they born?
4. *What* happened later?
5. *Why*—(Perhaps this is theological)?

Early attempts to answer these questions alternatively identified cosmic rays as the birth cries or the death gasps of matter. Millikan first contended that cosmic ray energy represented the difference between the atomic masses of the universally common elements and the larger sum of the masses of the hydrogen atoms

which presumably combined to form them in interstellar space (*cf.* Fig. 1-1). He later advocated the annihilation theory which envisaged the complete transformation in interstellar space of the rest mass of these same elements into cosmic-ray energy.

A great many ideas were proposed by many individuals, contemplating sources ranging from the sun to galaxies far beyond our own, and invoking acceleration mechanisms running the gamut from electric fields produced in stellar thunderstorms to the original act of creation of the universe. Even supernovae, currently regarded as a most likely cosmic-ray birthplace, were already receiving serious consideration as early as 1934 when W. Baade and F. Zwicky drew attention to the enormous energy released in a supernova explosion, and its potentiality as a cosmic fountainhead.

Before discussing the rationale for contemporary views on cosmic-ray origin, let us recall some of the observed characteristics for which an acceptable theory must account—the facts that keep the theorist honest.

A significant feature of the composition of the primaries is the relative overpopulation of heavy nuclei compared with universal abundances—exceedingly great for the L group, and less drastic for the M and H groups. Electrons are scarce and positrons are considerably rarer.

Primary cosmic-ray nuclei have spent a very long time, at least millions of years, in traversing roughly 3 gm/cm^2 of matter before reaching the earth. They arrive isotropically and appear to have been around in very roughly the same numbers for perhaps longer than a billion years.

Their energies extend at least up to 10^{20} eV, their numbers varying inversely as an almost constant power of the energy above 10^9 eV. Below this energy, although the exact form of the spectrum is uncertain, the differential intensity unquestionably continues toward lower energies until the galactic cosmic rays become indistinguishable from solar cosmic rays.

The energy density is roughly 10^{-12} ergs/cm^3, so the source must not only produce individual particles with energies a billion times that of the greatest laboratory accelerators, but it

must also put out a stupendous total energy, depending upon the size of the volume over which this energy density extends.

ACCELERATION MECHANISMS

Betatron Action. Although striking evidence for particle acceleration on a galactic scale has been amassed in recent years, earlier attempts to account for cosmic-ray energies in terms of then-known physical principles were based upon classical electromagnetic theory. Thus, in 1933, W. F. G. Swann pointed out that fluctuating stellar magnetic fields can, through electromagnetic induction, give rise to cosmic-ray energies. He emphasized that it is not the *magnitude* of the field, but rather its *time rate of change* that is important, and showed that fields varying at a rate comparable with that observed in sunspots, if spread over a sufficiently large area in a star, can easily produce 10^{10} eV even with fields much weaker than these and, in fact, unobservable spectroscopically. The principle discussed by Swann was subsequently utilized in the *betatron*. In this device, charged particles are speeded up by a homogeneous magnetic field which increases with time. The mechanism is analogous to that of an ordinary electrical transformer, in which there is a change of magnetic field that threads through a wire circuit, inducing an electromotive force which drives the current through the circuit. Of course, the wire is not necessary for the attainment of the emf. Electrically charged particles that happen to be in the vicinity of the changing magnetic field are accelerated by the emf, even though they do not form part of a material circuit.

Fermi Acceleration. The first quantitative theory which made predictions that could be compared with observations was proposed by E. Fermi in 1949. Most easily visualized in terms of a mechanical analogy, it is based upon the principle that charged particles can gain energy from random collisions with magnetized gas clouds under certain conditions.

One might think of a system which is full of cannon balls that are moving randomly, corresponding to plasma clouds with frozen-in magnetic fields, and BB shot, representing cosmic rays.

Equipartition sets in, so that, according to the principles of thermodynamics, the cannon balls will ultimately lose their energy to the BB shot, and will reach a state of equilibrium in which the average translational energy of each cannon ball is the same as that of each much more rapidly moving BB shot.

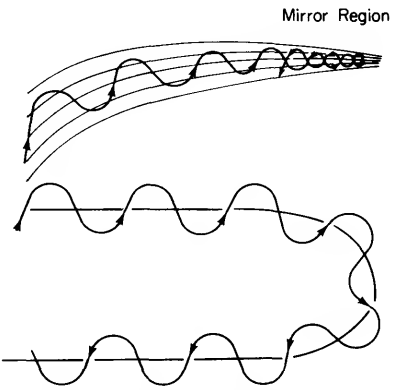

FIG. 8-1 "Collisions" of a charged particle with magnetic fields. The particle may mirror (top) or it may be guided around a sharp bend (bottom). If the magnetic field is in motion, the particle may either gain or lose energy in the encounter.

Fig. 8-1 shows the types of collision envisaged by Fermi. In one, the particle spiraling around a magnetic field line enters a region of greater field strength, increasing its *pitch angle* (the angle of the velocity vector of the particle with respect to the magnetic field) until the orbital plane is perpendicular to the field direction, in which case it *mirrors* like a geomagnetically trapped particle in the Van Allen belt. The other type of reflection is one in which the particle is guided along sharply bent field lines.

This statistical model provides a basis for computing the resulting energy spectrum. In head-on collisions between a particle with energy E and a magnetized cloud with velocity v_B, the particle gains energy, whereas it loses energy in overtaking collisions. Because the former are more probable, there is a net gain which averages per collision

$$dE = \beta^2 E, \tag{8-1}$$

where $\beta = v_B/c$. Thus the incremental energy gain increases with the particle energy—them as has gits!

After n collisions

$$\Delta E = n\beta^2 E, \tag{8-2}$$

whence an originally nonrelativistic particle will have attained an energy

$$E = \exp(\beta^2 n). \tag{8-3}$$

If the mean time between collisions is τ_c, the number of collisions experienced in time t is $n = t/\tau_c$ and the energy is

$$E(t) = E_i \exp\left(\beta^2 \frac{t}{\tau_c}\right) = E_i \exp(t/t_c), \tag{8-4}$$

where E_i is the *injection energy* and $t_c = \tau_c/\beta^2$. Now, particles are also lost, by catastrophic collisions with interstellar matter and by leakage out of the system, in a mean time t_l. The probability of surviving to an age greater than t is

$$P(>t) = \exp(-t/t_l). \tag{8-5}$$

Therefore, the number of particles with energy exceeding E is

$$j(>E) = KE^{-t_c/t_l}. \tag{8-6}$$

This is a power law integral spectrum identical to Eq. (5-1) with the value of the exponent $\gamma = t_c/t_l$. Experimentally, $\gamma = 1.5$, hence $t_c = 1.5\ t_l$. Since the mean lifetime for escape from the galaxy is at least as long as the mean time for removal by nuclear collisions, we can estimate t_l, by recalling that primary cosmic rays pass through ~ 3 gm/cm^2 of material. The density in the galactic disk is $\sim 10^{-24}$ gm/cm^3, so the distance traversed (remembering that gm/cm$^2 = \rho x$) is $3/10^{-24} = 3 \times 10^{24}$ cm. The corresponding time is $3 \times 10^{24}/c = 10^{14}$ sec, or about 3 million years. In the galactic corona, where the density is about 10^{-26} gm/cm^2, this becomes 10^{16} sec or 3×10^8 years.

This looks nice, but there is a catch. The particles lose energy by ionization, and gain energy in the collisions. The gains outweigh the losses only for particles exceeding a certain velocity. The relationships between energy gain and loss, respectively, and particle energy for protons are shown in Fig. 8-2. The inter-

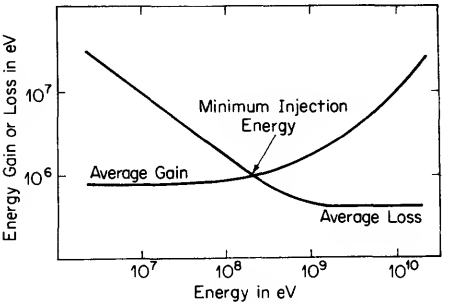

FIG. 8-2 Dependence of energy gain and loss upon energy for protons. For the Fermi acceleration mechanism to work, the minimum injection energy must be supplied by some other process.

section of the two curves marks the minimum injection energy required to make the Fermi acceleration go. Although it is only about 200 MeV for protons, heavier particles, because of their greater rate of ionization, require much higher injection energies—about 20 GeV for oxygen and 300 GeV for iron. This mechanism works well for protons, but even if the exorbitant injection energy were provided by some other mechanism, it is in trouble in accounting for the observed characteristics of the heavier nuclei. By virtue of their fragmentation probabilities they have correspondingly smaller mean free paths than do hydrogen nuclei. Consequently, the observed similarity in the energy spectra of the various components cannot be reconciled with this type of acceleration process.

A number of variations of this attractive principle have been proposed. For example, the arms of a spiral galaxy are essentially magnetic bottles, similar to the mirror machines that are utilized in fusion experiments. As is shown in Fig. 8-3, the magnetized plasmas near the ends of a tubular trap may approach each other, accelerating charged particles as they are reflected by the regions of denser magnetic field. And it is quite conceivable that conditions in the expanding envelope of a supernova may be especially congenial to the operation of the process originally conceived by Fermi.

Magnetohydrodynamic Mechanisms. H. Alfveń in 1959 showed that particles moving through magnetic fields with irregularities

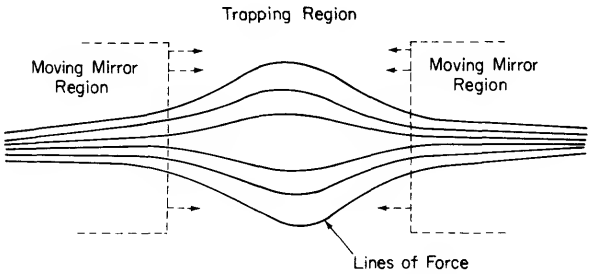

FIG. 8-3 Motion of mirror regions toward each other may accelerate particles. The effect is crudely analogous to what happens when a ping pong ball bounces between the table and a paddle that is rapidly moved toward the table top.

having dimensions very much smaller than the gyroradii of the particles would gain momentum in a process called *magnetic pumping*. If the increase in momentum at each stroke of the pump is proportional to the momentum, the differential spectrum has the form of a power law:

$$j(p)\,dp \propto p^{-1}\,dp. \tag{8-7}$$

This can be doctored to look like the observed spectrum by taking into account the diffusion of the particles after acceleration. This gives

$$j(p)\,dp \propto p^{-2+\zeta}, \tag{8-8}$$

where ζ is an unknown quantity in the range $-1 < \zeta < 1$, so that the result is not inconsistent with the experimental value $\gamma \simeq -2.5$. This type of mechanism, which can occur anywhere in space where the required conditions apply, has actually been utilized in plasma physics experiments.

Observations of radio galaxies and of radio emission from quasars show that particle acceleration happens, even on a galactic scale, in cosmic explosions. Spontaneous processes analogous to laboratory plasma experiments, in which explosive instability of quiescent plasma leads to the acceleration of some particles, undoubtedly occur throughout the cosmos. There is a cornucopia of stored energy residing in magnetic fields. Plasma instabilities can cause the sudden conversion of magnetic energy to particle energy. For example, metastable surfaces of sharp

field reversal, called the *cheek pinch,* can store a finite amount of energy, and then release it explosively.

Electromagnetic fluctuations composed of plasma oscillations, Alfvén waves, acoustic waves, or more complicated wave types known in plasma physics may also produce accelerations. The formation of shock waves provides a most effective means for imparting great energies to cosmic rays. Theories invoking this mechanism relate to a particular type of astronomical object in which conditions for this mode of energy transformation are extremely propitious—the supernova. The occurrence of shock waves is inferred from *wisps* or *ripples* of light emanating from central regions of the Crab Nebula with speeds of about $\frac{1}{3}$ *c*. S. A. Colgate and M. A. Johnson in 1960 first proposed a hydrodynamic process in which cosmic rays are blown off surface layers of an exploding supernova.

SOURCES

Sun and Stars. When cosmic rays were thought to be electromagnetic in nature, the absence of a day-night variation immediately disqualified the sun from further consideration. But later, as the direction-randomizing effects of magnetic fields on the electrically charged primaries were recognized, the sun again became a serious contender. Then, the observation, albeit rarely, of solar cosmic rays in the billion electron volt range coupled with the realization that energetic particles might be stored by magnetic fields in a volume centered at the sun resurrected the possibility that at least a good part of the local cosmic ray population was spawned there.

Solar particles with energies of the order of 10^{10} eV have been observed only once. Clearly, the sun (and, hence, ordinary stars of which it is typical) cannot be the source of the higher energy end of the spectrum. Furthermore, it is easy to demonstrate that the injection rate of all solar particles that can produce ground-level effects ($\gtrsim 0.5$ GV) falls far short of the required level. Of course, we haven't been in the monitoring business very long, and there may have been some very intense high-energy solar

cosmic-ray outbursts in the past. Could the particle density be maintained by storage in the interplanetary magnetic field? This question can be answered by referring to Eq. (4-5), which tells us that the radius of curvature r_g of a 10^{12} eV proton in the 5×10^{-5} gauss field is

$$r_g = pc/300zB \simeq 10^{12}/(300)(5 \times 10^{-5}) \simeq 10^{14}\,\text{cm}. \qquad (8\text{-}9)$$

This is about 10 AU, comparable to the radius of the solar wind cavity, hence particles of this energy would readily escape from the solar system.

The inverse correlation between cosmic-ray intensity and solar activity was the *coup de grâce* of the solar origin hypothesis for all except the very low-energy particles that are certainly domestic products. However, there still remains the possibility of storage and further acceleration on a galactic scale of cosmic rays injected into the great galactic reservoir by millions of ordinary stars like the sun. But, the significant differences between the composition of solar and galactic cosmic rays indicate that ordinary stars having the same relative elemental abundances as the sun do not constitute the main source. We must look for some astronomical objects with special properties.

Supernovae. The list of objects that differ from the typical sun-like stars includes *red giants, supergiants, magnetic stars, novae,* and *supernovae.* The most promising candidate is the supernova.

The theory of nucleosynthesis predicts that in supernova explosions the abundances of carbon and oxygen are enhanced compared with hydrogen and helium. Furthermore, the relative amounts of the heavier elements are increased above their general abundances. Both of these predictions are in agreement with the cosmic-ray observations (cf. Table 5-1).

Supernovae are the last stage in stellar evolution. The aging star becomes hotter, producing progressively heavier nuclides in its nuclear furnace, until it exhausts its fuel. As it loses its latent heat, the star slowly shrinks and its internal temperature rises, increasing the internal pressure. New exothermic nuclear reactions may then occur. The star is depleted of hydrogen first, then helium. Heavier nuclei are synthesized from alpha particles,

and the build-up proceeds. Eventually, at a temperature of about 7 billion degrees, the rapid conversion of iron to helium demands energy that can be supplied only by gravitational potential energy. This causes an *implosion* in a matter of seconds, followed by an unimaginable *thermonuclear explosion* when the lighter elements still left in the outer layers fall into the collapsing core.

A well-known example of a supernova is the *Crab Nebula,* observed in 1054 by the Chinese. At present it is an elliptical object of dimensions roughly 6×4 light years, and about 3500 light years away from the solar system. This stellar explosion was visible in daylight for 23 days, and its brightness was 350 million times the sun's!

Magnetic fields of $\sim 5 \times 10^{-4}$ gauss exist in the Crab, and strong synchrotron radiation is emitted. It is also the site of a copius x-ray source of small dimensions (Tau X-1). X-ray sources and cosmic-ray generators may belong to a common class of celestial objects.

Other well-known supernovae in our Galaxy are Tycho's star in Cassiopeia A (1572) and Keppler's star (1604), both discrete radio sources. The rate of supernova explosions in this galaxy is about two per century.

The stellar end-product of a supernova is a *neutron star.* These remnants of celestial detonations consist of nuclear matter, with densities of the order of 10^{15} gm/cm^3 (roughly a billion tons per cubic inch!). Their radii are about 10 km, their masses range from about 0.2 $M_\odot$ to 2 $M_\odot$, and their temperatures exceed a billion degrees Kelvin.

First recognized through the repetitive bursts of radiofrequency radiation which they emit, by virtue of which they were named *pulsars,* observations have revealed that neutron stars rotate with periods ranging from 33 millisec (the Crab pulsar, NP 0532) to 3.8 sec. The corresponding mechanical energy amounts to 10^{51}–10^{52} erg. Changes in their rotational periods have been observed, and in the case of the Crab pulsar $\Delta T = 3.70 \times 10^{-8}$ sec/day. This corresponds to a change in the rotational energy $-\Delta E \simeq 10^{38}$ erg/sec, the amount required to make the Crab shine. In addition to rf radiation, emissions covering a wide

frequency range, including the optical and x-ray regions of the spectrum, have been detected.

The rapid rotation of a neutron star, coupled with its 10^{13} gauss magnetic field, appears to be profoundly related to the origin of cosmic rays. As T. Gold pointed out in 1968, the pulsar's magnetosphere attains the velocity of light quite close to the rapidly spinning object (e.g. 1700 km from NP 0532), and this can indeed provide the means whereby particles acquire cosmic ray energies. Roughly 40 pulsars, a few hundred parsecs apart and 2500 light years away on the average, have been observed.

OUR GALAXY

The galaxy in which our solar system is located, the Milky Way, is a rotating quasi-spherical mass of 10^{11} stars with dust and gas and wandering masses of plasma in the space between. It consists of the *disk* and the quasi-ellipsoidal *halo,* as is shown in Fig. 8-4. The volume of the halo is about 50 times that of the

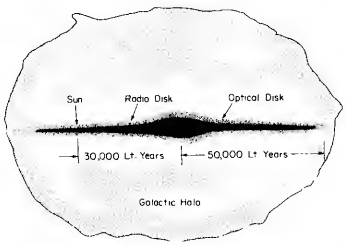

FIG. 8-4 Highly idealized map of our galaxy—the Milky Way.

disk. The radius R_d and thickness h_d of the disk are about 50,000 light years and 3,000 light years, respectively. The distribution of Population I (young) stars is similar to that of the gas clouds which move randomly through the interstellar space. Population II stars, concentrated around the galactic center, display random motions of about 100 km/sec or more, reflecting turbulent conditions early in their lives. Curving out from the galactic nucleus is a spiral structure, as represented schematically in Fig. 8-5, and the sun is located about two-thirds of the way out in one of the *spiral arms.*

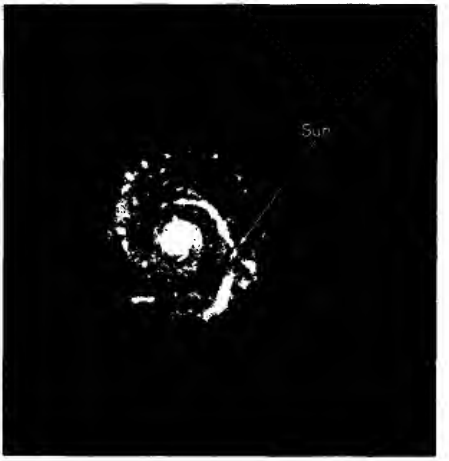

FIG. 8-5 Spiral structure of the galaxy.

The rotational period of the Galaxy is about 200 million years, and its age is approximately 10 billion years. In interstellar space, the density is $\simeq 10^{-24}$ gm/cm^3 (1 hydrogen atom per cubic centimeter) in the disk and about a hundredth of this in the halo. But there are also large islands with dimensions of some ten light years in which the density may be as much as 100 or 1000 times greater. These clouds of ionized gas are characterized by frozen-in magnetic lines of force. The turbulent motion produces disordered magnetic fields and large scale ordered fields, as evidenced by the polarization of starlight due to the magnetic orientation of nonspherical dust particles through which the light passes. The galactic magnetic field amounts to something of the order of 10^{-5} gauss in the disk, and 10^{-6} gauss in the halo. Stronger magnetic fields are present in discrete radio sources.

ORIGIN MODELS

In the formulation of theories of cosmic-ray origin, there is a choice between *galactic* and *metagalactic* models. The latter is called the *homogeneous* model if the energy density $W_g \simeq 10^{-12}$ ergs/cm^3 pervades the entire visible universe, that is, a region with dimensions R of the order of the photometric radius $R_{ph} \simeq$

5×10^{27} cm. In this case, the total energy in the form of cosmic radiation exceeds that of all other forms of energy except the mass of matter in the universe. *Local* metagalactic models confine the sources to regions with dimensions 10^{26} cm $\lesssim R \lesssim 10^{24}$ cm. The galactic size is $R \simeq 10^{22} - 10^{23}$ cm.

The disk and halo models differ mainly in terms of the volume occupied by cosmic rays. Whereas, in the first case, the volume $V_d \simeq R_d^2 h_d \simeq 10^{67}$ cm^3, in the second case $V_h \simeq R_h^3 \simeq 10^{68}$ cm^3, hence the total energy of cosmic rays differs by one order of magnitude:

$$\begin{aligned} E_d &\simeq W_g V_d \simeq 10^{55} \text{ ergs}, \\ E_h &\simeq W_g V_h \simeq 10^{56} \text{ ergs}. \end{aligned} \tag{8-10}$$

For purposes of comparison, let us list some significant cosmic energy densities. In addition to (1) the classical cosmic rays that constitute the subject of this book—energy density $\simeq 1$ eV/cm^3, there are (2) the very soft photons comprising the *background radiation* from a *big bang*—energy density $\simeq 0.4$ eV/cm^3, (3) hard photons, x rays and γ rays—energy density $\simeq 3 \times 10^{-5}$ eV/cm^3, and (4) neutrinos—energy density $\lesssim 10$ keV/cm^3. Other relevant forms of energy are (5) magnetic field in galactic disk—$B_g^2/8\pi \simeq 1$ eV/cm^3; (6) starlight in our part of the Galaxy—$\simeq 0.3$ eV/cm^3; and (7) random motions of gas clouds in our Galaxy—$\frac{1}{2}\rho v^2 \simeq 0.2$ eV/cm^3.

It is interesting and probably quite coincidental that some of these apparently unrelated quantities are so similar. On the other hand, it is known that in plasma, magnetic fields are coupled to particle motions.

In the financial world, the balance sheet reveals the fiscal soundness of an enterprise. Similarly, to be plausible, a theory of cosmic-ray origin must provide a balanced energy budget. This means that within the volume assumed to be occupied by cosmic rays there must be sources that are capable of maintaining the corresponding total energy carried by cosmic rays distributed throughout that volume. Consequently, arguments about the extent of the source region devolve upon the efficiency of the galaxy and its immediate surroundings as a trapping volume,

and the relative efficiencies of galactic and metagalactic energy sources.

The choice between galactic *vs* extragalactic origin is centered upon whether supernovae and explosions in the galactic nucleus on the one hand, or the strong radio sources on the other, are the principal cosmic-ray sources. Estimation of both the frequency of violent events and the energy released per event is required in either case.

Still a controversial matter, the distance of *quasars* is the key to the extragalactic hypotheses. What is the nature of a quasar? The red shift of the lines of the spectra of these quasi-stellar objects (QSO) can be explained either by (a) their participation in the general expansion of the universe, or by (b) their ejection at the observed speed from the galactic nuclei of nearby radio galaxies (i.e. 40 Mps)* or by (c) gravitational displacement of lines emitted by gas in the central part of an accumulation of neutron stars. The cosmological viewpoint (a) now seems to have the edge.

Homogeneous Metagalactic Model. The density of radiogalaxies is about $1.3 \times 10^{-4}/(\text{Mps})^3 \simeq 4 \times 10^{-78}/\text{cm}^3$. Therefore, on the average, each must inject cosmic rays with a total energy $10^{-12}/(4 \times 10^{-78}) \simeq 2 \times 10^{65}$ ergs $\simeq 10^{11}\ M_\odot c^2$. The mass of the largest galaxies is usually $<10^{12}\ M_\odot$. The maximum attainable value is more like $10^{61} - 10^{62}$ ergs or about $10^7\ M_\odot c^2$. This would give a cosmic-ray density less than $\simeq 10^{-16}$ ergs/cm^3.

Local Metagalactic Model. In the case of the local metagalactic model, the nearest potential source is the radio galaxy Centaurus A at a distance of 3.8 Mps. To fill a volume $V_{\text{mg}} \simeq 10^{75}$ cm^3 with a density $\simeq 10^{-12}$ ergs/cm^3 requires injection of 10^{63} ergs. But only about 10^{59} ergs are available for particle acceleration. Similarly, gravitational collapse to produce 10^{63} ergs requires a mass $M \simeq 10^{12}\ M_\odot$, whereas for the entire galaxy, $M \simeq 2 \times 10^{11}\ M_\odot$.

If a large part of the cosmic radiation comes from extragalactic sources, the intensity would show a large time variation over a period of less than about 10^8 years, which seems not to be in accord with observation. Nevertheless, such a source appears

*1 Mps $= 10^6$ parsecs $= 3 \times 10^{24}$ cm.

to be required to account for the particles at the top of the energy spectrum.

Galactic Model. The question of the disk and halo *vs* disk alone affects the high-energy end of the spectrum as well as the power that must be furnished by individual sources to meet the total energy quota. From Eq. (8-10) the total energies are $E_h \simeq 10^{56}$ ergs and $E_d \simeq 10^{55}$ ergs. But escape from the disk is easier, since the trapping time is shorter. Thus, for a lifetime of 10^6 years, the power must be 10^{55} erg/(10^6 yr) (3×10^7 sec/yr) $\simeq 10^{41}$ ergs/sec $\simeq 10^{35}$ watts. In the halo, where the lifetime is $\simeq 10^8$ years, the required power is 10^{56} ergs/(10^8 yr)(3×10^7 sec/yr) $\simeq 10^{40}$ ergs/sec $\simeq 10^{34}$ watts.

To summarize, the parameters of a plausible model are:

$R \simeq 3 - 5 \times 10^{22}$ cm,
Volume $\simeq 10^{68}$ cm^3,
Total Cosmic Ray Energy $\simeq 10^{56}$ ergs,
Escape Time $\simeq 3 \times 10^8$ years,
Power of Sources $\simeq 10^{40}$ ergs/sec.

Supernova outbursts in our galaxy occur about once in 50 years (1.5×10^9 sec). Therefore, the mean energy transferred to cosmic rays per outburst must be (10^{40} ergs/sec) (1.5×10^9 sec) $\simeq 10^{49}$ ergs. This is not asking too much. Besides, minor outbursts in the galactic nucleus that could also provide the required power of about 10^{40} ergs/sec have been observed.

But a prime candidate for the role of cosmic ray spawner is the neutron star. With about 3×10^{42} ergs/sec going into plasma energy, the Crab pulsar NP 0532 produces about 30 times the power needed to supply the cosmic ray energy density in the galaxy.

Hierarchy Theory. The increase in the slope of the cosmic-ray energy spectrum at about 10^{15} eV (see Fig. 5-1) has been attributed to the inability of the galaxy to retain particles with rigidities exceeding $10^{15} - 10^{16}$ volts. Referring to Eq. (8-9), the corresponding radius of curvature of a proton in a *homogeneous* magnetic field of 10^{-5} gauss is about one light-year and of an iron nucleus 0.04 light-years. It must be remembered in all our discussion of the bending of charged particles that the radius of

curvature could be considerably larger, and the container more transparent, if the field does not maintain some degree of regularity over the entire trajectory. As protons start to wander out of the galactic fold at the energy corresponding to the kink, the composition changes in the direction of an increase in the relative abundance of heavy nuclei (i.e. higher Z), for which the magnetic containment is more efficient.

Above 10^{18} eV, the flux of galactic cosmic rays falls below that of extragalactic particles, since near the upper limit of observed energies, the galactic storage mechanism breaks down. For example, at 10^{20} eV, the cyclotron radius of a proton in the $\leq 10^{-5}$ gauss galactic field would be $> 3 \times 10^4$ light-years. The corresponding diameter of $> 6 \times 10^4$ light-years is about 20 times the thickness of the galactic disk. Undoubtedly, the halo plays an essential role in storing the more energetic particles. But it is inconceivable that the galaxy could retain 10^{20} eV protons, several of which have been observed.

The recent discovery of low-energy black-body radiation, interpreted as a red-shifted remnant of the primeval fireball, has important implications with regard to the problem of cosmic-ray origin, particularly with respect to the distance of the sources. This thermal microwave radiation corresponding to a temperature of 3°K is assumed to pervade all space uniformly. It imposes an upper limit on the expected spectrum of cosmic-ray protons through the action of pion photoproduction, which has a threshold at 10^{20} eV and a rapidly rising cross section. For α particles and heavier nuclei, the upper limit would be encountered at lower total energies.

The reaction is

$$\begin{aligned} \gamma + \mathrm{p} &\rightarrow \pi^0 + \mathrm{p} \\ &\rightarrow \pi^+ + \mathrm{n}. \end{aligned} \tag{8-11}$$

With an average cross section of 2×10^{-28} cm^2, and a photon density of 600 photons/cm^3, Eq. (2-12) gives the mean free path $\lambda = 1/N\sigma \simeq 10^{25}$ cm $\simeq 10^7$ light-years. This is roughly the diameter of the "local group" of galaxies. Thus, the high-energy cutoff near 10^{20} eV would prevail unless the most energetic cosmic rays observed thus far are generated within this radius.

Another reaction that would affect particles traveling large distances in the metagalaxy is

$$\gamma + p \rightarrow e^+ + e^- + p. \qquad (8\text{-}12)$$

This also tends to reduce the energy at the high-energy end of the spectrum.

As to the origin of the primary electrons, the various acceleration mechanisms that we have discussed are expected to produce negative electrons exclusively, since, presumably, positrons are not available. Therefore, the latter can originate only in collisions of other forms of cosmic radiation with matter in the galaxy. Those interactions of cosmic-ray protons with interstellar hydrogen in which both protons survive yield equal numbers of positive and negative pions, which decay into positrons and electrons in the scheme π-μ-e. However, when protons turn into neutrons in the collisions, π^+ are emitted, and a positive excess results. Thus, the large observed excess of negative electrons indicates that most of the electronic component is accelerated directly, and is not the product of collisions of other types of cosmic radiation with interstellar hydrogen. Supernova remnants seem to be their most likely source.

In any event, the cosmic-ray electrons that reach the earth must all originate within the galaxy, since the background microwave photon radiation would obliterate extragalactic electrons by an inverse Compton effect that would convert their energy into x rays during the course of a longer journey. Furthermore, x-ray data indicate that the energy density of relativistic electrons in metagalactic space is less than $\sim 10^{-17}$ ergs/cm^3, which is very much below the observed cosmic-ray electron energy density of $\sim 10^{-14}$ ergs/cm^3.

The *mixed,* or *hierarchy,* theory of the origin of cosmic radiation ascribes different parts of the cosmic ray family to different sources. The diverse features that must be explained would seem to preclude a unique source and acceleration mechanism. Indeed, a number of different processes are capable of producing cosmic rays and are probably operating somewhere. This is brought home by the mounting evidence that charged particles are accelerated even by phenomena occurring within the earth's mag-

netosphere. A finite flux is actually injected into interplanetary space and, if we follow the historical pattern, we should call these particles *terrestrial cosmic rays.* This would surely confound the semanticist!

Perhaps there is some philosophical justification in the belief that if man can conceive of a physically sound method for producing cosmic rays, it is probably operative somewhere in the universe. In any case, the burden of telling us why such orderliness prevails amidst such a plethora of cosmic ray sources may have to be borne by the answer to question number 5—Why?

We dance round in a ring and suppose,
But the secret sits in the middle and knows.

ROBERT FROST

Appendix

TABLE A-1. *Dramatis Personae. Principal Elementary Particles in the Cosmic Radiation.*

Name	Symbol	Rest Mass M_0/m_0	Rest Energy M_0c^2, MeV	Charge q	Spin S, $\hbar/2\pi$	Magnetic Moment μ $\hbar e/2m_0c$	Proper Lifetime τ_0, sec.	Principal Decay Scheme	Anti-particle
*Leptons**									
Neutrino	ν	$<10^{-3}$	<500eV	0	$\frac{1}{2}$	$<10^{-7}$	—	—	$\bar{\nu}$
Electron	e^-	9.109×10^{-28} gm	0.511	-4.803×10^{-10} esu	$\frac{1}{2}$	1	—	—	e^+
Muon	μ^-	207	106	$-e$	$\frac{1}{2}$		2.2×10^{-6}	$e^- + \nu + \bar{\nu}$	μ^+
Bosons									
Photon	γ	—	—	0	1	0	—	—	itself
*Hadrons***									
Pion	π°	264	135	0	0	—	2.2×10^{-16}	$\gamma + \gamma$, $\gamma + e^+ + e^-$	itself
	π^+	273	140	$+e$	0	—	2.6×10^{-8}	$\mu^+ + \nu$	π^-
*Baryons***									
Proton	p	1836	938	$+e$	$\frac{1}{2}$	2.79	—	—	$\bar{p}$
Neutron	n	1839	939	0	$\frac{1}{2}$	−1.97	1020	$p + e^- + \bar{\nu}$	$\bar{n}$

* weak interactions
** strong interactions

Bibliography

BOOKS

A. E. Sandström, *Cosmic Ray Physics* (North-Holland Publishing Co., Amsterdam, 1965).

B. Rossi, *Cosmic Rays* (McGraw-Hill, Inc., New York, 1964).

V. L. Ginzburg and J. I. Syrovatskii, *The Origin of Cosmic Rays* (Pergamon Press, Oxford, 1964).

V. D. Hopper, *Cosmic Radiation and High Energy Interactions* (Prentice-Hall, Inc., New Jersey, 1964).

A. W. Wolfendale, *Cosmic Rays* (Philosophical Library Inc., New York, 1963).

T. E. Cranshaw, *Cosmic Rays* (Oxford University Press, London, 1963).

B. Peters, Editor, *Cosmic Rays, Solar Particles and Space Research* (Academic Press, New York, 1963).

E. N. Parker, *Interplanetary Dynamical Processes* (John Wiley and Sons, Inc., 1963).

H. Alfvén and C. G. Fälthammar, *Cosmical Electrodynamics* (Clarendon Press, Oxford, 1963).

A. Ramakrishnan, *Elementary Particles and Cosmic Rays* (Pergamon Press, Oxford, 1962).

C. F. Powell, P. H. Fowler, D. H. Perkins, *The Study of Elementary Particles by the Photographic Method* (Pergamon Press, New York, 1959).

J. E. Hooper and M. Scharff, *The Cosmic Radiation* (John Wiley and Sons, Inc., New York, 1958).

W. Heisenberg, Editor, *Kosmische Strahlung* (Springer-Verlag, Berlin, 1953).

B. Rossi, *High Energy Particles* (Prentice-Hall, Inc., New York, 1952).

D. J. X. Montgomery, *Cosmic Ray Physics* (Princeton University Press, New Jersey, 1949).

L. Jánossy, *Cosmic Rays* (Clarendon Press, Oxford, 1948).

W. Heisenberg, Editor, *Cosmic Radiation* (Dover Publications, New York, 1946).

E. Miehlnickel, *Höhenstrahlung* (*Ultrastrahlung*) (Theodor Steinkopff, Germany, 1938).

SERIES OF BOOKS AND JOURNALS CONTAINING REVIEW ARTICLES

Annual Review of Astronomy and Astrophysics (Annual Reviews, Inc., California).

Annual Review of Nuclear Science (Annual Reviews, Inc., California).

Handbuch der Physik [*Encyclopedia of Physics*] (Springer-Verlag, Berlin).

Proceedings of the International Conference on Cosmic Rays:
Eleventh, Budapest, Hungary, 1969 (Acta Physica Hungarica).
Tenth, Calgary, Canada, 1967 (Canadian Journal of Physics).
Ninth, London, England, 1965 (The Institute of Physics and the Physical Society, London).
Eighth, Jaipur, India, 1963 (unpublished).
Seventh, Kyoto, Japan, 1961 (Journal of the Physical Society of Japan).

Progress in Elementary Particle and Cosmic Ray Physics (North-Holland Publishing Company, Amsterdam).

Progress in Nuclear Physics (Pergamon Press, London).

Progress of Theoretical Physics (Research Institute for Fundamental Physics, Japan).

Reviews of Geophysics (American Geophysical Union, Virginia).

Space Science Reviews (D. Reidel, Holland).

Symbols, Abbreviations, Typical Units, and Values of Various Quantities

a—radius of earth $= 6.378 \times 10^3$ km.
A—atomic mass number = number of nucleons in a nuclide.
$\bar{A}$—amplitude (percent).
A_s—area (e.g. cm^2).
AU—astronomical unit (mean earth-sun distance) $= 1.496 \times 10^{13}$ cm.
barn—cross section $= 10^{-24}$ cm^2.
B—magnetic induction (gauss).
B_g—galactic magnetic field (gauss).
B_s—interplanetary magnetic field (gauss).
c_m—speed of light in a medium.
d—impact imparameter (e.g. cm).
dE/dx—specific energy loss (e.g. MeV/gm/cm^2).
D—diffusion coefficient (cm^2/sec).
eV—electron volt (1 eV $= 1.602 \times 10^{-12}$ erg).
E—kinetic energy (ev).
E_c—critical energy in radiation processes: $(dE_c/dx)_{ion} = (dE_c/dx)_{rad}$.
h_d—thickness of galactic disk.
I—intensity of electromagnetic radiation (photons/cm^2/sec/ster).
$j(E)dE$ or $dj(E)/dE$—differential unidirectional intensity between E and $E + dE$ (e.g. particles/cm^2/sec/ster/MeV).
$j(P)dP$ or $dj(P)/dP$—differential unidirectional intensity between P and $P + dP$ (e.g. particles/cm^2/sec/ster/GV).
$j(>E)$—integral unidirectional intensity above energy E (e.g. particles/cm^2/sec).

$j(>P)$—integral unidirectional intensity above rigidity P (e.g. particles/cm^2/sec).
j_p—primary specific ionization (e.g. ion pairs/cm).
j_t—total specific ionization (e.g. ion pairs/cm).
l—shower unit (eg. cm).
LY—light year $= 9.460 \times 10^{17}$ cm.
M_β—total mass, or mass of moving particle in coordinate system in which its speed is $v = \beta c$.
M_D—dipole moment of the earth $= 8.1 \times 10^{25}$ gauss cm.
M_0—rest mass, or mass of particle in coordinate system in which its speed is $v = 0$.
m_0—electron rest mass $= 9.109 \times 10^{28}$ gm.
$M_\odot$—solar mass $= 1.989 \times 10^{33}$ gm.
$M_\odot c^2$—solar mass energy $= 1.789 \times 10^{54}$ ergs.
N_p—particle density (e.g. particles/cm^3).
$N(P)$—counting rate attributable to primaries with rigidity P.
p—momentum (ev/c).
ps—parsec $= 3.26$ light years $= 3 \times 10^{18}$ cm.
P—magnetic rigidity $= pc/ze$ (volts) $= Br_g$ (gauss cm).
P_c—vertical threshold rigidity (GV).
P_s—minimum rigidity required for particle to reach earth at the equator from least favored direction $= 59.6$ GV.
P_{s_V}—vertical cutoff rigidity (Störmer cone) $= 14.9 \cos^4 \lambda_g$ GV.
rad—energy absorption $= 100$ ergs/gm.
r_e—classical electron radius $= e^2/m_0c^2 = 2.818 \times 10^{-13}$ cm.
rep—roentgen equivalent physical $= 93$ ergs/gm.
r_g—gyroradius or cyclotron radius (e.g. cm).
r_0—interplanetary magnetic field cavity (e.g. AU).
R—range (e.g. gm/cm^2).
R_i—astronomical dimension (e.g. Mps).
ster—unit solid angle (steradian).
torr—atmospheric pressure (1 torr $=$ 1 mm of Hg).
U—total energy $=$ kinetic energy $E +$ rest energy M_0c^2 (e.g. GeV).
v_B—speed of plasma cloud (e.g. km/sec).
v_p—speed of particle (e.g. cm/sec).
v_w—speed of solar wind (e.g. km/sec).
W—energy of electromagnetic radiation (e.g. MeV).

W_g—energy density in galaxy (ergs/cm^3).
X_0—radiation length (e.g. gm/cm^2).
z—charge in units of electron charge.
Z—atomic number = number of protons in nucleus (and electrons in neutral atom).

GREEK SYMBOLS

α—fine structure constant = $e^2/hc = 1/137.04$.
α_i—barometric pressure coefficient for component i (e.g. percent per torr).
β—particle speed/speed of light = v/c.
β_i—absorption coefficient = $1/\lambda_i$.
β_ℓ—linear absorption coefficient (cm^{-1}).
β_m—mass absorption coefficient (cm^2/gm).
ϵ—phase angle.
ϵ_0—permittivity (dielectric constant) in free space = 8.854×10^{-12} farad/m.
ϵ_c—critical energy in radiation processes: $-\int_{X_0}^{0}(dE/dx)_{\text{ion}}\,dx$.
λ_i—interaction mean free path (e.g. gm/cm^2).
λ_a—absorption (or attenuation) mean free path (e.g. gm/cm^2).
λ_g—geomagnetic latitude (degrees).
μ—micrometer = 10^{-4} cm.
ν—frequency (hertz).
ρ—density (e.g. gm/cm^3).
σ_i—cross section (e.g. barns. 1 barn = 10^{-24} cm^2).
σ_g—geometric cross section = $0.05A^{1/3}$ barns.
τ—mean lifetime = lifetime of unstable particle in coordinate system with respect to which it is moving (sec).
τ_c—bombardment or radiation age (e.g. year).
τ_0—proper lifetime = lifetime of unstable particle in coordinate system with respect to which it is at rest (sec).
ϕ—particle flux (e.g. particles/cm^2/sec).
Ω—angular velocity of sun = 2.7×10^{-6} rad/sec.

Index

VAN NOSTRAND REINHOLD MOMENTUM BOOKS

MOMENTUM BOOKS were conceived with a purpose . . . to serve the modern inquiring mind. Scientist, engineer, teacher, student, inquisitive layman . . . each will find that MOMENTUM BOOKS provoke new ideas, new questions and new answers while they provide an insight into experimental techniques and the disciplines of the scientific mind.

Each MOMENTUM BOOK is a lucid and accurate analysis of an area of modern or classical physics. Combining sound science with clear presentation, this series presents expositions in important topics in physics . . . ranging from its history to its applications.

WALTER C. MICHELS is Marion Reilley Professor of Physics at Bryn Mawr College. He received an E.E. degree from Rensselaer Polytechnic Institute in 1927, and a Ph.D. degree from the California Institute of Technology in 1930. He then spent two years as a National Research Fellow at Palmer Physical Laboratory, Princeton University, before joining the staff at Bryn Mawr College. Professor Michels is the author of *Electrical Measurements and Their Applications* (1957), and *Elements of Modern Physics* (with A. L. Patterson, 1951). He also served as editor-in-chief of the *International Dictionary of Physics and Electronics* (1961). He has been editor of the *American Journal of Physics* since 1959. Professor Michels has contributed to that journal, and to *Physical Review*, *Journal of the Optical Society of America*, the *American Journal of Psychology*, and *Scientific American* as well. He is a member of the American Association of Physics Teachers (President 1956-57), the American Physical Society, and the Optical Society of America.

C 6721-997-8

A VAN NOSTRAND REINHOLD MOMENTUM BOOK

PUBLISHED FOR THE COMMISSION ON COLLEGE PHYSICS
under the General Editorship of WALTER C. MICHELS
Morton Kelley Professor of Physics, Bryn Mawr College

ABOUT THIS BOOK: This book conveys to readers with a diversity of interests and backgrounds a sense of the excitement that pervades cosmic ray research, as well as a feeling for the broad range of fundamental physics that falls within its purview. Throughout the book, the emphasis is on ideas, rather than on experimental and theoretical details. The book begins with the story of the discovery of cosmic rays and the subsequent development of our understanding about them. The first chapter concludes with a survey of our current knowledge concerning their properties. The various interactions of cosmic rays with matter are then discussed, after which the many different experimental techniques utilized in cosmic ray research are described. The next chapter treats the propagation of cosmic rays through the earth's magnetic field, and through the atmosphere. The properties of galactic cosmic rays are then discussed in detail. The next chapter is devoted to cosmic ray intensity variations and their causes, and the final two chapters are concerned with solar cosmic rays, and the origin of the so-called galactic cosmic rays.

The Author: MARTIN A. POMERANTZ is Director, Bartol Research Foundation of The Franklin Institute and Professor of Physics, Temple University. The author of more than 100 scientific publications, Dr. Pomerantz is Editor, Journal of The Franklin Institute and a member of the Editorial Board of Space Science Reviews, Advances in Research Series (in Atomic and Molecular Physics). He received his A.B. degree from Syracuse University, his M.S. from University of Pennsylvania, and a Ph.D. from Temple University. He is a Fellow of the American Physical Society, a Fellow of the American Association for the Advancement of Science, and a Fellow of The American Geophysical Union.

VAN NOSTRAND REINHOLD COMPANY
450 West 33rd Street New York, N.Y. 10001

POMERANTZ Cosmic Rays